ULPGC
Universidad de
Las Palmas de
Gran Canaria

Doctorado en Ingenierías Química, Mecánica y de Fabricación

Las Palmas de Gran Canaria, marzo de 2025

ESTUDIO DE LAS PROPIEDADES DE ALEACIONES DE ALTA ENTROPÍA COMO BIOMATERIALES DE NUEVA GENERACIÓN

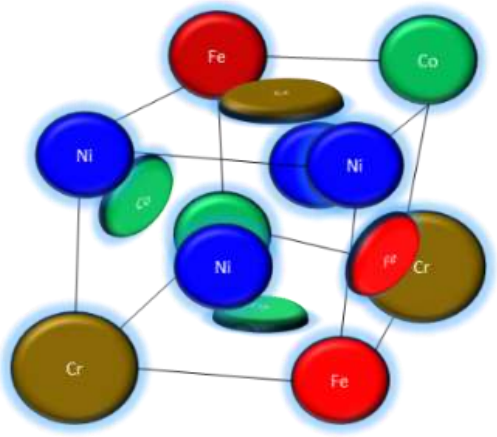

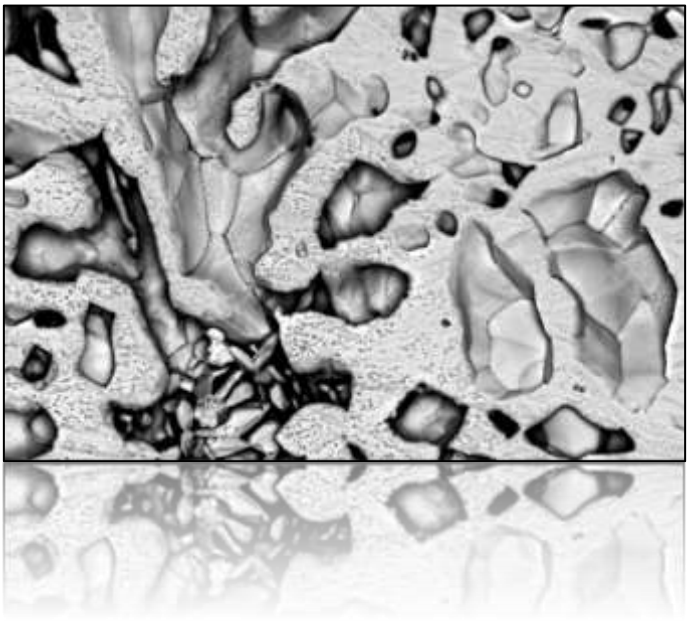

Autor:

Miguel López Ríos

Directoras:

Dra. Julia Claudia Mirza Rosca

Dra. Ionelia Voiculescu

SHEng
SMART HEAT-ICHE FABRICATION

Erasmus+ Programme – Cooperation partnerships
Project No.: 2023-1-RO01-KA220-HED-000159985

Co-funded by
the European Union

ULPGC
Universidad de
Las Palmas de
Gran Canaria

Doctorado en Ingenierías Química, Mecánica y de Fabricación

Escuela de doctorado de la ULPGC

Las Palmas de Gran Canaria, marzo de 2025

ESTUDIO DE LAS PROPIEDADES DE ALEACIONES DE ALTA ENTROPÍA COMO BIOMATERIALES DE NUEVA GENERACIÓN

Autor:

Miguel López Ríos

Directora:

Julia Claudia Mirza Rosca

Directora:

Ionelia Voiculescu

AGRADECIMIENTOS

Quisiera expresar mi más sincero agradecimiento a todas aquellas personas del grupo de investigación de nanomateriales y corrosión que, en distintos momentos, han coincidido conmigo durante este trabajo, como Néstor, Pedro, Iosif y Cristina, por su apoyo mutuo y por compartir conmigo sus conocimientos y experiencias. Y de forma más concreta, quisiera agradecer a Santiago su colaboración en los trabajos más recientes. Puede que él no sea consciente de lo mucho que me ha ayudado su participación en este proyecto, ya que no me refiero específicamente a sus aportaciones como investigador, sino también a su forma de trabajar y de ser. Tenerlo como compañero es un aliciente para avanzar y lograr objetivos.

A mi amigo Luis, compañero en la Escuela, y desde la escuela, por servirme de referencia en esto y en tantas otras cuestiones. Desde siempre.

A mis dos directoras de tesis, las doctoras Ionelia Voiculescu y Julia Mirza, gracias por su dedicación y generosidad. Su conocimiento en el área de investigación ha sido fundamental en este estudio, así como también lo ha sido en gran medida su disponibilidad y filosofía de trabajo. A las dos, mi más profundo agradecimiento. Y de forma especial, quisiera agradecer a Julia por su aportación humana, comprensiva en todo momento con mis circunstancias personales, algo que ha resultado indispensable para que yo haya reunido la voluntad y el tiempo necesarios para completar esta tarea. Su respaldo ha sido fundamental en mi desarrollo como investigador y como docente en el área de materiales.

A mis padres y hermanos, por su cariño y apoyo. A mi padre, desde el amor del recuerdo y a mi madre, desde la suerte de tenerla a "mi" lado, "cazando ratones". Gracias Toñito, por ser un viento fresco de propósitos y buenos deseos. Y especialmente, gracias Laura, porque sin tu llamada y sin tu ánimo, lo más probable es que nunca hubiese empezado nada de esto.

Finalmente, gracias a mis hijas que, sin saberlo todavía, me iluminan en el camino de querer ser mejor. Y, por supuesto, gracias a mi amada esposa, sustancia fundamental de mi vida, con quien cuento para cada aventura que emprendo. Mi agradecimiento hacia ti va mucho más allá de este trabajo.

A todos y cada uno de ustedes, gracias por creer en mí y por acompañarme en este viaje.

RESUMEN

El presente trabajo de investigación consiste en el análisis de distintas aleaciones de alta entropía (HEAs), propuestas como posibles materiales para aplicaciones biomédicas. Concretamente, analiza tres aleaciones formadas por las siguientes combinaciones de elementos: AlCoCrFeNi, MoNbTaTiZr y FeMoTaTiZr.

En los últimos años un nuevo tipo de materiales basado en aleaciones de múltiples elementos principales (MPEAs), ha abierto un extenso campo de estudio. Lo que inicialmente se valoró como aleaciones formadas por cinco o más elementos en proporciones equimolares, también denominadas aleaciones de alta entropía (HEAs), ha dado paso a un amplio abanico de posibilidades de combinaciones, resultando en nuevas aleaciones con propiedades especiales que mejoran las características físicas y químicas de las aleaciones tradicionales.

De forma lógica, el descubrimiento de un nuevo tipo de material, junto con la teorización de su estructura y composición, implica el estudio paralelo de sus propiedades, y la consecuente dirección de sus aplicaciones. En este sentido, la familia de las aleaciones de alta entropía, debido al enorme número de posibilidades de combinaciones de hasta cinco elementos que puede haber, está desarrollando nuevos materiales a una velocidad creciente, aumentando en mucho las posibles aplicaciones de estos. Esto ha generado un espacio grande para el estudio de las propiedades de las distintas HEAs, que apenas ha empezado a llenarse con investigaciones en todo el mundo.

La motivación principal de este trabajo radica en la necesidad de desarrollar biomateriales con propiedades mecánicas y de biocompatibilidad superiores a las aleaciones convencionales, actualmente utilizadas en implantes y dispositivos médicos. Es por esto que, dentro de la ingente cantidad de nuevas aleaciones de alta entropía que se están investigando en la actualidad, esta tesis se ha basado en aquellos sistemas de aleaciones constituidos principalmente a partir de elementos químicos con nula o escasa toxicidad para el cuerpo humano.

Con este fondo, el trabajo de investigación desarrollado tiene como **objetivo fundamental** caracterizar distintas aleaciones de alta entropía desde el punto de vista de la estructura, la dureza y el comportamiento ante la corrosión en ambientes que simulan el

interior del cuerpo humano, de manera que se puedan obtener conclusiones sobre la idoneidad de seguir avanzando en estas líneas de investigación acerca de la biocompatibilidad de este nuevo tipo de aleaciones para su uso como piezas para implantes médicos o instrumentos quirúrgicos.

Los objetivos específicos planteados para este trabajo de investigación se exponen a continuación:

1) En el sistema de aleaciones de alta entropía AlCoCrFeNix, determinar la influencia de diferentes proporciones de níquel (x = 1.0, 1.4 y 1.8) en la microestructura, en la microdureza y en el comportamiento a la corrosión en fluido corporal simulado.

2) Para dos sistemas de aleaciones de alta entropía similares, MoNbTaTiZr (NbHEA) y FeMoTaTiZr (FeHEA), determinar el efecto de la sustitución de niobio por hierro, tanto en la microestructura como en la resistencia a la corrosión en un entorno fisiológico simulado. Las muestras se ensayaron antes y después de la aplicación de tratamientos térmicos controlados, para mejor comprensión de cómo evolucionan las fases y su homogeneidad.

3) Caracterizar una nueva aleación de alta entropía basada en los elmentos FeMoTaTiZr, diseñada específicamente para aplicaciones médicas no implantables, analizándola en términos de microestructura, dureza y biocompatibilidad in vitro (citotoxicidad).

El estudio de las propiedades de aleaciones de alta entropía como biomateriales de nueva generación tiene relación con las siguientes líneas de investigación del programa de doctorado en Ingenierías Química, Mecánica y de Fabricación (QUIMEFA):

- Corrosión de metales.
- Nanomateriales.

El estudio de las propiedades de un metal que se pretende que tenga aplicaciones médicas requiere del estudio del comportamiento del mismo frente a la corrosión para concluir su idoneidad como herramientas quirúrgicas o implantes que van a estar sometidos al ataque de los fluidos corporales. En este sentido, la corrosión en los metales como línea de investigación está directamente relacionada con el tema de la tesis. Adicionalmente, algunas aleaciones de alta entropía presentan granos nanométricos, por lo que el estudio de

las HEAs genera la posibilidad de influir en la composición de fases y en la estructura del material a ese nivel.

La presente tesis doctoral cuenta con tres publicaciones en dos revistas científicas.

El primer trabajo se publicó en el artículo "*Effects of nickel content on the microstructure, microhardness and corrosion behavior of high-entropy AlCoCrFeNix alloys*" y consistió en el análisis del efecto que tiene variar el ratio atómico del níquel en este sistema de aleaciones de alta entropía formado por $AlCoCrFeNi_x$. Para esto, se fabricaron tres muestras de este sistema, en los que se variaba la composición según los valores de ratios atómicos x = 1.0, 1.4 y 1.8. Las aleaciones fueron sintetizadas mediante la técnica de fabricación de refundición por arco al vacío, y sometidas a tratamientos térmicos posteriores.

Se realizaron ensayos de microestructura mediante microscopía óptica y SEM, así como ensayos de microdureza Vickers y ensayos de corrosión mediante polarización potenciodinámica tras una inmersión prolongada en fluido corporal simulado.

Este trabajo fue publicado en la revista científica "Scientific Reports" (ISSN 2045-2322) en diciembre de 2020.

El segundo trabajo se publicó bajo el título "*Comparative Study of (Fe,Nb)MoTaTiZr High Entropy Alloys in Ringer Grifols Solution*". En este segundo artículo se presentó un análisis comparativo entre las aleaciones MoNbTaTiZr (NbHEA) y FeMoTaTiZr (FeHEA), en las que se mantuvieron proporciones similares del resto de los elementos, con el objetivo de analizar el efecto de la sustitución del niobio por el hierro. Este efecto se estudió en la microestructura, en la microdureza y en la resistencia a la corrosión en un medio fisiológico simulado (solución de Ringer).

Para la observación de la microestructura se utilizaron las técnicas de microscopía óptica y de espectroscopía electrónica de barrido (SEM). Esta información se completó además con los datos del ensayo de difracción de rayos X (XRD), que aportó información sobre las estructuras cristalinas presentes en las aleaciones. Finalmente, los datos arrojados por los ensayos de polarización potenciodinámica y por los ensayos de espectroscopia de impedancia electroquímica (EIS) permitieron evaluar la susceptibilidad a la corrosión y suponer los mecanismos involucrados en el proceso corrosivo.

Este trabajo fue publicado en la revista científica "Metals" (ISSN 2045-4701) en diciembre de 2024.

El tercer trabajo se publicó en el artículo "*NewFeMoTaTiZr High-Entropy Alloy for Medical Applications*". En este, se describe la síntesis y caracterización de una nueva aleación de alta entropía, formada por los elementos FeMoTaTiZr.

La aleación se fabricó mediante fusión por arco al vacío. La composición de las muestras fabricadas fue cuantificada mediante microscopía electrónica de barrido (SEM). Estos valores se compararon con los inicialmente proyectados para la fabricación de las muestras, lo que permitió validar el proceso de fabricación. Adicionalmente, las muestras fueron sometidas a tratamientos térmicos posteriores.

La microestructura se analizó con microscopía óptica y la composición con espectroscopía electrónica de barrido (SEM). La caracterización de las fases cristalinas se realizó mediante técnica de difracción XRD, ejecutada tanto antes como después de la aplicación de tratamientos térmicos. La dureza se evaluó mediante ensayos de microdureza Vickers. Y, adicionalmente, se realizó una evaluación de la biocompatibilidad mediante el ensayo de citotoxicidad basado en la actividad de la enzima lactata hidrogenasa (LDH).

Este trabajo fue publicado en la revista científica "Metals" (ISSN 2045-4701) en febrero de 2025.

ÍNDICE

1. INTRODUCCIÓN

1.1 ANTECEDENTES

Actualmente, una de las líneas de investigación más prometedoras en ciencia de materiales, con potencial para revolucionar la industria aeroespacial, biomédica y energética, es la de las aleaciones de alta entropía (HEAs).

Un primer estudio detallado de aleaciones multicomponentes formadas por un gran número de constituyentes en proporciones iguales o casi iguales fue llevado a cabo en 1981 por Vincent y continuado en 1997 por Knight, para ser posteriormente publicado en 2004 por Cantor et al. Ranganathan discutió tipos similares de aleaciones en 2003, describiéndolas como cócteles multimateriales y Yeh et al. hicieron lo propio en 2004, describiéndolas como aleaciones de alta entropía.

El término de "aleaciones de alta entropía" se ha aceptado para referirse a las aleaciones multicomponentes que consisten en un gran número de constituyentes en proporciones iguales o casi iguales. A menudo exhiben un número sorprendentemente pequeño de fases con amplios rangos de solubilidad, causado en parte por los efectos de alta entropía. De hecho, existen muchos tipos diferentes de aleaciones multicomponentes, tengan o no un gran número de componentes en proporciones iguales o casi iguales, dependiendo de su método de desarrollo (aleación convencional, aleación extendida, sustitución equiatómica, etc.), especies constituyentes (metálicas, no metálicas, semimetálicas, compuestas, etc.), método de fabricación (fundición, solidificación rápida, deposición de vapor, co-pulverización, etc.), y la estructura de fases y microestructura resultantes (solución sólida monofásica, dendrítica, eutéctica o peritéctica dúplex, multifásica, amorfa, etc) [1].

Así, la primera generación de HEAs estaba enfocada en aleaciones de cinco o más elementos en proporción atómica igual o casi igual. Uno de los ejemplos más representativos de esta época de publicaciones es la aleación CrMnFeCoNi, investigada por Cantor y su equipo. Estos estudios iniciales mostraron que este tipo de aleaciones podía presentar buenas propiedades, a pesar de la complejidad en su composición. Sin embargo, también se exponía la existencia de limitaciones en las propiedades mecánicas, sobre todo en términos de la combinación ductilidad-resistencia.

La segunda generación de HEAs surge entonces como un esfuerzo para superar las limitaciones de la primera generación. Estas aleaciones se caracterizan por un diseño más complejo, que a menudo implica la incorporación de múltiples fases para optimizar

combinaciones específicas de propiedades, mediante la adición de elementos minoritarios o la modificación de las proporciones de los elementos principales [2].

Así, dentro de la segunda generación de HEAs, la extensión del espacio de composición que se puede explorar es muy extenso. Alguna clasificación por familias se ha planteado para ordenar este campo de posibilidades, caracterizando las aleaciones de múltiples elementos principales (MPEAs) según la frecuencia de los elementos utilizados y las agrupaciones comunes de elementos. Miracle et al. [3] publicaron en 2017 una revisión de 408 aleaciones distintas que utilizaban 37 elementos, algunos de los cuales resultaban excepcionalmente comunes en las MPEAs. Plantearon una clasificación en siete familias de aleaciones complejas y concentradas (CCAs) como agrupaciones de elementos con una característica común, o como agrupaciones de elementos que probablemente producirían un conjunto particular de propiedades. Sin embargo, la propiedad de la aleación deseada a veces resultaba de una interacción no intuitiva entre dos o más elementos, de modo que la razón para seleccionar cada elemento en una familia podía no resultar obvia. Se están ideando familias nuevas de aleaciones a un ritmo rápido, y el enfoque actual para definir estas nuevas ramas de aleaciones se ha ampliado atendiendo a las propiedades o aplicaciones deseadas de estas nuevas familias.

La segunda generación de HEAs supone una evolución en el enfoque del diseño de aleaciones de este tipo. Ya no es suficiente formular una aleación de varios elementos en proporciones equimolares. En el estado actual del arte, lo que se busca es lograr combinaciones de propiedades superiores o adaptadas a aplicaciones específicas. Y esto se ha visto que es viable, en este tipo de aleaciones, gracias a la manipulación controlada de la microestructura, mediante ajustes en la composición y en el procesamiento del material.

1.2 OBJETIVOS

Dentro de las ingentes posibilidades de estudio que existen en este campo de nuevos sistemas de aleaciones, el presente trabajo de tesis doctoral se centra en aplicaciones biomédicas para la elección de los sistemas que se van a estudiar. Con lo anterior, el **objetivo principal** de la presente tesis de investigación es el de caracterizar distintas aleaciones de alta entropía desde el punto de vista de la estructura y de su comportamiento ante la corrosión en ambientes con condiciones similares a las del interior del cuerpo humano, de manera que se

puedan obtener conclusiones sobre la idoneidad de seguir avanzando en estas líneas de investigación acerca de la biocompatibilidad de este nuevo tipo de aleaciones para su uso como piezas para implantes médicos o instrumentos quirúrgicos.

Este fin se enfocará a través de los **objetivos específicos** siguientes:

1) Determinar cómo diferentes proporciones de níquel (x = 1.0, 1.4 y 1.8) influyen en la microestructura, la microdureza y el comportamiento a la corrosión en fluido corporal simulado en el sistema de aleaciones de alta entropía AlCoCrFeNix, fabricadas a partir de refundición por arco al vacío.

2) Determinar el efecto de la sustitución de niobio por hierro en la microestructura y la resistencia a la corrosión en un entorno fisiológico simulado (solución de Ringer Grifols) en las aleaciones de alta entropía MoNbTaTiZr (NbHEA) y FeMoTaTiZr (FeHEA).

3) Determinar el potencial de una nueva HEA FeMoTaTiZr específicamente diseñada para aplicaciones médicas no implantables, analizándola en términos de microestructura, dureza y biocompatibilidad in vitro (citotoxicidad).

El estudio de las propiedades de aleaciones de alta entropía como biomateriales de nueva generación tiene relación con las siguientes líneas de investigación del programa de doctorado en Ingenierías Química, Mecánica y de Fabricación (QUIMEFA):

- Corrosión de metales.
- Nanomateriales.

El estudio de las propiedades de un metal que se pretende que tenga aplicaciones médicas requiere del estudio del comportamiento del mismo frente a la corrosión para concluir su idoneidad como herramientas quirúrgicas o implantes que van a estar sometidos al ataque de los fluidos corporales. En este sentido, la corrosión en los metales como línea de investigación está directamente relacionada con el tema de la tesis. Adicionalmente, algunas aleaciones de alta entropía presentan granos nanométricos, por lo que el estudio de las HEAs genera la posibilidad de influir en la composición de fases y en la estructura del material a ese nivel.

1.3 JUSTIFICACIÓN

La presente tesis doctoral cuenta con tres publicaciones en dos revistas científicas de impacto, una de ellas ("Scientific Reports") indexada en el cuartil Q1, y la otra ("Metals") indexada en el cuartil Q2. Y en los tres artículos se ha mantenido siempre la constante de enfocar la elección de las aleaciones y la planificación de los ensayos realizados, hacia conocer la respuesta de estos nuevos materiales para el uso de aplicaciones biomédicas.

En investigaciones existentes, las aleaciones de alta entropía en el sistema CrCoFeMoMnNiNb microaleadas con Ta, Ti o Zr han demostrado características mecánicas especiales (resistencia a la compresión superior a 2000 MPa, buena capacidad de deformación bajo condiciones severas y buen comportamiento dinámico al impacto), excelente estabilidad química de la película pasiva (potencial de corrosión en un entorno biológico simulado) y citotoxicidad reducida, en comparación con las aleaciones clásicas utilizadas en dispositivos médicos de alta exigencia (aleaciones CoCr o CoCrMo) [4]. El primero de los artículos publicados en esta tesis doctoral se centra en el estudio de un sistema de aleación basado en esta familia de aleaciones (familia de CCAs de metales de transición 3d).

Por otro lado, dentro del estudio de las posibles aplicaciones de las aleaciones de alta entropía, parte de las investigaciones realizadas por la comunidad científica se ha centrado en HEAs refractarias basadas en sistemas como W-Nb-Mo-Ta y W-Nb-Mo-Ta-V. Posteriormente, se invirtió en producir aleaciones que incluyeran metales de transición como Nb-Mo-Ta-W, V-Nb-Mo-Ta-W, Ta-Nb-Hf-Zr-Ti, Hf-Nb-Ta-Ti-Zr y Mo-Nb-Ta-V-W, así como la aleación equiatómica Hf-Mo-Nb-Ta-Ti-Zr [5–9]. Desde una perspectiva de biocompatibilidad, es relevante indicar que la mayoría de estos elementos son biocompatibles. Al combinar el concepto de HEAs con la necesidad de asegurar la biocompatibilidad de las aleaciones, se han diseñado aleaciones de alta entropía biocompatibles a partir de los sistemas mencionados, con un uso potencial en implantes ortopédicos, obteniéndose resultados con respecto a la producción y el ensayo de HEAs en los sistemas TiNbTaZrMo, TiNbTaZrFe, TiNbTaZrW, TiNbTaZrCr y TiNbTaZrHf, los cuales presentan características de deformabilidad y biocompatibilidad superiores al titanio puro (considerado prácticamente el metal menos citotóxico). Las dos publicaciones restantes del presente trabajo de tesis doctoral se basan en aleaciones pertenecientes a esta otra familia de aleaciones (familia de CCAs de metales refractarios).

A continuación, se expone un resumen de cada una de estas publicaciones mencionadas.

"Effects of nickel content on the microstructure, microhardness and corrosion behavior of high-entropy AlCoCrFeNix alloys"

López Ríos, Miguel; Socorro Perdomo, Pedro Pablo; Voiculescu, I.; Geanta, V.; Crăciun, V., et al.

Fecha de publicación: 2020

Artículo

Localización: *Scientific Reports [EISSN 2045-2322], v. 10 (1), 21119, (Diciembre 2020)*

DOI: *10.1038/s41598-020-78108-5*

Este primer artículo explora el efecto de la concentración de níquel en las propiedades del sistema de aleaciones de alta entropía $AlCoCrFeNi_x$. Los elementos de este sistema de aleación fueron seleccionados por sus características de escasa toxicidad para el cuerpo humano. El níquel, siendo el único elemento que no cumple con esta condición, fue añadido a la aleación por su excelente resistencia a la corrosión, especialmente a la oxidación a temperaturas elevadas durante la exposición a tratamientos térmicos, así como por su tendencia en otras aleaciones existentes a mejorar las propiedades mecánicas de las mismas, incrementando la dureza y manteniendo niveles aceptables de ductilidad. Una aleación con buenas propiedades mecánicas y baja toxicidad, que no va a estar implantada dentro del cuerpo humano de forma permanente, por lo que la liberación de iones de los elementos de la misma es limitada, podría ser una buena solución para instrumentación quirúrgica. Así, para esta investigación, se fabricaron tres aleaciones con los mismos elementos, en los que se variaba principalmente la composición del níquel según los valores de ratios atómicos x = 1.0, 1.4 y 1.8.

Para la sintetización de las aleaciones se utilizó la técnica de fabricación de refundición por arco al vacío. Las muestras fueron sometidas a un recocido a 1100 grados centígrados durante 48 horas, y posterior temple en agua, con el objetivo de lograr una homogeneidad adecuada en la composición de las mismas. Se realizaron ensayos de microestructura mediante microscopía óptica y SEM, tanto en las muestras sin tratar, como en las muestras tratadas. También se realizaron estos ensayos en las muestras sometidas al ensayo de corrosión. Los resultados mostraron una evolución de la microestructura dendrítica con el aumento del contenido de níquel.

Para la caracterización de las propiedades mecánicas se realizaron ensayos de microdureza Vickers. Se observó una tendencia a la disminución de la dureza con el incremento de níquel.

Finalmente, para la determinación del comportamiento frente a la corrosión en fluido corporal simulado, se utilizó la técnica de polarización potenciodinámica. De manera significativa, las tres aleaciones demostraron una buena estabilidad en el entorno biológico simulado, con bajas tasas de corrosión.

"Comparative Study of (Fe,Nb)MoTaTiZr High Entropy Alloys in Ringer Grifols Solution"

López Ríos, Miguel; Brito García,Santiago; Mirza Rosca, Julia Claudia; Voiculescu, Ionelia

Fecha de publicación: 2024

Artículo

Localización: *Metals [ISSN 2075-4701], v. 14 (12), p. 1-16*

DOI: 10.3390/met14121430

Esta segunda investigación analiza el efecto de la sustitución de niobio por hierro en aleaciones de alta entropía basadas en los elementos MoTaTiZr, estudiando las diferencias en la microestructura y en la resistencia a la corrosión en un entorno fisiológico simulado.

La metodología consistió en la caracterización de la microestructura mediante microscopía óptica y la aplicación de espectroscopía electrónica de barrido (SEM). Se pudo observar morfología dendrítica y la distribución de los elementos constituyentes en las regiones dendríticas e interdendríticas.

El análisis de fases por difracción de rayos X (XRD) confirmó la presencia de varios tipos de estructuras cristalinas en ambas aleaciones.

La evaluación de la resistencia a la corrosión mediante polarización potenciodinámica y mediante espectroscopia de impedancia electroquímica (EIS), proporcionó datos cuantitativos sobre la susceptibilidad a la corrosión y los mecanismos involucrados en el proceso corrosivo.

Los resultados analizados revelaron una influencia significativa de la sustitución del niobio por el hierro en la segregación de elementos, con este último mostrando una mayor afinidad por las regiones interdendríticas, comparado con el niobio.

Por otro lado, el hallazgo de una mayor tasa de corrosión para la FeHEA en comparación con la NbHEA subraya la importancia de los elementos constituyentes en la estabilidad química de las HEAs en entornos biológicos.

Finalmente, las pruebas de microdureza complementaron la caracterización mecánica, indicando una mayor dureza para el FeHEA.

"New FeMoTaTiZr High-Entropy Alloy for Medical Applications"

López Ríos, Miguel; Mirza Rosca, Julia Claudia; Mates, Ileana.; Geanta, V.; Voiculescu, I.

Fecha de publicación: 2025

Artículo

Localización: *Metals [ISSN 2075-4701], v. 15 (3)*.

DOI: 10.3390/met15030259

Este tercer estudio describió la síntesis y caracterización de una nueva aleación de alta entropía formada con los elementos FeMoTaTiZr, diseñada para el campo de las aplicaciones médicas no implantables. La elección de estos elementos se basó en su escasa o nula toxicidad, según publicaciones especializadas en materiales biomédicos. Se trató de establecer el potencial de esta aleación en términos de microestructura, dureza y biocompatibilidad in vitro (citotoxicidad).

La metodología de fabricación mediante fusión por arco al vacío aseguró la obtención de la aleación con la composición deseada. Las muestras obtenidas fueron sometidas a microscopía electrónica de barrido para confirmar la composición final de la aleación. Estos valores se compararon con los inicialmente proyectados para la fabricación de las muestras, lo que permitió validar el proceso de fabricación. Las muestras fueron además sometidas a tratamientos térmicos posteriores: un recocido a 900°C durante 2 horas y un recocido a 900°C durante 15 horas.

La caracterización microestructural detallada a través de microscopía óptica y electrónica (SEM), así como difracción de rayos X (XRD) antes y después de tratamientos

térmicos controlados, permitió comprender la evolución de las fases y la homogeneidad de la aleación.

Las pruebas de microdureza Vickers permitieron cuantificar la influencia de los tratamientos térmicos aplicados en la dureza de las muestras.

La evaluación de la biocompatibilidad mediante el ensayo de citotoxicidad se basó en el estudio de la actividad de la enzima LDH. Para esto se pusieron en contacto las muestras de la aleación con células madre mesenquimales de hueso humano (hBMSC) y con células del tipo fibroplasto humano normal (NHF). Este ensayo proporcionó información sobre la interacción de la aleación con sistemas biológicos a nivel celular.

Los resultados más significativos incluyeron la confirmación de una microestructura dendrítica con segregación composicional, una modulación de la dureza a través de tratamientos térmicos posteriores (lo cual es importante para aplicaciones en herramientas) y una biocompatibilidad aceptable para aplicaciones no implantables, aunque se identificaron aspectos que debían estudiarse con mayor profundidad.

1.4 REFERENCIAS

1. Cantor, B. Multicomponent and High Entropy Alloys. *Entropy* **2014**, *16*, 4749–4768, doi:10.3390/e16094749.
2. Zhang, Y. *High-Entropy Materials A Brief Introduction*; 2019;
3. Miracle, D.B.; Senkov, O.N. A Critical Review of High Entropy Alloys and Related Concepts. *Acta Mater* 2017, *122*, 448–511.
4. Geanta, V.; Voiculescu, I.; Vizureanu, P. High Entropy Alloys for Medical Applications. In; 2019 ISBN 978-1-78985-947-8.
5. Todai, M.; Nagase, T.; Hori, T.; Matsugaki, A.; Sekita, A.; Nakano, T. Novel TiNbTaZrMo High-Entropy Alloys for Metallic Biomaterials. *Scr Mater* **2017**, *129*, 65–68, doi:10.1016/j.scriptamat.2016.10.028.
6. Saini, M.; Singh, Y.; Arora, P.; Arora, V.; Jain, K. Implant Biomaterials: A Comprehensive Review. *World J Clin Cases* **2015**, *3*, 52–57, doi:10.12998/wjcc.v3.i1.52.
7. Cantor, B.; Chang, I.T.H.; Knight, P.; Vincent, A.J.B. Microstructural Development in Equiatomic Multicomponent Alloys. *Materials Science and Engineering: A* **2004**, *375–377*, 213–218, doi:10.1016/J.MSEA.2003.10.257.

8. Wang, S.-P.; Xu, J. TiZrNbTaMo High-Entropy Alloy Designed for Orthopedic Implants: As-Cast Microstructure and Mechanical Properties. *Materials Science and Engineering: C* **2016**, *73*, doi:10.1016/j.msec.2016.12.057.

9. Tsai, M.; Yeh, J.-W. High-Entropy Alloys: A Critical Review. *Mater Res Lett* **2014**, *2*, 107–123, doi:10.1080/21663831.2014.912690.

2. PUBLICACIONES PRINCIPALES

"Effects of nickel content on the microstructure, microhardness and corrosion behavior of high-entropy AlCoCrFeNix alloys"

Rios, M.L.; Baldevenites, V.L.; Voiculescu, I.; Rosca, J.M. AlCoCrFeNi High Entropy Alloys as Possible Nuclear Materials. Microscopy and Microanalysis 2020, doi:10.1017/s1431927620014555

www.nature.com/scientificreports

scientific reports

OPEN

Effects of nickel content on the microstructure, microhardness and corrosion behavior of high-entropy AlCoCrFeNix alloys

M. López Ríos[1], P. P. Socorro Perdomo[1], I. Voiculescu[2], V. Geanta[3], V. Crăciun[4,5], I. Boerasu[4] & J. C. Mirza Rosca[1]✉

In this study the effect of three different nickel concentration on the microstructure, hardness and corrosion properties of high entropy alloys (HEAs) from AlCrFeCoNi system as an alternative material for medical instruments fabrication was investigated. The analyzed HEAs were AlCrFeCoNix obtained by vacuum arc remelting from high purity raw materials and having nickel atomic ratio x = 1.0, 1.4 and 1.8. The microscopy examination revealed the dendritic morphology for the reference alloy (AlCrFeCoNi) and that the extent of the interdendritic areas increased with the concentration of nickel while Cr was more segregated in the interdendritic areas than in dendrites. Hardness values decreased as the percentage of nickel increased due to the dissolution of the precipitates in a nickel-rich matrix and consequently the formation of continuous solid solutions. The corrosion properties of the synthesized HEAs were evaluated using a potentiodynamic polarization method. The alloys were immersed in Simulated Body Fluid during one week and the corrosion parameters were recorded. The low corrosion rates, low corrosion currents and high polarization resistance attest the good stability of these HEAs in simulated biological environment indicating their possible use for surgical and dental instruments.

Classic metallic alloys generally contain one metal in a high proportion, called the base metal, and very rarely two metals in similar proportions. Although small amounts of other elements are added, this can make a big difference in the characteristics of the obtained alloy. Due to the great advance of science and technology, new metallic alloys containing more than 2 base metals, with a different metallurgical concept, have been recently explored[1,2].

High-entropy alloys (HEAs) are one of the most promising results of the exploration of new chemical compositions for metallic materials with improved performance[3–5]. Originally, they were defined as an alloy with at least five metallic elements with atomic percentage between 5 and 35%[6].

One of the basic alloy from HEA category, AlCoCrFeNi, was discovered in 2014 by Zhang's group at University of Science and Technology from Beijing, China[2]. Many other groups have joined the research effort to understand this HEA microstructure[7,8], hardness[9,10], strength[11,12], friction and wear[13] and thermal resistance[14,15] particular properties. Although many interesting topics have been explored, only few studies deal with corrosion properties of this high-entropy alloy, in general depending of fabrication method: if is synthesized by laser additive[16], by electrospark process[17] and by spark plasma sintering with pre-alloy powders obtained through gas atomization[18]. Other studies, with different aluminium concentration were performed[19–21].

In the late last century, the progress of materials science led to the rapid development of biomedical materials. Nowadays, titanium alloys are widely used as implants and prosthesis in the human body because of their excellent biocompatibility and low density. However, titanium alloys do not have sufficient strength characteristics

[1]Mechanical Engineering Department, University of Las Palmas de Gran Canaria, Campus Universitario Tafira, Edif.Ingenieria, 35017 Gran Canaria, Spain. [2]Faculty of Industrial Engineering and Robotics, Politehnica University of Bucharest, 313 Splaiul Independentei, 060042 Bucharest, Romania. [3]Faculty of Materials Science and Engineering, Politehnica University of Bucharest, 313 Splaiul Independentei, 060042 Bucharest, Romania. [4]National Institute for Laser, Plasma and Radiation Physic, Magurele, Romania. [5]Extreme Light Infrastructure-Nuclear Physics, IFIN-HH, Magurele, Romania. ✉email: julia.mirza@ulpgc.es

for medical instruments used for surgery or prosthetic devices. The recent development of HEAs provides a new generation of biomaterials which may can be used for medical devices.

To be able to use the high-entropy alloys for the manufacturing of medical instruments (like cutters, saws, scalpels etc.), their mechanical characteristics and corrosion resistance in physiological fluids which contain 1% wt. NaCl, must be tested. Furthermore, if the material corrodes due to chemical attack, some corrosion products that will form can produce undesirable reactions at metal-tissue interface. To avoid this deleterious effect, the chemical composition of the new alloys must be carefully designed[22]. The material needs to be inert in contact with the human body, so it won´t cause any metal contamination when used internally. Together with the mechanical properties[23,24], corrosion resistance plays a critical role in determining the successful use of HEAs for biomedical applications[25,26]. In this study the effect of three different nickel concentrations on the microstructure, hardness and corrosion properties of high entropy alloys from AlCrFeCoNi system has been investigated. The reason for adding nickel is that nickel generally increases ductility and hardness. Nickel improves heat treatment properties by expanding the critical temperature level, it does not form oxides and this increases strength without decreasing ductility. The results presented below indicate that the structure and corrosion behavior of AlCrFeCoNix alloys strongly depends on the Ni content.

Experimental

Materials and samples preparation. The high entropy AlCrFeCoNix alloys (with x = 1.0, 1.4 and 1.8) were obtained in the ERAMET Laboratory of the Politehnica University of Bucharest, using the MRF ABJ 900 Vacuum Arc Remelting (VAR) installation[10,25]. The theoretical degree of assimilation of the chemical elements during melting and the possible losses by vaporization were taken into account for designing the metallic charge. Highly pure raw materials, including Al, Cr, Fe, Co and Ni (at least 99.5%) were used. In order to obtain the adequate homogeneity, the obtained alloys were flipped and re-melted in VAR equipment for 6 times (3 times on each part) under inert atmosphere of Argon.

Samples in the form of rods of about 10 cm long and 1 cm diameter were obtained. The rods were transversally cut and some samples were selected for homogenization (annealing to 1100 °C for 48 h followed by water quenching). For structural, compositional and mechanical analyses the samples were embedded into an epoxy resin cylinder and then their surface was prepared in 3 stages: (1) polishing with SiC abrasive papers of progressive grain size from 240 to 2000 grit; (2) final polishing with 0.1 µm alpha alumina paste; (3) cleaning in ultrasonic deionized water.

Test environment. All the measurements were performed in Ringer Grifols solution (from Grifols Laboratories, Barcelona, Spain) with the following composition in mmol/l: Na^+ 129.9; K^+ 5.4; Ca^{2+} 1.8; Cl^- 111.7 and $C_3H_5O_3^-$ 27.2. It is a modified physiological solution in which part of the sodium ions are replaced by calcium and potassium ions and parts of the chlorine ions by lactate ions. The lactate ions are transformed into bicarbonate ions allowing a regulation of the solution pH. The tests were conducted at 37 ± 0.1 °C in a thermostatic bath.

Microstructural characterization. To study the microstructure of the alloys by optical microscopy, their surface was etched by electrochemical route using a solution of 10% oxalic acid, a current of 5 A and an immersion time of 4 s. The observations of the surface were made using an OLYMPUS PME 3-ADL microscope.

Scanning electron microscope (SEM) observations were made using a S LoVac of the Apreo Field Emission Scanning Electron Microscope (THERMO FISHER SCIENTIFIC, Co., USA) equipped with a TEAM EDX spectrometer. For ensuring the best high vacuum imaging and analytic conditions the microscope was set to run at 20 kV voltage and 1.6 nA beam current, for working distance of 10.0 mm.

Electrochemical measurements. The electrochemical measurements were made with a conventional three-electrode electrochemical cell: the sample as working electrode, Pt as counter electrode and a saturated calomel electrode (SCE) as reference electrode. The used potentiostate was a SP-150 (BioLOGIC Science Instruments) controlled by a computer with EC-LAB software package.

Open circuit potential (OCP). Open circuit potential measurements during 3 days were performed, followed by potentiodynamic polarization measurements. All tests were performed three times and data were processed using EC-LAB software.

Potentiodynamic polarization studies—polarization resistance and Tafel slopes. In order to calculate the Tafel slopes for the partial anodic processes (b_a), and the Tafel slopes for the partial cathodic processes (b_c), the linear polarization curves have been shifted from E_{OCP} − 150 mV to E_{OCP} + 150 mV using a scanning rate of 10 mV/s. The polarization studies to evaluate the passivation process continued with measurements from − 800 mV (vs. SCE) to + 500 mV (vs.SCE), increasing the potential at a scanning rate of 1 mV/s. SP-150 potentiostate was used to perform the tests and data were processed using EC-LAB software, both from BioLOGIC Science Instruments. Results showed the potentiodynamic polarization curves and the breakdown potential.

Microhardness measurements. The HEAs Vickers microhardness has been measured by an indentation test using a REMET HX-1000 Microhardness Tester. The samples, with the surfaces polished to mirror quality for good vision of the prints, were indented every 0.5 mm along the diameter. The tests were carried out according to the regulation UNE-EN ISO 6507-1:2006, applying a load of 100 g during 15 s. A minimum of 5

indentations were made on each sample and the average value was calculated, expressing it as the Vickers hardness (HV).

XRD analysis. X-ray diffraction experiments were performed with the aid of an empyrean diffractometer (MALVERN-PANALYTICAL). The instrument was working with a Cu Kα anode at a power of 45 kV and 40 mA in the Bragg–Brentano geometry. The samples were rotated during acquisition to ensure a better data collection. The acquired patterns were simulated to extract the crystalline phase present, lattice parameter and grain size with the aid of HighScore Plus software from MALVERN-PANALYTICAL.

Results and discussions

Microstructure. The phase structure of an alloy is critical for its biocompatibility and depends on the solubility of the alloying elements. The interaction between the phase structure and the biologic environment determines which elements will be released and, therefore, how the body will respond to the alloy. The grain size affects the corrosion processes because the grain boundaries influence the corrosion behaviour. The smaller the grain size of the samples, the higher the critical current density they will have as the edges of the grains store internal energy that promotes the corrosion[27].

The microstructures of the analysed HEAs before corrosion tests are shown in Fig. 1a–f. The overall look of the optical microstructures is dendritic (Fig. 1a–c). The different concentrations of the alloying elements involves the morphology of the phases. Thus, in the case of AlCrFeCoNi the aspect of the dendrites is quite round, while in the $AlCrFeCoNi_{1.4}$ sample we can observe needle forms that are oriented in different directions. The $AlCrFeCoNi_{1.8}$ sample combines rounded phases with needle-like phases, consistent with the observation reported by Cao et al.[28].

Chrome induces the formation of a protective and compact oxide layer on the surface of nickel alloys, the optimum corrosion resistance being obtained with Cr contents of about 16–27%. If the Cr content is lower, the alloy may not be able to develop a passive film adequate for a good corrosion resistance. AlCrFeCoNi has a spinodal structure quite typical for high entropy alloys, as we reported before[5]. This structure determines the smaller dimension of the phases and higher interfaces area increasing the hardness value.

The SEM observations are presented in Fig. 1d–f. The microstructural aspect is similar to that observed by optical microscopy. In the case of Ni_1 alloy, the crystalline grains with crystallites are observed, organized like Chinese letters, bordered by linear limits (Fig. 1d). As the Ni content increases in the $Ni_{1.4}$ alloy, the appearance of acicular phases is observed (Fig. 1e). As further increase of nickel content in $Ni_{1.8}$ alloy the acicular phases become rounded (Fig. 1f).

The elements Al, Co and Ni can form continuous solid solutions with the same composition in the matrix of dendritic and interdendritic zones while Cr and Fe segregated more in the spherical precipitates of dendritic region[5,7]. This suggests that the partitioning of elements from the solution phase of HEA is inherently related to the enthalpy and miscibility between the various atoms present[22].

The heat treatment performed after casting promoted homogenization of chemical composition and changes of microstructure aspect (Fig. 1g–i). The linear appearance of the grain boundaries was replaced by curved connections and the amount of needle phase decreased. In Fig. 1g three types of phases can be distinguished, as follows: a majority phase (light gray) with dendritic appearance, an inter-dendritic phase (dark gray) and thin needle like phase formed inside the majority phase. As the nickel concentration increased (Fig. 1h,i), there was a compositional change of the 2 major phases (dark gray and light gray) and a decreasing of the needle-like phase number.

The surface of the samples was examined also after performing heat treatment and corrosion test. For all the samples, pitting corrosion was observed. The images of the corroded surfaces highlight the acicular-looking phases that formed in the microstructure after the heat treatment (see Fig. 1j–l). It is observed how the chemical solution partially dissolved the surface film and preferentially attacked the alloy phases. As the Ni content in sample $Ni_{1.8}$ increases to 31 at.% (Fig. 1l), more extended corrosion effects on the alloy phases are observed.

EDS analysis. The EDS analyses have been performed on micro-zones, having the same square area, see Fig. 1g–l. The results of the chemical composition for the three alloys are presented in Table 1.

Analyzing the EDS results from Table 1 it is observed that Al concentration decreases in all samples that were simultaneously heat treated and corroded, from about 10 at% to 2.57–3.03 at%. A similar evolution is observed in terms of Ni concentration, which decreases from the maximum values existing in the heat treated samples (24.99 at% for Ni_1 to 37.68 at% for $Ni_{1.8}$) to just over half of the initial values (12.73 at % Ni for Ni_1 to 25.14 at% Ni for $Ni_{1.8}$). Cr and Fe maintain their concentrations within tight limits (maximum variations of 5 at%), and Co records the largest increases in concentration for simultaneously heat-treated and corroded samples. This behavior emphasizes the high chemical stability of Co in the metal matrix of the analyzed alloys.

Based on the EDS analysis performed on different phases, following the initial values of Co and Cr content in those phases, the specific tendency of segregation and association of these elements to form common phases is observed on atoms distribution maps (see Fig. 2).

In the case of Ni_1 (AlCrFeCoNi) TT sample, the chemical microanalysis on light grey phase indicates that it contains about 5.08 at% Al, 9.14 at% Co, 31.76 at% Cr, 29.80 at% Fe and 20.51 at% Ni. The dark grey phase contains 27 at % Al, 8.55 at% Co, 10.37 at% Cr, 14.15at% Fe and 38.26 at% Ni.

Regarding $Ni_{1.4}$ ($AlCrFeCoNi_{1.4}$) TT sample, the light grey phase contains 4.40 at % Al, 7.16 at % Co, 34.18 at % Cr, 28.96 at % Fe and 21.42% Ni. The dark grey phase contains 23.53 at% Al, 7.21 at % Co, 13.35 at % Cr, 15.21 at % Fe and 39.23 at % Ni.

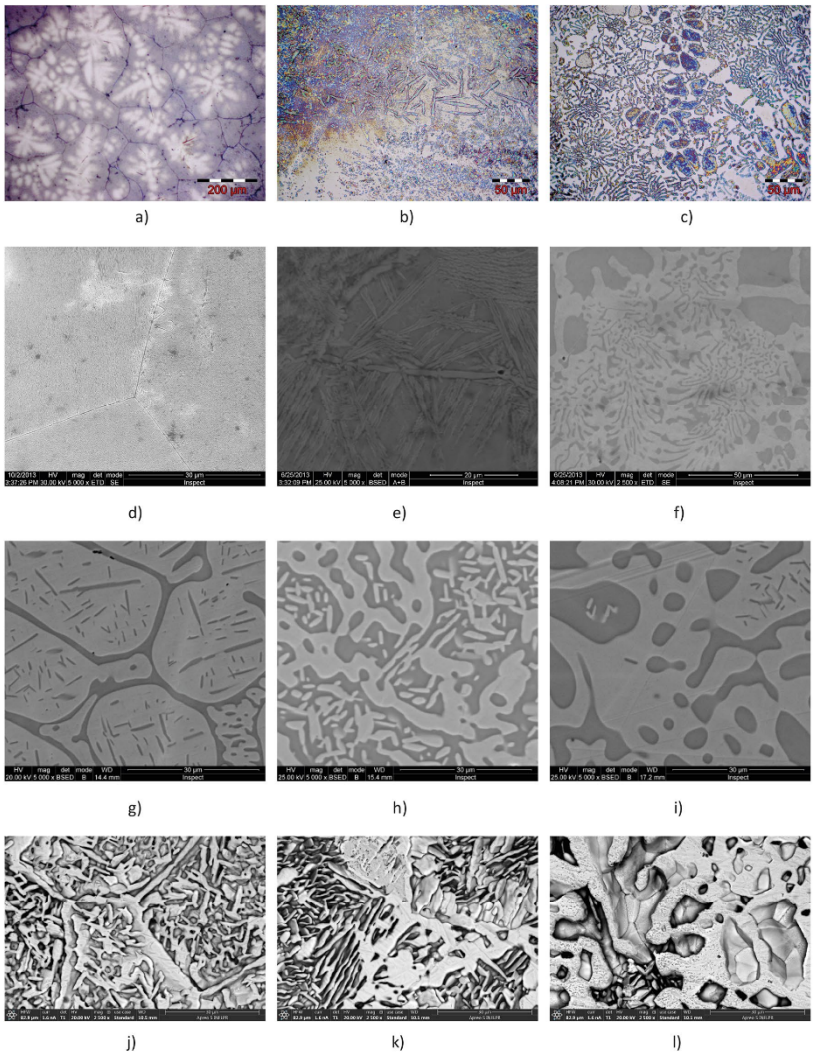

Figure 1. Microstructure evolution of HEAs (Ni_1, $Ni_{1.4}$ and $Ni_{1.8}$) during thermal and chemical processing: (**a**), (**b**), (**c**) optical microstructure; (**d**), (**e**), (**f**) SEM as-cast microstructure; (**g**), (**h**), (**i**) SEM heat treated microstructure; (**j**), (**k**), (**l**) Thermal treated and corroded microstructure.

Finally, in the case of $Ni_{1.8}$ ($AlCrFeCoNi_{1.8}$) TT sample, the light grey phase contains 21.73 at% Al, 5.31 at %Co, 9.85 at% Cr, 12.82 at% Fe and 48.88 at% Ni. The dark grey phase contains 5.51 at % Al, 6.02 at % Co, 29.06 at% Cr, 24.98 at.% Fe and 31.01at % Ni.

These results highlight the tendency of Al and Ni to form stable compounds (dark grey phase) and quite equal distribution of the other elements in light grey phase or in the acicular phases.

	Ni_1			$Ni_{1.4}$			$Ni_{1.8}$		
Element	**Corr**	**TT**	**T + C**	**Corr**	**TT**	**T + C**	**Corr**	**TT**	**T + C**
Al, at%	**12.00**	**9.89**	**2.57**	**11.68**	**14.28**	**3.03**	**10.59**	**10.46**	**2.77**
wt%	6.33	5.14	1.29	6.12	7.54	1.52	5.47	5.37	1.38
Error,%	5.47	5.43	4.13	2.84	5.47	5.74	2.92	5.82	5.76
Co, at%	**6.59**	**8.48**	**21.85**	**3.75**	**7.40**	**21.49**	**3.34**	**5.36**	**20.49**
wt%	7.58	9.62	24.07	4.29	8.54	23.46	3.77	6.01	22.33
Error,%	5.34	5.02	1.79	3.32	4.43	1.79	3.88	4.51	1.76
Cr, at%	**28.72**	**26.98**	**31.83**	**32.61**	**22.67**	**28.51**	**29.62**	**22.95**	**26.16**
wt%	29.17	27.01	30.93	32.93	23.07	27.46	29.50	22.71	25.15
Error, %	1.93	1.90	1.90	1.99	2.00	1.95	2.04	2.11	1.97
Fe, at%	**26.56**	**26.40**	**26.41**	**24.75**	**21.52**	**23.52**	**22.94**	**21.39**	**21.07**
wt%	28.98	28.38	27.57	26.85	23.53	24.33	24.54	22.73	21.76
Error,%	2.05	1.95	1.87	1.81	2.11	1.94	1.90	2.30	1.99
Ni, at%	**23.28**	**24.99**	**12.73**	**24.78**	**31.13**	**19.62**	**31.33**	**37.68**	**25.14**
wt%	26.58	28.24	13.97	28.26	35.78	21.33	35.24	42.10	27.29
Error,%	2.12	1.94	2.05	1.73	2.11	1.93	1.67	1.98	1.85
O, at%	**2.38**	**2.46**	**3.54**	**1.39**	**2.22**	**2.77**	**1.08**	**1.61**	**3.25**
wt%	0.74	0.76	1.06	0.43	0.70	0.82	0.33	0.49	0.96
Error, %	5.15	4.57	4.13	2.78	5.21	4.40	2.73	6.24	4.28

Table 1. EDS global analyses on micro areas for HEAs after different processing stages. Corr, corroded; TT, Thermal treated; T + C, Thermal treated and corroded.

X-ray diffraction. The XRD patterns acquired from as-cast samples are displayed in Fig. 3. The Ni_1 sample exhibited a pure primitive cubic phase (space group Pm-3m, number 221), matched very well by reference pattern 04-018-5047, Al0.4Co0.4Cr0.4Fe0.4Ni0.4. Increasing the Ni content resulted in the appearance of a new FCC phase (Fm-3m, group 225, a = 3.5643 Å), that was matched by reference pattern 04-022-2301, $Co_{0.25}Cr0.25Fe_{0.25}Ni_{0.25}$ and indicated by symbol # in front of the Miller indices in Fig. 3. Also, $Al_{0.9}Ni_{4.22}$ (pattern 00-050-1294) with a slightly different lattice parameter (FCC, a = 3.5700 Å) and $Cr_{0.10}Fe_{0.65}Ni_{0.25}$ (pattern 04-019-2390) with a slightly different lattice parameter (FCC, a = 3.5920 Å) are good matches. The presence of an Al-Ni FCC type compound after the thermal treatment is strongly supported by the EDS results. After corrosion treatment, a strong decrease in Ni and Al concentrations was observed, which was probably caused by the dissolution of this compound, while the others elements were not that much affected. SEM images of the corroded surface also suggest that a phase initially present was dissolved and disappeared from the surface region.

XRD patterns acquired from samples after the thermal treatment exhibited a mixture of two cubic phases: a primitive one and a FCC one (Fig. 3), with the relative percentage displayed in Table 2, although the presence of other FCC type compounds as those mentioned above could not be ruled out. The patterns also displayed narrower diffraction peaks, indicative of grain growth. The lattice parameters of the Pm-3 m and FCC phases, also displayed in Table 2 did not significantly changed with the increase of Ni content or the thermal treatment.

With the increasing of nickel concentration, the lattice parameter of the primitive cubic phase varies very slightly, from 2.876 Å to 2.870 Å, while the grain size remains almost the same (from 398 to 414 and 365 Å) for as-cast samples. For the FCC phase, the lattice parameters also vary very slightly but the grain size increases with the nickel content for both as-cast andannealed samples. It can be seen that, for all the studied alloys, the lattice parameter of the two phases varies marginally, which was also reported for other HEAs[29].

The results show a good homogeneity of the samples with two main solid solutions formed and some minor compounds segregating in the dendritic zone.

After the thermal treatment, the elemental composition of HEAs does not change; however, after the corrosion stage, the Al concentration in the surface region significantly dropped, followed by Ni; Co concentration went up, while Fe and Cr did not change much.

To explain these results, the formation after the thermal treatment of an Al-Ni compound is hypothesized, which should be corroded faster than the main HEA phase. There are several Al-Ni compounds having an FCC lattice and a lattice parameter very close to that of FCC AlCoCrFeNi HEA that could explain the results.

Open circuit potential (OCP). Open circuit potential measurement curves during one-week immersion are shown in Fig. 4.

For all analyzed HEAs, after a short immersion time of about some hours, there is an increase in the corrosion potential due to the growth of passive layers on the surface of the alloys. During the first 24 h, the OCP for all the three alloys increases with 30–50 mV due to the build-up of the passive layers on the surface of the HEAs. The maximum value of OCP is 236 mV for AlCrFeCoNi and 235 $AlCrFeCoNi_{1.8}$ and almost half of this value, 102 mV, for $AlCrFeCoNi_{1.4.}$

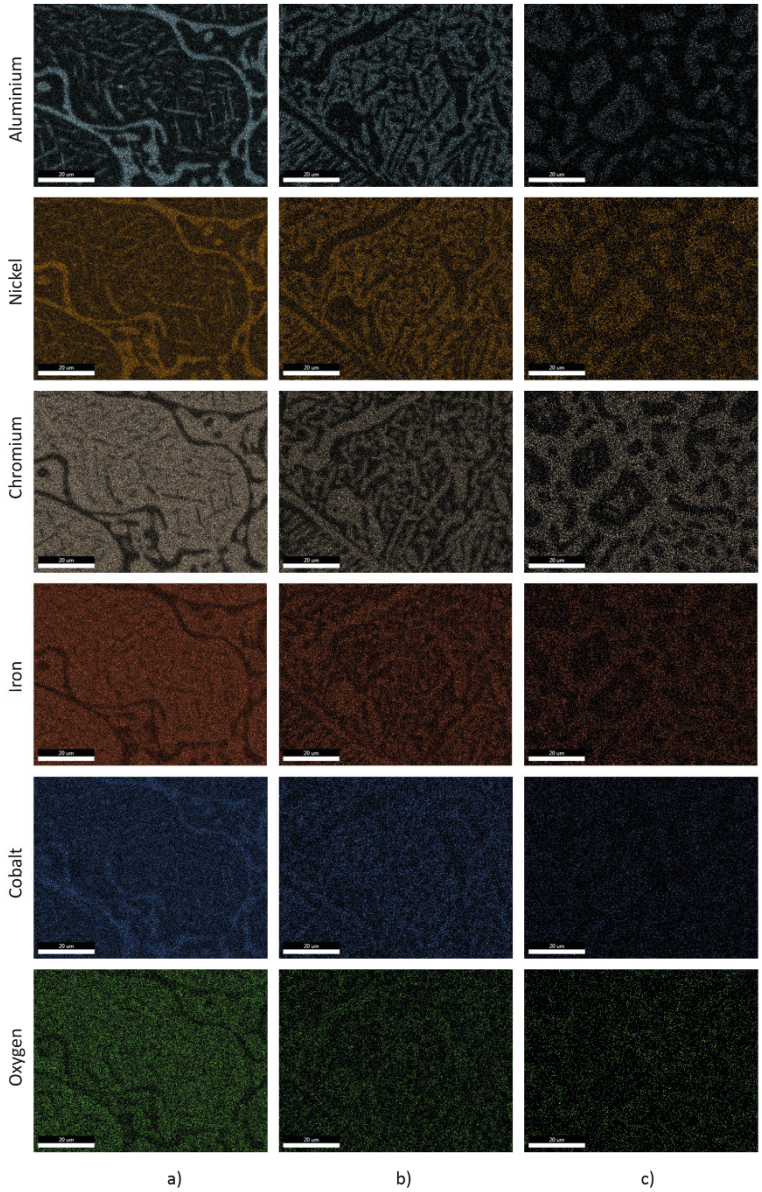

Figure 2. Atoms distribution of main elements of HEAs micro-area. (**a**) in Ni_1 TT sample; (**b**) $Ni_{1.4}$ TT sample; (**c**) $Ni_{1.8}$ TT sample.

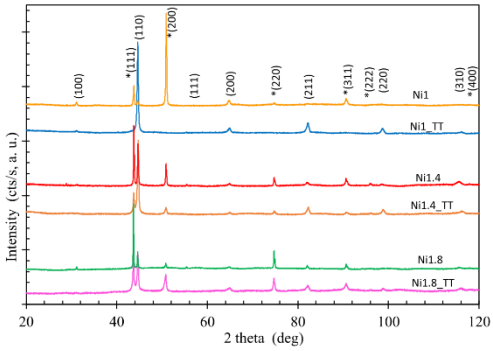

Figure 3. XRD patterns acquired from as-cast samples and from thermal treated samples (Miller indices for the new FCC phase induced by a higher Ni content are marked by symbol #).

	Pm-3m (PDF 04-018-5047)			Fm-3m (PDF 04-022-2301)		
Sample	Content (%)	Lattice parameter (Å)	Grain size (Å)	Content (%)	Lattice parameter (Å)	Grain size (Å)
Ni_1	100	2.876	398	–	–	–
$Ni_{1.4}$	78	2.870	414	22	3.595	327
$Ni_{1.8}$	37	2.873	365	63	3.599	402
Ni_1_TT	16	2.875	574	84	3.588	562
$Ni_{1.4}$_TT	73	2.871	937	27	3.591	1813
$Ni_{1.8}$_TT	75	2.872	1258	25	3.591	1259

Table 2. Samples phase composition, lattice parameters and grain size.

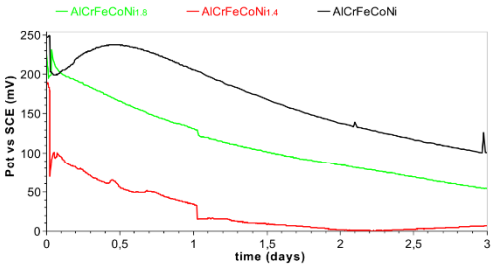

Figure 4. Variation of open circuit potential with time for the three alloys (AlCrFeCoNi, $AlCrFeCoNi_{1.4}$, $AlCrFeCoNi_{1.8}$) in Ringer solution.

After the OCP reaches the maximum value, it begins to decrease. This decrease is due to the changes in the characteristics of the surface film.

From the curves can be seen continuous breakages and repairs of the passive layer.

Potentiodynamic polarization result. Polarization techniques have been used respecting the indications of ASTM Subcommittee G01.11 on Electrochemical Measurements in Corrosion Testing regarding the reproducibility of cyclic potentiodynamic polarization measurements for determining the susceptibility to localized corrosion[30].

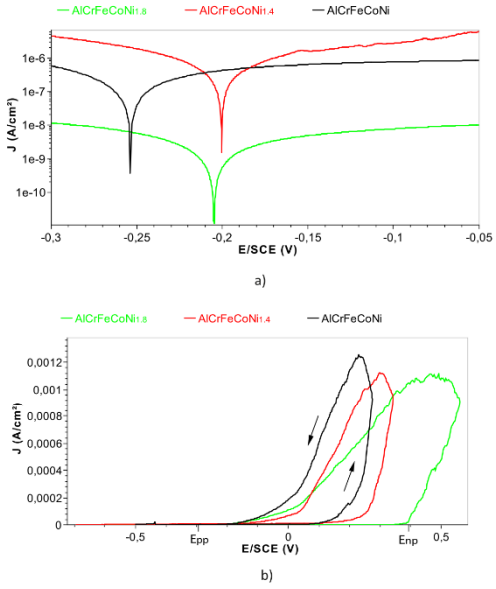

Figure 5. (**a**) Tafel curves for $AlCrFeCoNi_1$, $AlCrFeCoNi_{1.4}$ and $AlCrFeCoNi_{1.8}$ after one-week immersion. (**b**) Potentiodynamic polarization curves for AlCrFeCoNi, $AlCrFeCoNi_{1.4}$, $AlCrFeCoNi_{1.8}$ presented in linear axis in order to reveal the nucleation pitting potential and pitting protection potential).

Alloy	E_{corr} (mV)	i_{corr} (nA/cm^2)	b_a (mV)	b_c (mV)	Corrosion rate (mmpy)
AlCrFeCoNi	− 255.59	428	638.4	255.1	5.92E−03
$AlCrFeCoNi_{1.4}$	− 199.7	748	169.2	124.5	3.00E−02
$AlCrFeCoNi_{1.8}$	− 206.86	374	347	185.8	1.25E−02

Table 3. Electrochemical parameters of corrosion process estimated through Tafel approximation.

1. Plots in a semi-logarithmic version between − 150 mV (vs OCP) and + 150 mV (vs OCP) after 1 week in Ringer solution are displayed (see Fig. 5a).
   The values of E_{corr}, i_{corr}, b_a, b_c and V_{corr} were determined by EC-Lab software and presented in Table 3. An alloy will corrode if b_c is greater than b_a and will be subjected to passivity if b_c is smaller than b_a. The higher values of b_a vs b_c for all the three alloys indicates an anodic control of the corrosion process which implies the existence of a passive layer on the sample's surface. The point resulted in the intersection of the two Tafel slopes has the coordinates i_{corr} and ZCP (zero current potential). It can be seen that in all the cases, the difference between OCP and ZCP is only few mV. This indicates that the errors introduced into the values of kinetic parameters are negligible with the variations of the charging current.
   The corrosion current densities obtained for the analyzed HEAs are much lower than that of the 304SS[31], which means that these HEAs are more resistant to general corrosion than 304SS.
   With the increase of Ni content, the corrosion rate of the alloy presents a non-linear trend mainly due to the fact that Ni content is not the only factor affecting the corrosion process (for example: microstructure, element distribution, etc.).
2. Pitting potential
   The pitting potential (or pit nucleation potential E_{np}) is one of the most important parameter characterizing the susceptibility of HEA to pitting corrosion. It is the potential at which the passive film formed on the HEA surface is damaged and the current density begins to increase drastically in the passive range due to the pits nucleations. Plots in a linear version of I vs E between − 0.8 V and + 0.5 V vs Ref (see Fig. 5b) were performed in order to determine the pit nucleation potential (pitting potential) and pitting protection potential (the potential in the reverse scan associated with a drop in current density caused by the repasivation of pits).

A scan rate of 1 mV/s was used and considered to be sufficiently slow to prevent any distortion of the curves. The values of nucleation pitting potential were 185 mV for AlCrFeCoNi, 245 mV for $AlCrFeCoNi_{1.4}$ and 385 mV for $AlCrFeCoNi_{1.8}$. The obtained values characterize the resistance of the analyzed HEA to pitting corrosion and can therefore be considered a measure of the susceptibility of HEA in simulated body fluid. $AlCrFeCoNi_{1.8}$ has the most positive pit nucleation potential: the more positive Enp, the more resistant the alloy is to pitting.

Among the three tested alloys, the difference between E_{np} and E_{pp} for $AlCrFeCoNi_{1.8}$ is the largest, which suggests that the repasivation tendency of pits on this alloy is large and only at higher potential these pits can transform to stable pits.

Microhardness. Five indentations have been made for each sample and the average value was calculated. The hardness values decrease with the increase of nickel concentration (562HV for AlCrFeCoNi, 455HV for $AlCrFeCoNi_{1.4}$ and 316HV for $AlCrFeCoNi_{1.8}$) as a result of dissolution of Cr and Fe precipitates in the nickel-rich matrix, forming a stable solid solution as we reported before[10]. For other HEA system, substitution of Al with different Zr concentrations, determine changes in the microhardness values, attributed to the phase changes in the alloy structure[23].

As has been demonstrated in a few studies[11,24] most metals and alloys exhibit strengthening effect by grain refinement due to the boundaries that function as impediments to dislocations. The decreasing of grain boundary density lead to the microhardness (and equivalent yield strength) values decreasing in HEAs which is consistent with the concept that the lattice of the crystal is seriously distorted and dislocations movement is more difficult than in conventional alloys[32,33].

Conclusions

In this study, the effects of nickel content on the microstructure, microhardness and corrosion behavior of high-entropy entropy $AlCoCrFeNi_x$ alloys in simulated body fluid were investigated and following conclusions were drawn:

1. The microscopy examination revealed the dendritic morphology for as cast alloy $AlCrFeCoNi_{1.0}$ and the increase of the extent of the interdendritic areas by increasing the nickel concentration for $AlCrFeCoNi_{1.4}$ and $AlCrFeCoNi_{1.8}$. The annealing determined a more uniform distribution of the phases for the three high-entropy alloys and the modification of the morphology of the grain boundaries. It also resulted in a significant increase of the grain sizes.
2. The formation after the annealing treatment of an Al-Ni compound is hypothesized, which should be corroded faster than the main HEA phase. There are several Al-Ni compounds having an FCC lattice and a lattice parameter very close to that of FCC AlCoCrFeNi.
3. The low corrosion rates and low corrosion currents demonstrate the good stability of the studied samples of $AlCoCrFeNi_x$ (x = 1.0, 1.4 and 1.8) in simulated biological environment.
4. The lattice parameter of the cubic phase varies very slightly, from 2876 to 2870 Å by increasing the Ni content, but the grain size decreases considerably (from 398 to 206 Å) for as-cast samples. For the FCC phase, the lattice parameters also vary very slightly but the grain size increases with the nickel content for both as-cast and annealing samples.
5. The results proved that by manipulating the composition and structure of HEAs their mechanical and chemical performance could be optimized to meet the requirements for their usage as novel medical instruments materials.

Data availability

The datasets generated during the current study are available from the corresponding author on reasonable request.

Received: 4 June 2020; Accepted: 17 November 2020
Published online: 03 December 2020

References

1. Yeh, J. W. & Lin, S. J. Breakthrough applications of high-entropy materials. *J. Mater. Res.* **33**, 3129–3137 (2018).
2. Zhang, Y. *High-Entropy Materials A Brief Introduction*. https://doi.org/10.1007/978-981-13-8526-1 (2019).
3. Ching, W. Y. *et al.* Fundamental electronic structure and multiatomic bonding in 13 biocompatible high-entropy alloys. *npj Comput. Mater.* **6**, 1–10 (2020).
4. Zhang, C. *et al.* Understanding phase stability of Al-Co-Cr-Fe-Ni high entropy alloys. *Mater. Des.* **109**, 425–433 (2016).
5. Csaki, I. *et al.* Researches regarding the processing technique impact on the chemical composition, microstructure and hardness of AlCrFeNiCo high entropy alloy. *Rev. Chim.* **67**, 1373–1377 (2016).
6. Yeh, J. W. *et al.* Nanostructured high-entropy alloys with multiple principal elements: Novel alloy design concepts and outcomes. *Adv. Eng. Mater.* **6**, 299-303+274 (2004).
7. Wang, Y. P., Li, B. S., Ren, M. X., Yang, C. & Fu, H. Z. Microstructure and compressive properties of AlCrFeCoNi high entropy alloy. *Mater. Sci. Eng. A* **491**, 154–158 (2008).
8. Ye, Y. F., Wang, Q., Lu, J., Liu, C. T. & Yang, Y. High-entropy alloy: challenges and prospects. *Mater. Today* **19**, 349–362 (2016).
9. Alabd Alhafez, I., Ruestes, C. J., Bringa, E. M. & Urbassek, H. M. Nanoindentation into a high-entropy alloy—an atomistic study. *J. Alloys Compd.* **803**, 618–624 (2019).
10. Voiculescu, I., Geanta, V., Stefanoiu, R., Patrop, D. & Binchiciu, H. Influence of the chemical composition on the microstructure and microhardness of alcrfeconi high entropy alloy. *Rev. Chim.* **64**, 1441–1444 (2013).

11. Li, Z., Zhao, S., Ritchie, R. O. & Meyers, M. A. Mechanical properties of high-entropy alloys with emphasis on face-centered cubic alloys. *Prog. Mater. Sci.* **102**, 296–345 (2019).
12. Chen, C., Pang, S., Cheng, Y. & Zhang, T. Microstructure and mechanical properties of. *J. Alloys Compd.* **659**, 279–287 (2016).
13. Yang, S., Liu, Z. & Pi, J. Microstructure and wear behavior of the AlCrFeCoNi high-entropy alloy fabricated by additive manufacturing. *Mater. Lett.* **261**, 127004 (2020).
14. Chen, J. *et al.* A review on fundamental of high entropy alloys with promising high-temperature properties. *J. Alloys Compd.* **760**, 15–30 (2018).
15. Miracle, D. B. & Senkov, O. N. A critical review of high entropy alloys and related concepts. *Acta Mater.* **122**, 448–511 (2017).
16. Shon, Y., Joshi, S. S., Katakam, S., Shanker Rajamure, R. & Dahotre, N. B. Laser additive synthesis of high entropy alloy coating on aluminum: corrosion behavior. *Mater. Lett.* **142**, 122–125 (2015).
17. Li, Q. H., Yue, T. M., Guo, Z. N. & Lin, X. Microstructure and corrosion properties of alcocrfeni high entropy alloy coatings deposited on AISI 1045 steel by the electrospark process. *Metall. Mater. Trans. A Phys. Metall. Mater. Sci.* **44**, 1767–1778 (2013).
18. Zhou, P. F., Xiao, D. H. & Yuan, T. C. Microstructure, mechanical and corrosion properties of AlCoCrFeNi high-entropy alloy prepared by spark plasma sintering. *Acta Metall. Sin. (English Lett.)* **33**, 937–946 (2020).
19. Yamanaka, K. *et al.* Corrosion mechanism of an equimolar AlCoCrFeNi high-entropy alloy additively manufactured by electron beam melting. *npj Mater. Degrad.* **4**, 1–12 (2020).
20. Shi, Y. *et al.* Homogenization of AlxCoCrFeNi high-entropy alloys with improved corrosion resistance. *Corros. Sci.* **133**, 120–131 (2018).
21. Shi, Y. *et al.* Corrosion of Al x CoCrFeNi high-entropy alloys : Al-content and potential scan-rate dependent pitting behavior. *Eval. Program Plann.* **119**, 33–45 (2017).
22. Chen, H. Y. *et al.* Effect of the substitution of Co by Mn in Al-Cr-Cu-Fe-Co-Ni high-entropy alloys. *Ann. Chim. Sci. Mater.* **31**, 685–698 (2006).
23. Feng, X. *et al.* Effect of Zr addition on microstructure and mechanical properties of CoCrFeNiZrx high-entropy alloy thin films. *Appl. Nanosci.* https://doi.org/10.1007/s13204-019-01057-7 (2019).
24. Huang, Y. C., Su, C. H., Wu, S. K. & Lin, C. A study on the hall-petch relationship and grain growth kinetics in FCC-structured high/medium entropy alloys. *Entropy* **21**, 297 (2019).
25. Geanta, V., Voiculescu, I., Vizureanu, P. & Victor Sandu, A. High entropy alloys for medical applications. *Eng. Steels High Entropy Alloys* https://doi.org/10.5772/intechopen.89318 (2020).
26. Qiu, Y. *et al.* Corrosion characteristics of high entropy alloys corrosion characteristics of high entropy alloys. *Mater. Sci. Technol.* **31**, 1235–1243 (2015).
27. Guérin, M. *et al.* Identification of the metallurgical parameters explaining the corrosion susceptibility in a 2050 aluminium alloy. *Corros. Sci.* **102**, 291–300 (2016).
28. Cao, L. *et al.* Microstructural evolution, phase formation and mechanical properties of multi-component AlCoCrFeNix alloys. *Appl. Phys. A Mater. Sci. Process.* **125**, 1–11 (2019).
29. Krapivka, N. A., Firstov, S. A., Karpets, M. V., Myslivchenko, A. N. & Gorban, V. F. Features of phase and structure formation in high-entropy alloys of the AlCrFeCoNiCux system (x = 0, 0.5, 1.0, 2.0, 3.0). *Phys. Met. Metallogr.* **116**, 467–474 (2015).
30. Baboian R. & Haynes, S. G. *Cyclic polarization measurements-experimental procedure and evaluation of test data*. https://doi.org/10.1520/STP28038S (1981).
31. Chen, Y. Y., Duval, T., Hung, U. D., Yeh, J. W. & Shih, H. C. Microstructure and electrochemical properties of high entropy alloys—a comparison with type-304 stainless steel. *Corros. Sci.* **47**, 2257–2279 (2005).
32. Liu, W. H., Wu, Y., He, J. Y., Nieh, T. G. & Lu, Z. P. Grain growth and the Hall–Petch relationship in a high-entropy FeCrNiCoMn alloy. *Scr. Mater.* https://doi.org/10.1016/j.scriptamat.2012.12.002 (2013).

Acknowledgements

The research was supported by the Romanian National Authority, Executive Agency for Higher Education, Research, Development and Innovation (CNCS CCDI—UEFISCDI), project number PN-III-P1-1.2-PCCDI-2017-239/60PCCDI and Romanian National Nucleu Program LAPLAS VI – contract nº. 16N/2019.

Author contributions

M. López Ríos—Conceptualization, methodology, writing—original draft preparation, investigation. P. Socorro Perdomo—data curation (Figs. 4, 5 and Table 3). V. Geanta—investigation, Figs. 1, 2 and Table 1, resources. I. Voiculescu—investigation (Figs. 1, 2, Table 1), data curation, writing—review and editing. V. Craciun—investigation (Fig. 3 and Table 2), data curation, writing—review and editing. I. Boerasu –investigations. J.Mirza Rosca: data curation, project administration, visualization, writing—review and editing (data curation, supervision, validation of data). All authors reviewed the manuscript and agreed to the published version of the manuscript.

Competing interests

The authors declare no competing interests.

Additional information

Correspondence and requests for materials should be addressed to J.C.M.R.

Reprints and permissions information is available at www.nature.com/reprints.

Publisher's note Springer Nature remains neutral with regard to jurisdictional claims in published maps and institutional affiliations.

"Comparative Study of (Fe,Nb)MoTaTiZr High Entropy Alloys in Ringer Grifols Solution"

Lopez-Rios, M.; Brito-Garcia, S.; Mirza-Rosca, J.; Voiculescu, I. Comparative Study of (Fe,Nb)MoTaTiZr High Entropy Alloys in Ringer Grifols Solution. Metals (Basel) 2024, 14, doi:10.3390/met14121430.

metals

MDPI

Article

Comparative Study of (Fe,Nb)MoTaTiZr High Entropy Alloys in Ringer Grifols Solution

Miguel Lopez-Rios [1], Santiago Brito-Garcia [1], Julia Mirza-Rosca [1,2,*] and Ionelia Voiculescu [3]

[1] Mechanical Engineering Department, University of Las Palmas de Gran Canaria, 35001 Las Palmas de Gran Canaria, Spain
[2] Materials Engineering and Welding Department, Transilvania University of Brasov, 500036 Brasov, Romania
[3] Quality Engineering and Industrial Technologies Department, Faculty of Industrial Engineering and Robotics, National University of Science and Technology Politehnica of Bucharest, 060042 Bucharest, Romania
* Correspondence: julia.mirza@ulpgc.es

Abstract: High-entropy alloys (HEAs) are a family of materials that, because of their particular characteristics and possible uses in a variety of industries, have garnered a lot of interest recently. One such promising HEA is the MoNbTaTiZr high-entropy alloy, which displays excellent corrosion resistance and biocompatibility alongside good mechanical properties. Another promising HEA that has attracted researchers for its potential applications in various fields is FeMoTaTiZr. Exchanging one of the elements may result in important variation of properties of a material. This work studies two different samples of high-entropy alloys, MoNbTaTiZr (named NbHEA) and FeMoTaTiZr (named FeHEA), both generated in a laboratory context using electric-arc remelting technology, keeping similar atomic percentage of the elements in both alloys. Optical microscopy and scanning electron microscopy techniques were used to characterize the microstructure of the alloys. Replacing Nb for Fe affects the distribution proportion of the other four elements, since Fe has a higher tendency than Nb to form part of the inter-dendrite region. An evaluation of the properties related to the corrosion process was accomplished using the polarization method along with electrochemical impedance spectroscopy (EIS), performed under a simulated biological environment. As a result, FeHEA showed a higher corrosion rate in simulated body fluid than NbHEA.

Keywords: high-entropy alloys; corrosion resistance; microstructure; microscopy; biomaterial; EIS

Citation: Lopez-Rios, M.; Brito-Garcia, S.; Mirza-Rosca, J.; Voiculescu, I. Comparative Study of (Fe,Nb)MoTaTiZr High Entropy Alloys in Ringer Grifols Solution. *Metals* **2024**, *14*, 1430. https://doi.org/10.3390/met14121430

Academic Editors: Yonggang Yao and Yong Zhang

Received: 20 November 2024
Revised: 10 December 2024
Accepted: 11 December 2024
Published: 13 December 2024

1. Introduction

Conventional alloys consist mainly of a principal element acting as a matrix where other elements are included to improve the properties of the material, giving rise to an alloy based on the main element. Classic metallic alloys are often made with one metal in a large proportion, known as the base metal, and small amount of other elements, though some alloys with two metals in similar quantities can be discovered. These other elements, even in small proportions, can entail important differences in the characteristics of the resulting material.

The traditional approach to alloy development has been extremely limited in its ability to explore the entire spectrum of potential alloys [1]. A relatively fresh class of materials, HEAs have drawn plenty of concern in materials research and engineering since their discovery in the early 2000s. Unlike traditional alloys, several main components are present in HEAs in about equal concentrations. The development of HEAs over the last 10 years has provided fresh impetus for the study of novel materials intended for high-performance applications [2], considering that the arrangement of different atomic species in HEAs can offer several advantages compared to single element-based alloys.

Yeh [3] proposed in 2006 that four core effects could be proposed to characterize the behavior of HEAs: high-entropy, sluggish diffusion, severe lattice distortion, and "cocktail" effects. One accepted and usually used definition for HEAs describes them as

alloys comprising five or more elements in a compositional range of 5–35 at % each. These elements tend to form a single solid-solution phase. However, other stipulations can be read in the literature extending the range of multicomponent alloys over single-phase formation. Some of those expressions are multiprincipal element alloys (MPEAs), complex concentrated alloys (CCAs), and high-entropy materials (HEMs) [4,5].

Orthopedic implants have been mainly based in titanium alloys due to their biocompatibility and corrosion resistance of the passive film formed on the surface [6]. For example, a recent study advances the use of Ti-Mo-based materials because of the cytocompatibility and enhanced osseointegration [7,8]. The future of medical improvements is to be accompanied by a new generation of metallic biomaterials showing superior mechanical properties and higher biocompatibility, a combination that can be found in the new high-entropy alloys.

Since the component elements of Ti-rich Ti-Nb-Ta-Zr (TNTZ) alloys with a bcc phase are non-toxic and allergy-free, they have been studied as improved Ti-based metallic biomaterials [9]. The combination of Ta, Nb, Mo, Zr, and Ti promotes the development of a single solid solution phase in HEAs [10]. The formation of a solid solution gives rise to deformability and a severely distorted lattice. After Senkov et al. [11] introduced refractory HEAs featuring a solitary bcc phase in W-Nb-Mo-Ta and W-Nb-Mo-Ta-V alloy systems, researchers analyzed other bcc HEAs by incorporating early transition metals, such as zirconium [12]. The ions of zirconium, niobium, and tantalum that are released are titanium-like ions and do not typically exhibit toxicity when interacting with biomolecules. This is because the active ions readily bond with a nearby water molecule or an anion to create an oxide, hydroxide, or inorganic salt [13].

Some studies of both equiatomic and non-equiatomic MoNbTaTiZr HEA have been developed in the past recent years [14,15] as a consequence of the biomaterial concept of the alloy, but there are still many composition and fabrication possibilities to investigate. The Mo-Nb-Ta-Ti-Zr system alloy recipes were based on the choice of chemical elements with low bio-toxicity for the human body [16], which are currently being tested both for the manufacture of surgical instruments and for orthopedic applications [17]. The excellent biocompatibility of HEAs MoNbTaTiZr places these alloys as a new class of metallic biomaterials showing exceptional characteristics. For this reason, a new high-entropy alloy was obtained with iron in place of niobium, FeMoTaTiZr, taking into account that the iron does not tend to accumulate in tissues being metabolized [18].

In this work, two non-equiatomic MoNbTaTiZr and FeMoTaTiZr HEA, both being produced in an electric-arc remelting furnace, are tested for microstructure characterization and corrosion resistance behavior under a simulated physiological environment. Most of the elements that compose these alloys are refractory, so in order to ensure a better dissolution in the molten matrix and a better homogeneity of the alloy, Nb, which has a high melting point (2477 °C), was substituted with Fe (1538 °C), a component that is additionally essential in the human body.

2. Materials and Methods

2.1. Materials and Samples Preparation

The MoNbTaTiZr and FeMoTaTiZr high-entropy alloys (named NbHEA and Fe-HEA, respectively) were produced in an MRF ABJ 900 Vacuum Arc Remelting (VAR) furnace(Allenstown, NH, USA). Elements with a purity of at least 99.0% were utilized as raw materials, including Fe, Mo, Ta, Nb, Ti, and Zr (see Table 1).

The raw materials, melted and mixed under the action of the electric arc, were then cooled to be flipped and re-melted for 8 times under an argon atmosphere, in order to homogenize the distribution of the different elements, since the sample contained high melting temperature elements such as Nb (2477 °C), Mo (2623 °C), and Ta (3017 °C), compared to Fe (1538 °C), Ti (1668 °C), and Zr (1855 °C).

Table 1. NbHEA and FeHEA samples composition in atomic and weight percentage.

Element	wt %		at %	
	FeHEA	**NbHEA**	**FeHEA**	**NbHEA**
Mo	20.45	17.32	18.66	17.98
Ta	32.45	38.95	15.71	21.45
Ti	12.67	13.21	23.18	27.49
Zr	18.97	17.45	18.21	19.06
Fe	15.46	-	24.24	-
Nb	-	13.07	-	14.02

The obtained ingots had a mass of approximately 30 g (+/−0.2 g) and dimensions of 25 × 9 mm. The ingots were cut using an abrasive disk under cooling liquid jet and then embedded into an epoxy resin cylinder. The exposed surface of the NbHEA sample out of the resin is 0.652 cm^2, whereas for the FeHEA sample, the exposed surface is 0.695 cm^2. Preparation for the metallographic test was performed using abrasive paper with grit sizes between 240 and 2000 and then alpha alumina suspension of 3 µm and 0.1 µm. Finally, the surface was cleansed with deionized water using an ultrasonic cleaning system, consistent with ASTM E3-11(2017) [19].

2.2. Microstructural Characterization

To examine the sample's surface, Kroll reactive solution was used for etching. The OLYMPUS PME 3—ADL microscope (Olympus Corp., Tokyo, Japan) was then utilized to make observations.

The phase analysis was characterized using the Bruker D8 ADVANCE diffractometer (Billerica, MA, USA) to measure the X-ray diffraction data of the samples. This study was conducted using CuKα radiation (λ = 1.5418 Å) in Bragg–Brentano geometry with a step size of 0.02° and a power of 40 kV (LYNXEYE XE high-speed position-sensitive detector, Billerica, MA, USA) in the range of 2θ = 5–80°.

Additionally, the alloy was analyzed using a scanning electron microscope FE-SEM Zeiss Sigma 300 VP (Carl Zeiss, Jena, Germany), equipped with an energy dispersive X-ray spectrometer (Edax Inc., Mahwah, NJ, USA). The SEM micrographs were acquired in high-vacuum mode. A cathode voltage of 25 kV was used, keeping a working distance of 10 mm. A backscattered electron detector (BSD) along with a Z contrast revealed the different phases within the sample.

2.3. Electrochemical Measurements

Electrochemical measurement is one effective analytical technique for corrosion investigation. An electrochemical cell with three electrodes was employed. A saturated calomel electrode (SCE) served as the reference electrode. The working electrode was the HEA sample, whereas Pt was the counter electrode. The electrolyte was Ringer Grifols composed of (values in mmol/L): Na^+ 129.9; K^+ 5.4; Ca^{2+} 1.8; Cl^- 111.7; $C_3H_5O_3^-$ 27.2. Essays were performed at 37 ± 0.1 °C using a thermostatic bath. A computer with EC-Lab® software 9.55 package together with a SP-150 potentiostate (Biologic Science Instruments, Seyssinet-Pariset, France) was in the support tool for the experiment.

The open circuit potential was measured during 24 h. Then, potentiodynamic polarization measurements were registered. OCP provides qualitative findings regarding the state of corrosion but provides no information regarding the rate of corrosion.

The polarization curve can be used to determine the corrosion potential, whereas the Tafel slope can be used to fix the corrosion rate. Tafel slopes for both anodic processes (b_a) and cathodic processes (b_c) were calculated shifting linear polarization curves. The ASTM G 5-87 Standard Reference Test Method for Making Potentiostatic and Potentiodynamic Anodic Polarization Measurements was followed in varying the samples' potential throughout a range of values [20]. Current through the electrode is then monitored during

the scanning of potential values. A scan rate of 300 μV/1807 ms was the pattern for the potentiodynamic polarization accomplished [21].

The EIS experiment used a sinusoidal round potential E, set to the constant value of the open circuit potential to perform impedance testing into potentiostatic arrangement [22]. The cell current was stabilized after 24 h open circuit potential test. Scanning from 100 kHz to 100 mHz and an amplitude of 10 mV from peak to peak was carried out.

2.4. Microhardness

An indentation test was performed at 25 °C and 45% humidity. The equipment used was a Shimadzu HMV 2T microhardness tester (Shimadzu, Kyoto, Japan) to ascertain the microhardness of the samples. Before taking perpendicular microhardness measurements, the sample was previously polished to a mirror finish, and then viewed under an optical microscope. Following the diameter of the sample, indentations were made at intervals of 0.5 mm, with a low load of 9.1 mN (1 gf). A dwelling time of 10 s was performed for the loads. Up to ten indentations were produced for every sample, based on ISO 14577-1:2015 [23]. From these values, the Vickers hardness (HV) was computed for each sample.

3. Results and Discussions

3.1. Microstructural Characterization

The microstructure of the FeHEA and NbHEA can be observed through the optical microscopy of the two samples at 20× magnification in Figure 1. In both cases, grain microstructure is observed. The composing elements' distribution through solidification may result in the creation of a dendrite phase (light grey contrast in the images) and an inter-dendrite phase (dark grey contrast in the images).

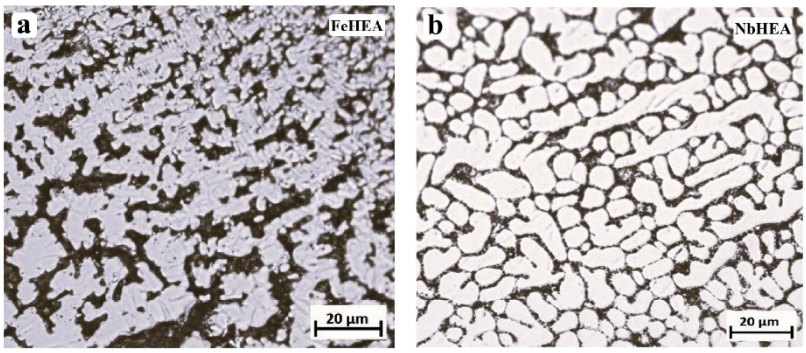

Figure 1. Optical microscopy at 20× magnification of (**a**) FeHEA microstructure and (**b**) NbHEA microstructure.

X-ray diffraction (XRD) analyses were performed, and the data obtained were subjected to Rietveld refinement processing using the TOPAS V6 program.

Factors R_p and R_{wp} are defined as follows:

$$R_p = \frac{\sum |Y_i(obs) - Y_i(calc)|}{\sum Y_i(obs)} \quad (1)$$

$$R_{wp} = \left\{ \frac{\sum w_i [Y_i(obs) - Y_i(calc)]^2}{\sum w_i [Y_i(obs)]^2} \right\}^{\frac{1}{2}} \quad (2)$$

Table 2 illustrates the resulting lattice parameters after refinement, as well as after Rietveld refinement analysis, for the MoNbTaTiZr sample.

Table 2. Lattice parameters and Rietveld refinement results for the MoNbTaTiZr alloy.

Phase	Lattice Parameters (Å)			Crystallite Size (nm)	Mass Proportion (%)	Space Group	Reliability Factors		
	a	b	c				R_p	R_{wp}	R_{exp}
MoNbTa	3.24 (9)			16 (1)	16.36	Im-3m (229) (bcc)	7.85	10.94	1.92
Ti_4Nb	3.19 (8)	4.87 (5)	4.60 (7)	102 (2)	3.80	Cmcm (orthorombic)			
Ta	2.82 (9)		5.34 (5)	16 (6)	74.22	P63/m (hexagonal)			
$Ti_{0.879}Nb_{0.121}$	3.11 (9)	5.09 (7)	4.62 (1)	81 (1)	5.62	Cmcm (orthorombic)			

The results obtained from the Rietveld analysis indicated the presence of Ta as the main phase, crystallized in the hexagonal system. Alongside it, in smaller proportions, MoNbTa solid solution appears, crystallized in the BCC system, and the compounds $Ti_{0.879}Nb_{0.121}$ and Ti_4Nb, both crystallized in the orthorhombic system.

Table 3 illustrates the resulting lattice parameters after refinement, as well as after Rietveld refinement analysis, for the FeMoTaTiZr sample.

Table 3. Lattice parameters and Rietveld refinement results for the FeMoTaTiZr alloy.

Phase	Lattice Parameters (Å)			Crystallite Size (nm)	Mass Proportion (%)	Space Group	Reliability Factors		
	a	b	c				R_p	R_{wp}	R_{exp}
Ti_2Fe	11.336 (14)			26.7 (27)	39.63	Fd-3m (fcc)	5.18	8.37	1.68
MoTa	3.2093 (40)			38.3 (51)	23.40	Im-3m (bcc)			
Mo	3.1421 (39)			28.2 (25)	20.68	Im-3m (bcc)			
(Fe Mo) Zr	5.2103 (64)		8.502 (11)	28.7 (15)	16.13	P63/mmc (hexagonal)			
Ti_7Zr_3	2.989 (20)		4.683 (97)	70 (16)	0.16	P63/mmc (hexagonal)			

These results indicated the presence of three main phases, crystallized in the cubic system: Ti_2Fe, MoTa, and Mo. In addition to these three main constituents, small proportions of solid phase (Fe Mo) Zr and Ti_7Zr_3 compound were also identified.

Mitsuharu Todai et al. [10] have published SEM-back scattering electron images of the MoNbTaTiZr HEA, both as-cast and annealed samples. Also, X-ray diffraction results for MoNbTaTiZr HEA are published by Takao Hori et al. [24]. Those XRD patterns of MoNbTaTiZr alloy showed a main bcc phase and a minor bcc phase (with a different lattice constant), and no indication of any intermetallic compound phases or bcc-based ordered phases. The annealing in Todai's study did not lead the decomposition of bcc solid solution phases to other phases, concluding that the formation of bcc HEA keeps a high phase stability [10]. The review on HEAs as biomaterials shows that the vast majority have a bcc structure [25].

SEM images of the MoNbTaTiZr sample at higher magnification, along with EDS graphs, are shown in Figure 2. Composition of elements in the dendrite and interdendrite regions have been aimed, performing EDS analyses on micro-zones with the same area. The results of the global and punctual chemical composition for the samples are presented in Table 4.

SEM images of FeHEA at the same magnification as for NbHEA and their respective EDS graphs are presented in Figure 3. In the same way as with the previous alloy, EDS analyses are used to obtain composition of elements both in the dendrite and interdendrite regions. The chemical composition for the different points is exposed in Table 5.

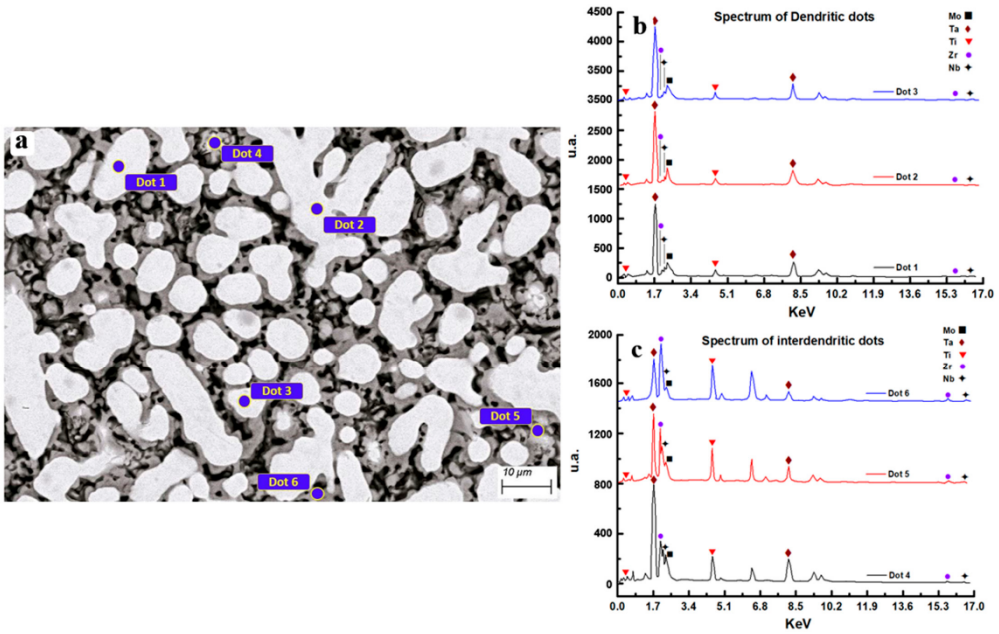

Figure 2. (**a**) SEM and EDS analysis for Area 1, Area 2, and Area 3 of MoNbTaTiZr high-entropy alloy; (**b**) compositional spectrum in dendritic areas; (**c**) compositional spectrum in interdendritic areas.

Table 4. EDS quantification results of atomic and weight percentage on dendritic (D) and interdendritic (ID) microstructures of MoNbTaTiZr high-entropy alloy.

Spot	1		2		3		4		5		6	
	D		D		D		ID		ID		ID	
Elements	**wt %**	**at %**	**wt %**	**at %**	**wt %**	**at %**	**wt %**	**at %**	**wt %**	**at %**	**wt %**	**at %**
Ti	6.20	15.74	5.89	14.99	6.21	15.84	10.46	23.53	14.26	28.48	19.94	36.16
Zr	3.66	4.88	4.04	5.41	3.72	4.98	20.74	24.49	31.30	32.82	39.60	37.70
Nb	10.68	13.97	9.07	11.91	9.87	12.97	9.80	11.36	10.23	10.53	9.04	8.45
Mo	20.30	25.71	21.90	27.85	20.25	25.76	11.60	13.03	10.24	10.21	6.11	5.53
Ta	59.15	39.71	59.10	39.85	59.95	40.45	39.52	23.53	33.97	17.96	25.32	12.16

Attending to compositions obtained, segregation factor is calculated for every element in both NbHEA and FeHEA. This factor is a parameter that helps to evaluate the segregation degree of an alloy and that facilitates comparison between the different elements for those two alloys. The segregation factor relates element concentration in the dendritic compared to the interdendritic area, following the formula:

$$S_R = \frac{\text{Element concentration in Dendritic area}}{\text{Element concentration in Interdendritic area}} \quad (3)$$

The results are shown in Table 6. Both dendrite and inter-dendrite regions contain all the constituent elements, but whereas Mo and Ta show a tendency towards the dendrite region, Ti, Zr, and Fe have an inclination to the inter-dendrite region.

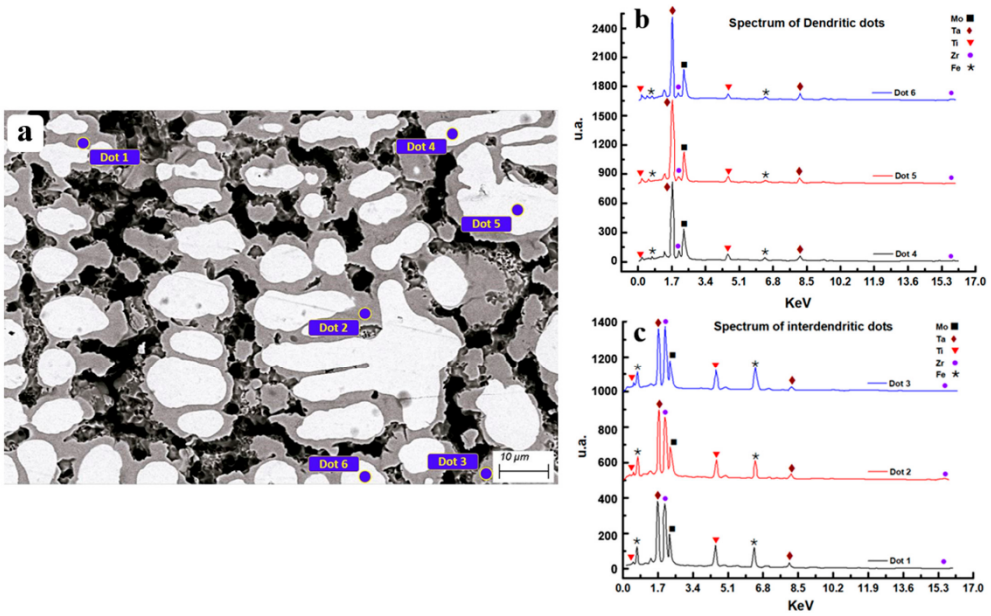

Figure 3. (**a**) SEM and EDS analysis for Area 1, Area 2, and Area 3 of FeMoTaTiZr high-entropy alloy; (**b**) compositional spectrum in dendritic areas; (**c**) compositional spectrum in interdendritic areas.

Table 5. EDS quantification results of atomic and weight percentage on dendritic (D) and interdendritic (ID) microstructures of FeMoTaTiZr high-entropy alloy.

Spot	**1**		**2**		**3**		**4**		**5**		**6**	
	ID		**ID**		**ID**		**D**		**D**		**D**	
Elements	**wt %**	**at %**	**wt %**	**at %**	**wt %**	**at %**	**wt %**	**at %**	**wt %**	**at %**	**wt %**	**at %**
Ti	10.58	18.18	10.81	18.48	11.14	18.54	9.14	18.09	7.61	15.97	7.60	15.85
Fe	14.68	21.62	14.78	21.65	16.50	23.54	5.24	8.89	3.30	5.94	3.41	6.10
Zr	37.44	33.77	36.07	32.34	39.38	34.41	9.47	9.83	3.51	3.86	4.35	4.76
Mo	23.51	20.16	25.45	21.70	23.03	19.13	50.27	49.64	54.29	56.85	54.32	56.55
Ta	13.79	6.27	12.89	5.83	9.95	4.38	25.88	13.55	31.29	17.38	30.32	16.74

Table 6. Composition average results in dendritic (D) and interdendritic (ID) areas and S_R values for FeHEA and NbHEA.

	Parameters	**Ti**	**Zr**	**Mo**	**Ta**	**Nb**	**Fe**
FeHEA	D	8.12	5.78	52.96	29.19	-	3.98
	ID	10.84	37.63	24.00	12.21	-	15.32
	S_R	0.75	0.15	2.21	2.39	-	0.26
NbHEA	D	7.19	8.04	18.51	54.43	9.86	-
	ID	17.10	35.45	8.18	29.65	9.64	-
	S_R	0.42	0.23	2.26	1.84	1.02	-

For the analysed samples, the distribution of the constituents inside the dendrite, so as through the inter-dendrite areas, shows that all the composing elements are contained in

both regions. This is consistent with the formation of multicomponent solid solution phases. For the NbHEA, a phase in the main-dendrite region is enriched with Ta, Nb, and Mo, and a minor phase the inter-dendrite region accumulates higher Ti and Zr concentrations.

The distribution of the constituents can be described with the enthalpy of mixing, attending to the high-melting-temperature elements (Mo, Nb, and Ta). During the solidification process, the dendrite phase is formed. Nb, Mo, and Ta are elements with high melting temperature, which forces Ti and Zr to be expelled from the phase as a consequence of the positive values of the enthalpy of mixing for the different combinations Ta-Zr, Ta-Ti, Nb-Zr, and Nb-Ti. This results in the enrichment of the inter-dendrite region with Ti and Zr. The enthalpy and miscibility between the different atoms in the solution phase of HEA are intrinsically linked to the partitioning of elements [10].

For the FeHEA, the main-dendrite region is also supported with Ta and Mo, and the inter-dendrite region also contains Ti and Zr, as explained for the NbHEA. However, Fe is now also added to the inter-dendrite region, showing a much higher tendency to be expelled from the dendrite than Nb. Again, high-melting-temperature elements keep a tendency to occupy dendrite phases. Following the former, Ti and Zr (in both alloys), and now also Fe, show segregation factors with a lower value than the unit, which make them the main constituents of the inter-dendrite regions. Additionally, the shift in the segregation factor values indicates that with the addition of Fe instead of Nb, dendrite regions' compositions are reinforced with Ta and Ti, while Mo proportions keep mainly steady. The microstructure and composition of cast FeMoTaTiZr high-entropy alloy, with dendrites based on Mo and Ta, dispersed in Ti, Fe, and Zr matrix [26], are in agreement with the results obtained in this study.

3.2. Corrosion Tests

3.2.1. Open Circuit Potential (OCP)

Open circuit potential measurement curves during 24 h immersion for both NbHEA and FeHEA are shown in Figure 4.

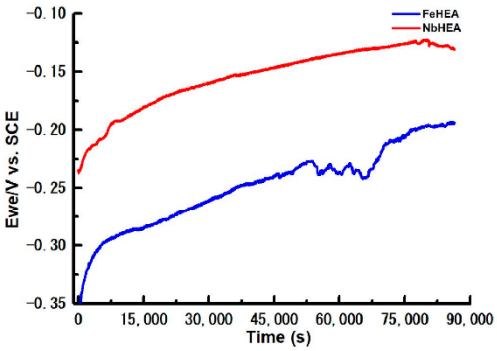

Figure 4. Open circuit potential variation with time for the two samples FeHEA and NbHEA in Ringer solution.

The open circuit potential (OCP) of metallic samples refers to the voltage difference between a reference electrode and a metal sample when there is no external current flowing between them. The OCP of a metal depends on its electrochemical properties, such as its standard electrode potential. Metals with higher standard electrode potentials tend to have more positive OCP values compared to those with lower standard electrode potentials. This is because metals with higher electrode potentials have a greater tendency to lose electrons and undergo oxidation, resulting in a more positive potential. The chemical composition of the metal, particularly the presence of alloying elements, can influence its electrochemical

behavior and, consequently, its OCP. Niobium has a relatively cathodic standard electrode potential of ca. −1 V vs. standard hydrogen electrode (SHE) ($E^0_{Nb/Nb3+} \sim -1.1$ V and $E^0_{Nb/Nb5+} \sim -0.96$ V) while iron has $E^0_{Fe/Fe2+} \sim -0.45$ V vs. SHE. It can be observed that the OCP for both samples are shifting to more positive values during the immersion time (see Figure 4). The variation of open circuit potential (OCP) to more positive values during the time of immersion can be explained by several factors related to the electrochemical behavior of the metallic sample in the Ringer solution. Both studied alloys develop a passive oxide layer on their surface during the immersion, and this passive film acts as a barrier that reduces the rate of corrosion by preventing direct contact between the metal and corrosive agents. As the passive film forms and stabilizes, it causes the OCP to shift to more positive values. This shift indicates that the alloys are becoming more passive and less reactive towards corrosion. In aqueous Ringer environments, oxygen reduction reactions occur on the surface of metals, leading to the consumption of dissolved oxygen in the solution. As the concentration of oxygen decreases near the metal surface, the OCP tends to shift to more positive values due to the decrease in the cathodic reaction rate. The oscillations (increasing and decreasing) of OCP for FeHEA sample can be explained by the depassivation process, which occurs when the passive layer breaks down, causing a decrease in OCP, but after it, the stable passive layer forms again, leading to an increase in OCP.

3.2.2. Potentiodynamic Polarization

Following the potentiodynamic polarization, plots in a semi-logarithmic version are displayed in Figure 5.

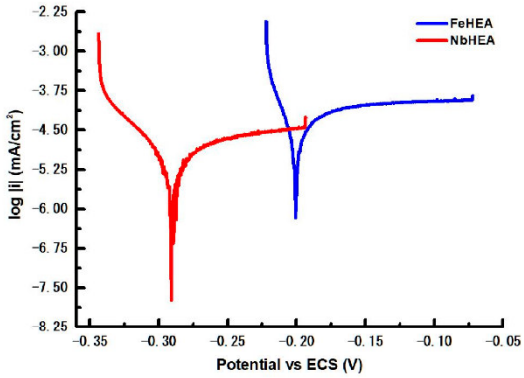

Figure 5. Tafel curves for the two samples of FeHEA and NbHEA after 24 h immersion in Ringer solution.

Potentiodynamic polarization is a widely used electrochemical technique for studying the corrosion behavior of metallic materials. When potentiodynamic polarization data were plotted in a semi-logarithmic version (i.e., with the logarithm of the current density on the *y*-axis), several corrosion parameters can be obtained: corrosion potential, corrosion current density, Tafel slopes, and corrosion rate. By using EC-Lab® software, the analytic results of E_{corr}, i_{corr}, b_a, b_c, and V_{corr} are presented in Table 7.

It can be observed (see Table 7) that FeHEA, with the higher corrosion current, is experiencing more corrosion or corroding at a faster rate. This is due to factors such as passivation and the formation of a less protective oxide layer, all of which contribute to deteriorating the corrosion resistance. The dissolution of Fe in the Ringer Grifols solution was associated with the anodic portion of the polarization curve (above E_{corr}), whereas the cathodic region (below E_{corr}) was associated with the cathodic reaction of oxygen. E_{corr} of

NbHEA presents a more negative (active) potential value compared to that of FeHEA by −90 mV, whereas the corrosion current density (I_{corr}) shows a growth from 10 nA cm^{-2} to 39 nA cm^{-2}. The rate of degradation for the FeHEA was probably accelerated by substitution of Nb with Fe, and the average of the degradation rate (mmpy) became almost four times higher for FeHEA than for NbHEA. The corrosion current density of FeHEA is comparable with that of Ti6Al4V [27].

Table 7. Electrochemical parameters estimated through Tafel approximation.

	E_{corr}	i_{corr}	b_c	b_a	V_{corr}
	mV	**μA·cm^{-2}**	**mV dec^{-1}**	**mV dec^{-1}**	**mmpy**
FeHEA	−200.51	0.039	26.90	202.10	4.9×10^{-4}
NbHEA	−290.78	0.010	45.50	325.50	1.3×10^{-4}

3.2.3. Electrochemical Impedance Spectroscopy (EIS)

Electrochemical impedance spectroscopy (EIS) is a powerful technique for analyzing corrosion processes due to its ability to provide detailed information about the electrochemical behavior of metallic systems. EIS can provide insight into the kinetics of corrosion processes by analyzing impedance data over a range of frequencies. Changes in impedance spectra, such as the shape and position of impedance arcs, can reveal information about the corrosion rate, corrosion mechanism, and the formation of passive films or corrosion products.

The Nyquist representation of the EIS analysis is displayed in Figure 6. Both the FeHEA and NbHEA samples, in the high-to-low frequency region, display a semicircle formation. There is a direct correspondence between the semicircular portion of a Nyquist plot and the limited process of electron transfer at the metal surface through the solution interface. For the corrosion process, the diameter of these semicircles can be used to interpret the electron transfer resistance. It is clear, when comparing the two Nyquist plots, that an important reduction of the electron transfer resistance is shown for the FeHEA sample, which indicates that the substitution of Nb with Fe produced an acceleration of the corrosion rate for this FeHEA.

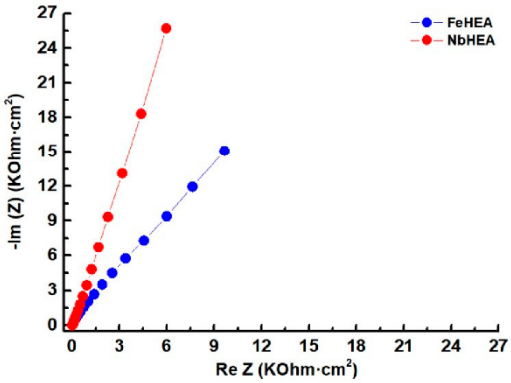

Figure 6. Nyquist vs. Eocp curves for the two samples of FeHEA and NbHEA.

In the Bode-Z plots shown in Figure 7, overlapping curves are formed for the range of frequency displayed. It can be observed that the impedance of both HEA improved linearly with decreasing frequency in the range of 10^3–10^{-1} Hz, indicating that the passive film on the samples surface have optimal corrosion resistance.

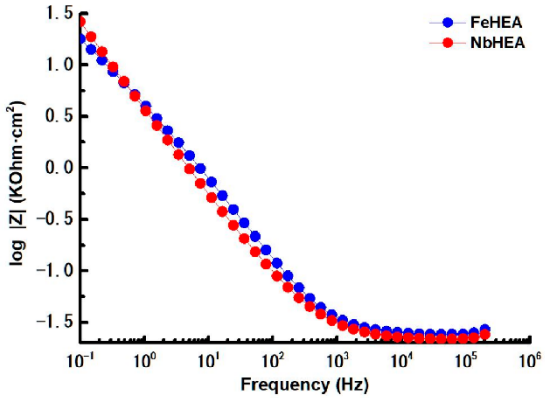

Figure 7. Bode Z vs. Eocp curves for the two samples of FeHEA and NbHEA.

For the open circuit potential versus the Reference electrode, the phase displacement in proportion to frequency is displayed via the Bode-phase plot in Figure 8. It can be observed from the curves that theta changes in a more significant way in the low-frequency region for the FeHEA. At low frequencies, the system has increased time to equilibrate, allowing electrochemical processes to predominate the impedance response. The phase angle diminishes due to the presence of a resistive component in these processes, which mitigates the overall capacitive phase shift. The diffusion of ions to and from the alloy surface in simulated human fluid is constrained by mass transport restrictions. At low frequencies, imperfections or ion diffusion within the passive layer may become prominent, affecting the phase angle and leading to its reduction.

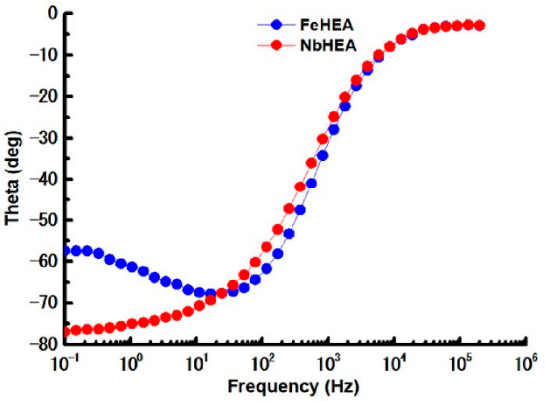

Figure 8. Bode Theta vs. Eocp curves for the two samples of FeHEA and NbHEA.

When considering metals to be inside the human body, those with an electrode potential slightly higher than zero may be degraded. Degradation process and the grade of the corrosion kinetics are influenced by characteristics of the inner human body environment (e.g., flow and pH). Another specific parameter to take into account is the surface film condition.

In the physiological conditions, the electrochemical deportment of HEA occurs in an oxygen absorption mode, increasing the pH value of the solution, and can be expressed through the following reactions:

$$\text{Anodic reaction: Me} \rightarrow \text{Mex}^{+} + \text{xe}^{-} \quad (4)$$

$$\text{Cathodic reaction: } O_2 + 2H_2O + 4e^{-} \rightarrow 4OH^{-} \quad (5)$$

During the anodic oxidation, the passive film is predominantly formed by stable oxides such as: TiO_2, ZrO_2, MoO_3, MoO_2, and Ta_2O_5. In the case of NbHEA, the passive film also contains Nb_2O_5. In the case of FeHEA, the iron reactions in physiological conditions (pH = 7.4 and T = 37 °C) with the corresponding enthalpy calculated with common Standard Enthalpy of Formation values [28] are:

$$Fe \rightarrow Fe^{2+} + 2e^{-} \quad \Delta H = -87.9 \text{ kJ/mol} \quad (6)$$

$$Fe^{2+} + 2OH^{-} \rightarrow Fe(OH)_2 \quad \Delta H = +57.9 \text{ kJ/mol} \quad (7)$$

$$Fe^{2+} \rightarrow Fe^{3+} + e^{-} \quad \Delta H = +40.2 \text{ kJ/mol} \quad (8)$$

$$Fe^{3+} + 3OH^{-} \rightarrow Fe(OH)_3 \quad \Delta H = -2.3 \text{ kJ/mol} \quad (9)$$

The proposed equilibrium equations are shown in equations:

$$Fe(OH)_2 + Cl^{-} \rightarrow FeClOH + OH^{-} \quad (10)$$

$$FeClOH + H^{+} \rightarrow Fe^{2+} + Cl^{-} + H_2O \quad (11)$$

$$Fe^{2+} + O_2 + 3OH^{-} \rightarrow Fe(OH)_3\downarrow + O^{2-} \quad (12)$$

$$Fe(OH)_3 + 2Cl^{-} \rightarrow FeCl_2OH + 2OH^{-} \quad (13)$$

Chloride ions have been identified in solid intermediate species during the precipitation of Fe(III) hydroxide from aqueous chloride solutions, suggesting that this species is stable in weakly acidic solutions with low chloride concentrations. Nonetheless, the stability of FeClOH and $FeCl_2OH$, if it indeed exists, is minimal, and these species are not regarded as significant [29].

Both the electrochemical oxidation and reduction of iron in the presence of oxygen and the stability conditions of compounds that may originate in processes involving the gaseous phase have been examined [30]. Fe is particularly prone to selective dissolution due to the low stability of iron species in comparison to other species.

For additional EIS data interpretation, an analogous electric circuit is proposed. A precise fit and interpretation of EIS data depend on the correct choice of the circuit. In addition to being as simple as possible while retaining the key elements of the system, it is a requisite that the equivalent circuit is physically meaningful and pertinent to the electrochemical system under study.

The corrosion process characteristics were modelled using the equivalent circuit depicted in Figure 9, pretending to be a suitable compromise between physical significance and simplicity based on the impedance. The electrolyte resistance is presented as R_e in the figure. Capacitance Q_p and resistance R_p represent the impedance of the pores. It is supposed to be in the passive film, strongly involved with the conduction of ions through the passive layer structure. This gives an idea of the protection level that the passive film can represent for the base alloy when facing corrosion. Finally, both the capacitance Q_c and the resistance R_c stand for the polarization resistance at the interface between the alloy and passive film, since the electrolyte is thought to enter into the pores.

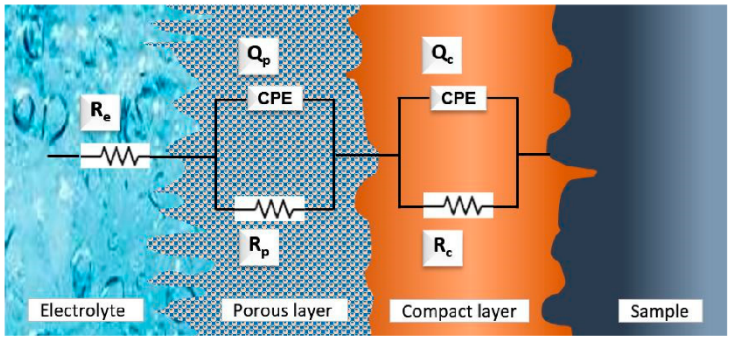

Figure 9. Equivalent circuit used for the EIS experimental data and its interpretation in the interface for the two samples of FeHEA and NbHEA.

ZSimpWin 3.60 software was utilized to analyze the impedance spectra. Data were computed to assess the fit quality by contrasting the simulated and experimental data [31]. The equivalent circuit impedance can be calculated with the following equation:

$$Z = R_e + \frac{R_p}{1 + R_p Y_p (jw)^{n_p}} + \frac{R_c}{1 + R_c Y_c (jw)^{n_c}} \quad (14)$$

The value of the different parameters is displayed in Table 8.

Table 8. Parameter values of the equivalent circuit for FeHEA and NbHEA.

	R_c	Y_c	n_c	R_p	Y_p	n_p	R_e
	[Ω·cm²]	[S·sⁿ cm⁻²]	-	[Ω·cm²]	[S·sⁿ cm⁻²]	-	[Ω·cm²]
FeHEA	24.37	1.00×10^{-4}	0.7950	2.77×10^{3}	$7.99 \cdot 10^{-5}$	0.8183	8.91×10^{4}
NbHEA	27.78	7.37×10^{-5}	1	5.72×10^{5}	$1.47 \cdot 10^{-4}$	0.7117	1.39×10^{4}

Since the distance between the working electrode and the reference electrode affects the resistance of the electrolyte R_e, it was aimed to be constant in both experiments. The pores' resistance in the passive film can be deducted from R_p and Y_p values, which show lower values for the FeHEA, indicating a likely higher ion conduction through the structure of the passive film. The n factor gives an idea of the proximity of the Y variable to the capacitor behavior, where similar n-values can be seen for both samples. A higher ability of the electrolyte to enter into the pores of the FeHEA can be fathomed. Finally, a lower polarization resistance can be seen through R_c values, referring to the interface between the passive film and the base alloy.

3.3. Microhardness

Imprints measurement is used to obtain Vickers Hardness. The results for the two samples are plotted in Figure 10.

For the NbHEA, an average value of 496.70 kgf·mm^{-2} is obtained, with a standard deviation of 17.72 kgf·mm^{-2}. For the FeHEA, an average value of 628.80 kgf·mm^{-2} is obtained, with a standard deviation of 24.13 kgf·mm^{-2}.

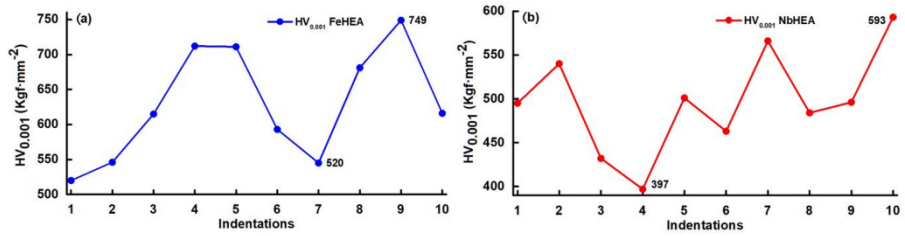

Figure 10. $HV_{0\text{-}01}$ microhardness test results for sample of (**a**) FeHEA and (**b**) NbHEA.

No big difference is shown between the two samples, though FeHEA exhibits higher microhardness results than NbHEA. Changes in the material structure process may be caused by the cutting process, enabling the formation of thin layers of altered material. These layers may influence the results. Also, the corrosion layers' formation can affect the hardness values when using low loads. Efforts were made to minimize those effects through additional polishing of the samples. Hardness values are similar for both samples, showing higher results for the FeHEA. This level qualifies the alloy for the manufacture of medical devices subjected to high mechanical stress.

4. Conclusions

In the present study, two different samples of HEAs MoNbTaTiZr and FeMoTaTiZr were analyzed. Both samples were produced with electric-arc remelting technology at a laboratory. The alloys were formed keeping similar atomic percentage of the elements in both alloys. Optical microscopy and scanning electron microscopy techniques were used to characterize the microstructure of the alloys. Replacing Nb with Fe has an influence on the layout proportion of the other four elements, with Fe leaving the dendrite towards the inter-dendrite region, whereas Nb has a tendency to stay in both regions. As for the corrosion properties, the synthesized alloys showed some differences. Both samples were evaluated under simulated biological environment using the potentiodynamic polarization method and electrochemical impedance spectroscopy (EIS). The tests proved that FeHEA has a higher corrosion rate than NbHEA. Both alloys represented by the same equivalent electrical circuit allows us to propose that the similar composition of those two alloys let them show similar corrosion products and layers formation. But the influence of the lower stability of the iron species offers a selective dissolution that probably increases the corrosion rate of the FeHEA compared to the NbHEA. In order to better characterize the FeHEA corrosion behavior, further studies focused on this matter should be aimed. Taking this into account, it would also be interesting to perform further microhardness tests on corroded samples so that the influence of iron corrosion effects on the hardness can be better analyzed.

Author Contributions: M.L.-R.: investigation, methodology and conceptualization, writing of the original draft; S.B.-G.: investigation, methodology, writing—review and editing; I.V.: investigation (Table 1) and review of the writing; J.M.-R.: data validation, project administration, visualization, review and editing. All authors have read and agreed to the published version of the manuscript.

Funding: This research received no external funding.

Data Availability Statement: The original contributions presented in this study are included in the article. Further inquiries can be directed to the corresponding author.

Acknowledgments: We hereby acknowledge the project "The Smart Healthcare Engineering (SHEng)", with number 2023-1-RO01-KA220-HED-000159985, co-funded by the European Union.

Conflicts of Interest: The authors declare no conflicts of interest.

References

1. Cantor, B.; Chang, I.; Knight, P.; Vincent, A.J.B. Microstructural Development in Equiatomic Multicomponent Alloys. *Mater. Sci. Eng. A* **2004**, *375–377*, 213–218. [CrossRef]
2. Li, D.; Liaw, P.K.; Xie, L.; Zhang, Y.; Wang, W. Advanced High-Entropy Alloys Breaking the Property Limits of Current Materials. *J. Mater. Sci. Technol.* **2024**, *186*, 219–230. [CrossRef]
3. Yeh, J.-W. Recent Progress in High-Entropy Alloys. *Ann. Chim. Sci. Mat.* **2006**, *31*, 633–648. [CrossRef]
4. Miracle, D.; Senkov, O. A Critical Review of High Entropy Alloys and Related Concepts. *Acta Mater.* **2016**, *122*, 448–511. [CrossRef]
5. Tsai, M.; Yeh, J.-W. High-Entropy Alloys: A Critical Review. *Mater. Res. Lett.* **2014**, *2*, 107–123. [CrossRef]
6. Rosca, J.; Santana, E.D.; Castro, J.; Lopez, A.; Vasilescu, E.V.; Drob, P.; Vasilescu, C. Characterisation of Anodic Films Formed on Titanium and Its Alloys. *Mater. Corros.* **2005**, *56*, 692–696. [CrossRef]
7. Jimenez-Marcos, C.; Mirza-Rosca, J.C.; Baltatu, M.S.; Vizureanu, P. Experimental Research on New Developed Titanium Alloys for Biomedical Applications. *Bioengineering* **2022**, *9*, 686. [CrossRef]
8. Baltatu, M.S.; Spataru, M.C.; Verestiuc, L.; Balan, V.; Solcan, C.; Sandu, A.V.; Geanta, V.; Voiculescu, I.; Vizureanu, P. Design, Synthesis, and Preliminary Evaluation for Ti-Mo-Zr-Ta-Si Alloys for Potential Implant Applications. *Materials* **2021**, *14*, 6806. [CrossRef]
9. Surmeneva, M.; Grubova, I.; Glukhova, N.; Khrapov, D.; Koptyug, A.; Volkova, A.; Ivanov, Y.; Cotrut, C.M.; Vladescu, A.; Teresov, A.; et al. New Ti–35Nb–7Zr–5Ta Alloy Manufacturing by Electron Beam Melting for Medical Application Followed by High Current Pulsed Electron Beam Treatment. *Metals* **2021**, *11*, 1066. [CrossRef]
10. Todai, M.; Nagase, T.; Hori, T.; Matsugaki, A.; Sekita, A.; Nakano, T. Novel TiNbTaZrMo High-Entropy Alloys for Metallic Biomaterials. *Scr. Mater.* **2017**, *129*, 65–68. [CrossRef]
11. Senkov, O.; Wilks, G.; Miracle, D.; Chuang, C.; Liaw, P. Refractory High-Entropy Alloys. *Intermet. Barking* **2010**, *18*, 1758–1765. [CrossRef]
12. Lin, S.; Lai, W.; Vogel, F.; Tong, X.; You, D.; Li, W.; Wang, X. Mechanical and Corrosion Properties of Biomedical (TiZr)90-XNbxTa5Mo5 Medium Entropy Alloys. *Int. J. Refract. Metals Hard Mater.* **2023**, *116*, 106361. [CrossRef]
13. Hanawa, T. Metal Ion Release from Metal Implants. *Mater. Sci. Eng. C* **2004**, *12*, 745–752. [CrossRef]
14. Akmal, M.; Park, H.-K.; Ryu, H.J. Plasma Spheroidized MoNbTaTiZr High Entropy Alloy Showing Improved Plasticity. *Mater. Chem. Phys.* **2021**, *273*, 125060. [CrossRef]
15. Günen, A.; Ceritbinmez, F.; Patel, K.; Akhtar, M.A.; Mukherjee, S.; Kanca, E.; Karakas, M.S. WEDM Machining of MoNbTaTiZr Refractory High Entropy Alloy. *CIRP J. Manuf. Sci. Technol.* **2022**, *38*, 547–559. [CrossRef]
16. Matsuno, H.; Yokoyama, A.; Watari, F.; Uo, M.; Kawasaki, T. Biocompatibility and Osteogenesis of Refractory Metal Implants, Titanium, Hafnium, Niobium, Tantalum and Rhenium. *Biomaterials* **2001**, *22*, 1253–1262. [CrossRef] [PubMed]
17. Ishimoto, T.; Ozasa, R.; Nakano, K.; Weinmann, M.; Schnitter, C.; Stenzel, M.; Matsugaki, A.; Nagase, T.; Matsuzaka, T.; Todai, M.; et al. Development of TiNbTaZrMo Bio-High Entropy Alloy (BioHEA) Super-Solid Solution by Selective Laser Melting, and Its Improved Mechanical Property and Biocompatibility. *Scr. Mater.* **2021**, *194*, 113658. [CrossRef]
18. Gąsior, G.; Szczepański, J.; Radtke, A. Biodegradable Iron-Based Materials—What Was Done and What More Can Be Done? *Materials* **2021**, *14*, 3381. [CrossRef] [PubMed]
19. *ASTM E3-11*; Standard Guide for Preparation of Metallographic Specimens. ASTM International: West Conshohocken, PA, USA, 2017.
20. *Designation: G 5-87*; Standard Reference Test Method for Making Potentiostatic and Potentiodynamic Anodic Polarization Measurements. ASTM International: West Conshohocken, PA, USA, 2003.
21. *ASTM G 102-89*; ASTM-Standards Standard Practice for Calculation of Corrosion Rates and Related Information from Electrochemical Measurements. ASTM International: West Conshohocken, PA, USA, 1999; Volume 89, pp. 1–7.
22. *ISO 16773-1-4*; Electrochemical Impedance Spectroscopy (EIS) on Coated and Uncoated Metallic Specimens. ISO: Geneva, Switzerland, 2016.
23. *ISO 14577-1*; Metallic Materials—Instrumented Indentation Test for Hardness and Materials Parameters—Part 1: Test Method. ISO: Geneva, Switzerland, 2015.
24. Hori, T.; Nagase, T.; Todai, M.; Matsugaki, A.; Nakano, T. Development of Non-Equiatomic Ti-Nb-Ta-Zr-Mo High-Entropy Alloys for Metallic Biomaterials. *Scr. Mater.* **2019**, *172*, 83–87. [CrossRef]
25. de Oliveira, T.G.; Fagundes, D.; Capellato, P.; Sachs, D.; da Silva, A.A.A.P. A Review of Biomaterials Based on High-Entropy Alloys. *Metals* **2022**, *12*, 1940. [CrossRef]
26. Codescu, M.; Vladescu, A.; Geanta, V.; Voiculescu, I.; Pana, I.; Dinu, M.; Kiss, A.; Braic, V.; Patroi, D.; Virgil, M.; et al. Zn Based Hydroxyapatite Based Coatings Deposited on a Novel FeMoTaTiZr High Entropy Alloy Used for Bone Implants. *Surf. Interfaces* **2021**, *28*, 101591. [CrossRef]
27. Kovacı, H.; Şenel, K.; Acar, T.; Bozkurt, Y.; Çelik, A. Comparative Investigation of Structural, Morphological, Mechanical, Tribological and Electrochemical Properties of TiO2 Films Formed on Cp-Ti, Ti6Al4V and Ti45Nb Alloys. *Surf. Coat. Technol.* **2024**, *487*, 131024. [CrossRef]
28. Lemire, R.; Berner, U.; Musikas, C.; Palmer, D.; Taylor, P.; Tochiyama, O. *Chemical Thermodynamics of Iron, Chemical Thermodynamics, Part 1*; OECD Nuclear Energy Agency: Seine Saint-Germain, France, 2013; No. 6355.

29. Waite, T.D. Chapter 7. Thermodynamics of the Iron System in Seawater. In *The Biochemistry of the Iron System in Seawater*; Turner, D.R., Hunter, K.A., Eds.; John Wiley and Sons, Ltd.: Hoboken, NJ, USA, 2001; pp. 292–340.
30. Pourbaix, M.; Zhang, H.; Pourbaix, A. Presentation of an Atlas of Chemical and Electrochemical Equilibria in the Precence of a Gaseous Phase. *Mater. Sci. Forum* **1997**, *251*, 143–148. [CrossRef]
31. Boukamp, B.A. A Nonlinear Least Squares Fit Procedure for Analysis of Immittance Data of Electrochemical Systems. *Solid. State Ion.* **1986**, *20*, 31–44. [CrossRef]

"New FeMoTaTiZr High-Entropy Alloy for Medical Applications"

López-Ríos, M.; Mirza-Rosca, J.; Mates, I.M.; Geanta, V.; Voiculescu, I. New FeMoTaTiZr High-Entropy Alloy for Medical Applications. Metals (Basel) 2025, 15, doi:10.3390/met15030259.

metals

MDPI

Article

New FeMoTaTiZr High-Entropy Alloy for Medical Applications

Miguel López-Ríos [1], Julia Mirza-Rosca [1,2,*], Ileana Mariana Mates [3], Victor Geanta [4] and Ionelia Voiculescu [5]

[1] Mechanical Engineering Department, University of Las Palmas de Gran Canaria, 35001 Las Palmas de Gran Canaria, Spain
[2] Materials Engineering and Welding Department, Transilvania University of Brasov, 500036 Brasov, Romania
[3] Central Military Hospital Carol Davila, Calea Plevnei 134, 010242 Bucharest, Romania
[4] Faculty of Materials and Science Engineering, Politehnica University of Bucharest, 060042 Bucharest, Romania
[5] Faculty of Industrial Engineering and Robotics, Politehnica University of Bucharest, 060042 Bucharest, Romania
* Correspondence: julia.mirza@ulpgc.es

Abstract: High-entropy alloys are novel metallic materials distinguished by very special mechanical and chemical properties that are superior to classical alloys, attracting high global interest for the study and development thereof for different applications. This work presents the creation and characterisation of an FeMoTaTiZr high-entropy alloy composed of chemical constituents with relatively low biotoxicity for human use, suitable for medical tools such as surgical scissors, blades, or other cutting tools. The alloy microstructure is dendritic in an as-cast state. The chemical composition of the FeMoTaTiZr alloy micro-zone revealed that the dendrites especially contain Mo and Ta, while the inter-dendritic matrix contains a mixture of Ti, Fe, and Zr. The structural characterisation of the alloy, carried out via X-ray diffraction, shows that the main phases formed in the FeMoTaTiZr matrix are fcc $(Ti_7Zr_3)_{0.2}$ and hcp Ti_2Fe after annealing at 900 °C for 2 h, followed by water quenching. After a second heat treatment performed at 900 °C for 15 h in an argon atmosphere followed by argon flow quenching, the homogeneity of the alloy was improved, and a new compound like $Fe_{3.2}Mo_{2.1}$, $Mo_{0.93}Zr_{0.07}$, and $Zr(MoO_4)_2$ appeared. The microhardness increased over 6% after this heat treatment, from 694 to 800 $HV_{0.5}$, but after the second annealing and quenching, the hardness decreased to 730 $HV_{0.5}$. Additionally, a Lactate Dehydrogenase (LDH) cytotoxicity assay was performed. Mesenchymal stem cells proliferated on the new FeMoTaTiZr alloy to a confluence of 80–90% within 10 days of analysis in wells where the cells were cultured on and in the presence of the alloy. When using normal human fibroblasts (NHF), both in wells with cells cultured on metal alloys and in those without alloys, an increase in LDH activity was observed. Therefore, it can be considered that certain cytolysis phenomena (cytotoxicity) occurred because of the more intense proliferation of this cell line due to the overcrowding of the culture surface with cells.

Keywords: high-entropy alloys; chemical composition; microstructure; microhardness

Academic Editors: Chao Yang and Jiro Kitagawa

Received: 8 January 2025
Revised: 22 February 2025
Accepted: 26 February 2025
Published: 27 February 2025

Citation: López-Ríos, M.; Mirza-Rosca, J.; Mates, I.M.; Geanta, V.; Voiculescu, I. New FeMoTaTiZr High-Entropy Alloy for Medical Applications. *Metals* **2025**, *15*, 259. https://doi.org/10.3390/met15030259

1. Introduction

High-entropy alloys (HEA) are currently widely studied and developed due to their special mechanical and chemical properties, sometimes highly superior to those of conventional alloys [1–5]. Alloys containing chemical elements with extremely low toxicity have recently been obtained and tested for use in medical applications [6–8]. A wide variety of chemical compositions can be designed through combinations of highly corrosion-resistant and non-toxic elements to obtain concentrated solid solutions or high-entropy alloys from alloying systems such as W-Nb-Mo-Ta and W-Nb-Mo-Ta-V. Furthermore, another research

direction is focused on obtaining HEAs with a BCC structure, consisting of combinations between transitional metallic elements such as Nb-Mo-Ta-W, V-Nb-Mo-Ta-W, Ta-Nb-Hf-Zr-Ti, Hf-Nb-Ti-Mo-Ta-Ti-Zr, or the equiatomic alloy Hf-Mo-Nb-Ta-Ti-Zr. Such high-entropy alloys feature high yield strength (σ_y = 900–1600 MPa) at ambient temperature, as well as significant compressive strength [9]. Except for vanadium, most of the chemicals used to make these alloys are biocompatible. These alloys have recently been studied in the medical field for the manufacture of orthopedic implants (hip, knee, and shoulder prostheses), tending to replace pure titanium alloys or other alloys like Co-Cr-Mo alloys and stainless steels [10,11].

The stability of the solid BCC or FCC solutions in HEA alloys can be predicted by the valence electron concentration (VEC) values [12–14]. This stability is important for predicting the evolution of mechanical characteristics during successive decontamination stages at high temperatures. As high-entropy alloys (HEAs) are metallic compounds characterised by significant chemical heterogeneity arising from the combination of elements with substantial disparities in atomic diameters and diverse mutual solubility, the performance of heat treatments after alloy preparation was a solution used by most researchers in the field to achieve homogeneous matrices [15,16].

Chemical elements considered to have low toxic effects were added to the composition of the new alloy [17–19]. In some studies, Fe is considered a biocompatible element [20], but for a high concentration of iron in the blood, several unpleasant biochemical effects can occur, such as damage to DNA, proteins, lipids, or other cellular compounds [21]. In the long term, exposure to Fe-ions can even cause death. Titanium and zirconium alloys exhibit the highest biocompatibility of all metals in the body. Also, some alloys like Ti–Ta and Ti–Zr are used in dentistry due to their high wear resistance [21].

Heat treatments of high-entropy alloys can yield either hardening effects or enhanced flexibility and toughness, depending on the heating parameters and cooling methods employed [16,22–24]. Annealing for homogenisation can mitigate or eradicate the segregation consequences of chemical components that arise during the casting of high-entropy alloys [25,26]. This results in microstructures closer to equilibrium, either by dissolving the metastable phases or by the nucleation of the equilibrium phases, the formation of which was suppressed during rapid cooling. The result of annealing can also be the reduction of microscopic or macroscopic residual stress levels [21,26].

After solution treatment, the ultimate tensile strength of Ti–8Fe–8Ta–4Zr and Ti–10Fe–10Ta–4Zr alloys increased by 6% to 10% (1051 and 1092 MPa), this improvement being larger than those obtained after heat treatments of conventional biomedical titanium alloys such as Ti–6Al–4V ELI [27].

Regarding matrix hardening, in the case of high-entropy alloys, the main explanation is based on the precipitation hardening effects and the transition from FCC to the BCC + B2 hard phase. If the hard phase formed in the alloy is brittle, then the maximum strength reached is lower [28–31]. Even if they are intended for medical applications that do not involve long-term maintenance with biological tissue, such alloys must also be tested to highlight their biocompatibility and corrosion resistance [32].

This study presents some aspects regarding the attainment and characterisation of a new FeMoTaTiZr high-entropy alloy that can be used for non-implantable medical applications. The objective of this study was to obtain a strong enough alloy that can be used for medical instruments, such as surgical scissors, blades, or other cutting tools. The experimental alloy, obtained by melting high-purity raw materials, was microstructurally characterised to highlight the different types of phases and the distribution of chemical components inside the dendritic constituents. The measurement of the microhardness before and after performing of heat treatment showed that the homogenised metal matrix

strengthens after heat procedures between 3 and 6%, depending on the heating period and cooling media.

Cytotoxicity tests were performed by determining LDH (Lactate dehydrogenase) activity in human cells. The results accredited the idea that several bio ceramic coating layers must be cladded to improve the biocompatibility of the alloy. The pH values were between 7.6 and 7.7, similar in simple media, media incubated with alloys and media incubated with alloys and human fibroblasts. In media incubated with alloys and mesenchymal stem cells, moderately alkaline pHs of 7.8–7.9 were found, which normally favour the proliferation and osteogenic differentiation of these cells.

2. Materials and Methods

2.1. Material Preparation

The FeMoTaTiZr experimental alloy consisted of chemicals with extremely low biotoxicity for the human body, so it could be used for non-implantable medical devices. The experimental high-entropy alloys were obtained in the MRF ABJ 900 vacuum arc melting furnace (Allenstown, NH, USA) of the ERAMET-SIM-UPB Laboratory. For the experimental alloys, there were high-purity (over 99.5 wt.%) raw materials (metal elements), which were cleaned in an ultrasonic tank, in ethanol solution, before being introduced into the melting furnace. The metallic materials were weighed and dosed in equiatomic ratios for the composition of the alloy recipe, each batch weighing about 40 g.

Each micro-ingot was obtained via electric arc melting in an inert argon environment. For a molar mass of 472 g/mol, the design of chemical composition of the FeMoTaTiZr equiatomic alloy was as follows (wt.%): Fe = 11.88, Mo = 20.34, Ta = 38.34, Ti = 10.17, and Zr = 19.27, corresponding to the preliminary analysis of the local chemical composition performed using an EDAX Z2e sensor provided on the SEM Inspect S-FEI microscope (FEI Co., Eindhoven, The Netherlands), in wt.%: Fe = 12.46, Mo = 20.05, Ta = 36.25, Ti = 11.27, and Zr = 19.97. To obtain the melting conditions, the air in the installation was removed by blowing argon and successive vacuuming until a pressure of 5×10^{-3} mbar was obtained in the working chamber. The actual melting was performed in an argon environment at a pressure of 1.2 bar by slowly moving the electric arc along the load between the tungsten electrode and the metal batch. The melting operations were performed on each side of the mini-ingots, rotating them 8–10 times by 180°, to ensure the homogenisation and uniform distribution of the elements in the alloys.

After the successive melting operations, the batches were cooled under an argon atmosphere in the wells of the forced water-cooled copper plate. Within the experimental program, 6 batches were obtained, which were used for heat treatments as well as mechanical and microstructural characterisation.

The HEA mini ingots were weighed to calculate the efficiency of the production process used to assess the level of losses by vaporisation, oxidation, or projection in the form of drops in the electric arc. The small losses that were recorded after weighing the experimental alloys (between 0.1 and 0.3 g) showed the efficiency and good repeatability of the melting process. Each sample has dimensions of 9 mm × 15 mm × 60 mm (Figure 1).

2.2. Chemical Composition

Due to their high hardness (over 690 $HV_{0.5}$), the cast FeMoTaTiZr alloy samples used for morphological and structural characterisation were cut by spark electro-erosion. In order not to alter the values of the chemical composition, the samples were not etched with chemical reagents. The chemical composition of the experimental alloys determined on the central area of the sample using a SEM microscope (Hitachi TM3030Plus, Hitachi, Tokyo, Japan) equipped with energy dispersive spectrometry (EDS, Bruker, Germany).

The phase composition of the coatings was determined through X-ray diffraction (XRD) utilising CuKα radiation (SmartLab, Rigaku, Houten, The Netherlands) over a range of 20° to 80° with a step size of 0.02°/min. The values of the chemical composition were in good agreement with those calculated, because of the correct preparation, weighing, and melting procedure.

(**a**) (**b**)

Figure 1. (**a**) The metallic load placed on the copper plate of the VAR equipment and (**b**) FeMoTaTiZr mini-ingots of high-entropy alloy obtained by melting in RAV.

2.3. Microstructural Characterisation

Preliminary operations were performed on the samples, embedding them in epoxy resin, sanding afterwards with abrasive paper (360 to 2500 grain size), and polishing with alpha alumina abrasive paste (grain size between 0.3 and 0.01 µm) using Struers TegraPol-11 polishing equipment (Copenhagen, Denmark). These metallographic preparation techniques complied with ASTM E3-11 (2017) [33]. The Kroll reactive solution was employed for etching to analyse the surface of the sample. The OLYMPUS PME 3-ADL microscope (OlympusCorp., Tokyo, Japan) was subsequently employed for observations.

The morphological and structural characterisation was performed using the Auriga FESEM-FIB field emission scanning electron microscope (Carl Zeiss SMT, Oberkochen, Germany), with Gemini column for electron beam. The analysis involved X-ray diffraction conducted with the D8 Discover diffractometer (Bruker, Ettlingen, Germany). The setup included primary optics featuring a copper radiation tube (λ = 1.540598 Å) and a Göebel mirror (Bruker, Ettlingen, Germany), along with secondary optics equipped with a 1D LynxEye detector (Bruker, Ettlingen, Germany).

2.4. Heat Treatments and Microhardness

The heat treatments were performed using a Nabertherm LT 15/12/P320 furnace (Bremen, Germany) equipped with an automate regulator to maintain the parameters of the treatment. The micro-hardness was measured using the Shimadzu HMV 2T automatic tester (Shimadzu, Kyoto, Japan). In-line measurements were performed, spaced at about 1000 µm, on the homogenised zones of the ingots, before and after performing the heat treatments.

Based on the literature documentation on the effects of heat treatments performed on complex alloys with high Fe, Mo, Ta, Ti, and Zr content, it was found that the treatment temperature applicable to the FeMoTaTiZr multicomponent alloys should be in the range 900–1150 °C [29,31]. The chosen temperature for annealing was of 900 °C. The complete heat treatment procedure included the following sequence: annealing at 900 °C for 2 h in a Nabertherm furnace, followed by water quenching. The heating time was 65 min, the holding time within the maximum temperature range was 90 min, and the cooling time was 5 s. Finally, additional annealing was applied. The sample was heat-treated for 15 h in a controlled atmosphere (argon) at a temperature of 900 °C, followed by rapid cooling via argon flow purging.

2.5. Lactate Dehydrogenase (LDH) Cytotoxicity Assay

The cells used to evaluate the biocompatibility of the alloys were human bone mesenchymal stem cells (hBMSCs) isolated in the laboratory of the University of Tg. Mures (Targu Mures, Romania) and a cell line of normal human fibroblasts (NHF). Culture medium (cleared by centrifugation before testing) was analysed in duplicate for lactate dehydrogenase using the Cobas Integra 400 Plus biochemical analyzer (Roche Diagnostics, Barcelona, Spain). The activity of lactate dehydrogenase (LDH) was assessed using the UV enzymatic technique, which is frequently employed to evaluate cytotoxicity by detecting the activity of cytoplasmic enzymes released from compromised cells.

Cells in close contact with the HEA samples were examined using a Leica DMi8 (Leica Microsistemas SLU, L´Hospitalet de Llobregat, Spain) inverted microscope, employing filter cubes for FITC and Rhodamine fluorescence, followed by incubation with Calcein AM and Propidium Iodide. The study was conducted according to the ISO 10993 standard [34].

3. Results and Discussion

3.1. Microstructure

The alloy recipe was developed based on the equimolar participation of the constituent elements, considering that the elements should have atomic percentages as close as possible in the metal matrix. Mixing entropy for 5-element alloy over 1.5R, where R is the molar gas constant, is one of the values used to define the alloy as high-entropy alloy. The second-generation HEAs mainly refer to a class of HEAs containing more than four main elements and having a multiphase structure. Also, bulk metallic glasses or intermetallic compounds can be obtained from high-entropy combinations of elements. The δ-ΔH_{mix} Criteria and Ω Criteria serve as essential indicators for predicting solid solution formation [35]. Additionally, the effect of the alloy valence electron concentration is considered when evaluating the stability of the solid solution. The bond between the components will become disordered when the concentration of valence electrons fluctuates or surpasses a particular threshold, which reduces the stability of the solid solution and is beneficial for the creation of intermetallic compounds. These characteristics provide insight into atomic interactions, structural stability, and possible mechanical properties of the FeMoTaTiZr high-entropy alloy. To fully understand the way it functions, thorough experimental data (e.g., X-ray diffraction and mechanical testing) are frequently necessary.

As stated above, the design of chemical composition of the FeMoTaTiZr alloy in wt.% is Fe = 11.88; Mo = 20.34; Ta = 38.34; Ti = 10.17; Zr = 19.27, and the corresponding atomic concentrations are (at%): Fe = 20.06; Mo = 19.99; Ta = 19.98; Ti = 20.04; Zr = 19.92.

Theses atomic percentages will be used in the following calculations.

Mixing entropy ΔS_{conf} is obtained with the following formula:

$$\Delta S_{conf} = -R\sum_{i=1}^{n} c_i ln c_i \quad (1)$$

where R is the gas constant, and c_i is the atomic ratio of the *i*-th element. Then, the calculated value is 1.609R, which is greater than 1.5R.

The δ parameter quantifies the atomic size discrepancy among the constituent elements in a high-entropy alloy. A bigger difference in atomic radii results in a larger δ value, which might affect the development of solid solutions or the long-term stability of the alloy.

The formula for δ parameter is

$$\delta = 100\sqrt{\sum_{i=1}^{n} c_i\left(1-\frac{r_i}{r_0}\right)^2} \quad (2)$$

where c_i and r_i are the atomic ratio and atomic radius of the component i, and r_0 is the weighted average of the atomic radii of all elements in the alloy. The atomic size of an element is affected by the surrounding atoms. The most useful radii for discussing metallic alloys are probably those for a coordination number of 12. Atomic radii used for the calculation are [36,37]: 127.4 pm (Fe), 140 pm (Mo), 146.7 pm (Ta), 146.2 pm (Ti), and 160.2 pm (Zr), resulting in the value r_0 = 145.89 pm. Then, the calculated delta parameter value is $\delta \approx 7.4\%$.

The formula for the mixing enthalpy (ΔH_{mix}) is

$$\Delta H_{mix} = \sum_{\substack{i=1 \\ i \neq j}}^{n} c_i c_j 4 \Delta H_{mix}^{AB} \quad (3)$$

where c_i and c_j are the atomic ratio of components i and j, respectively; r_0 is the weighted average of the atomic radii of all elements in the alloy; and ΔH_{mix}^{AB} is the mixing enthalpy of the binary alloy consisting of the i-th and j-th component in regular solution obtained through Miedema model. Mixing enthalpy values are shown in Table 1 [38]. Then, the calculated mixing enthalpy parameter value is $\Delta H_{mix} = -11.1$ kJ/mol.

Table 1. Values of the mixing enthalpy (kJ/mol) of the binary alloy for FeMoTaTiZr system.

Binary Alloy	Mixing Enthalpy (kJ/mol)
Fe-Mo	−2.0
Fe-Ta	−15.0
Fe-Ti	−16.8
Fe-Zr	−24.6
Mo-Ta	−4.9
Mo-Ti	−3.6
Mo-Zr	−6.2
Ta-Ti	1.4
Ta-Zr	2.7
Ti-Zr	−0.2

It can be found that solid solution phase formation is fixed for an atomic radius difference under 6.6% and when the mixing enthalpy of the alloy is within a certain range ($-20 < \Delta H_{mix} < 5$ kJ/mol). Under these conditions, the solid solution phase of the multicomponent alloy is easily formed with respect to the amorphous phase and the intermetallic compound [35]. Following the diagram published by Zhang et al. [39] that relates δ to the mixing enthalpy of the as-cast multicomponent alloys, it can be seen that for the atomic radius difference obtained (δ = 7.4%) and the mixing enthalpy of −11.1 kJ/mol, the alloy is out of the solid solution phase formation range. For this point in the diagram, intermediate phase formation is expected.

More multicomponent alloy systems have been calculated by other scientists, and the resulting impact of mixing enthalpy on phase stability was illustrated by Guo et al. [40], where solid solutions can develop when δ is small ($\delta < 6.6\%$) and ΔH_{mix} is either slightly positive or negligibly negative ($-11.6 < \Delta H_{mix} < 3.2$ kJ/mol); the formation of the amorphous phase is almost exactly contrary to these requirements when δ is large ($\delta > 6.4\%$) and ΔH_{mix} is noticeably negative ($\Delta H_{mix} < -12.2$ kJ/mol). Then, intermetallic compounds can develop under intermediate conditions regarding δ and ΔH_{mix}.

So, for the FeMoTaTiZr samples, δ-ΔH_{mix} criteria are not fulfilled because of the δ value being slightly over the limit. Following this analysis line, a single-phase solid solution may not be obtained, but intermediate phases and intermetallic compounds can.

The Ω Criterion is presented to take into account the influence of the thermodynamic stability of configurational entropy (ΔS_{mix}). It is calculated using the following formula:

$$\Omega = \frac{T_m \Delta S_{mix}}{|\Delta H_{mix}|} \tag{4}$$

where ΔS_{mix} is the configurational entropy, and T_m is the weighted average of the components melting point. The mixing enthalpy opposes the formation of a solid solution, whereas $T_m \Delta S_{mix}$ is favourable to its formation. Thus, values of $\Omega > 1$ may determine the formation of solid solution [35].

ΔS_{mix} can be obtained with the following formula:

$$\Delta S_{mix} = \Delta S_{conf} = -R \sum_{i=1}^{n} c_i \ln c_i \tag{5}$$

where R is the molar gas constant.

A value of Ω = 2.9 is obtained, which creates the possibility of solid solution formation.

For multicomponent high-entropy alloys, the VEC of the alloy is obtained with the following formula:

$$\mathrm{VEC} = \sum_{\mathrm{i}=1}^{\mathrm{n}} \mathrm{c_i VEC_i} \tag{6}$$

where $(\mathrm{VEC})_\mathrm{i}$ and $\mathrm{c_i}$ are the VEC and the atomic ratio for the *i*-th element, respectively.

The following $(\mathrm{VEC})_\mathrm{i}$ values were used [41]: 8 (Fe), 6 (Mo), 5 (Ta), 4 (Ti), and 4 (Zr). Then, the calculated value of the valence electron concentration for the alloy is 5.40. The stability of FCC and BCC solid solutions in high-entropy alloys was investigated by Guo et al. from Hong Kong Polytechnic University in relation to the valence electron concentration (VEC) [42]. The FCC solid solution phase is thought to be stable when VEC $\geq$ 8.6, whereas the BCC solid solution phase is thought to be relatively stable when VEC < 6.87. However, it cannot be used as a criterion for the formation of a high-entropy alloy phase; rather, it can only be used to determine which structure of the solid solution in the high-entropy alloy is easier to form [41].

Figure 2 displays optical images of the sample, before and after annealing at 900 °C for 2 h in furnace atmosphere, showing both a dendritically structure. Figure 2b shows the oxidation effects located preferentially on the interdendritic area (black mini area) that were produced by keeping the heated alloy in an unprotected atmosphere. For this reason, another annealing was performed in a controlled atmosphere (argon) at the same temperature but with a longer holding period (15 h). This time, cooling was performed in an argon flow medium (Figure 3). SEM images of samples after annealing at the same temperature but for different maintanance times are presented in Figure 3a (2 h, in furnace atmosphere) and Figure 3b (15 h in argon atmosphere).

Analing the SEM images of a cross-section through the ingot (Figure 3), it was observed that the appearance of the dendrites was modified after the second annealing, and they became rounded. Also, the oxidation effects were reduced, resulting in better alloy homogeneity. The semi-quantitative composition spectra of the zone integrated with elemental mapping for the central zone of the analysed alloy (Figure 3a) are presented in Figure 4, highlighting the composition of the alloy (wt.%): 26.9% Zr, 25.8% Ta, 17.9% Mo, 15.2% Fe, 13.1% Ti, and 1.1% Si. The distribution map of the elements providing indications regarding the constituents is shown in Figure 5. The presence of small amounts of oxygen

and Si (1.1 wt.%) probably comes from grit paper (SiC and Al_2O_3), being located mainly in dendrites, along with Mo and Ta. All chemical elements from the alloy are well distributed in the dendritic metallic matrix.

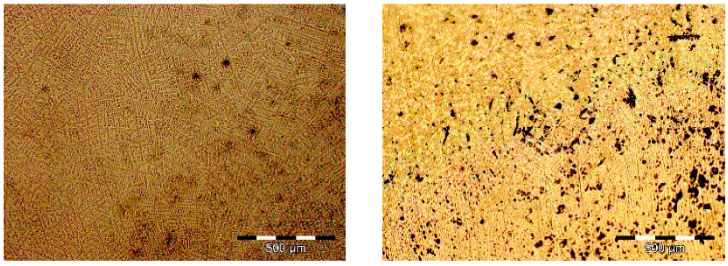

(**a**) (**b**)

Figure 2. Optical images of the the FeMoTaTiZr multicomponent alloy: (**a**) before first heat treatment and (**b**) after heat treatment.

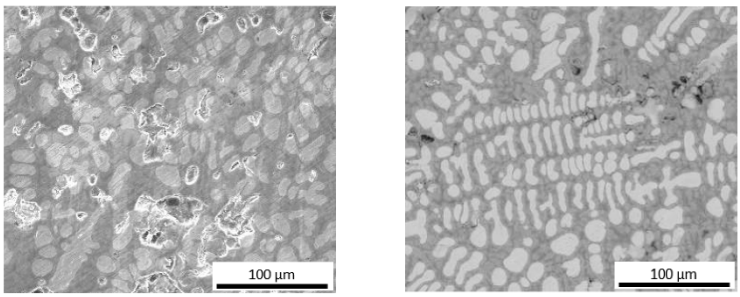

(**a**) (**b**)

Figure 3. SEM images of the FeMoTaTiZr multicomponent alloy: (**a**) after annealing at 900 °C for 2 h in furnace atmosphere; (**b**) after annealing at 900 °C for 15 h in argon atmosphere.

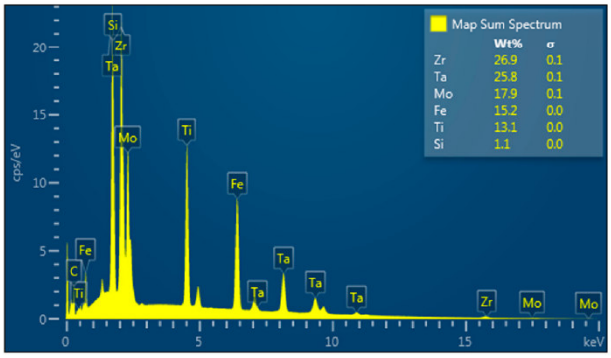

Figure 4. Semi-quantitative composition spectra of the area integrated with elemental mapping from Figure 3a.

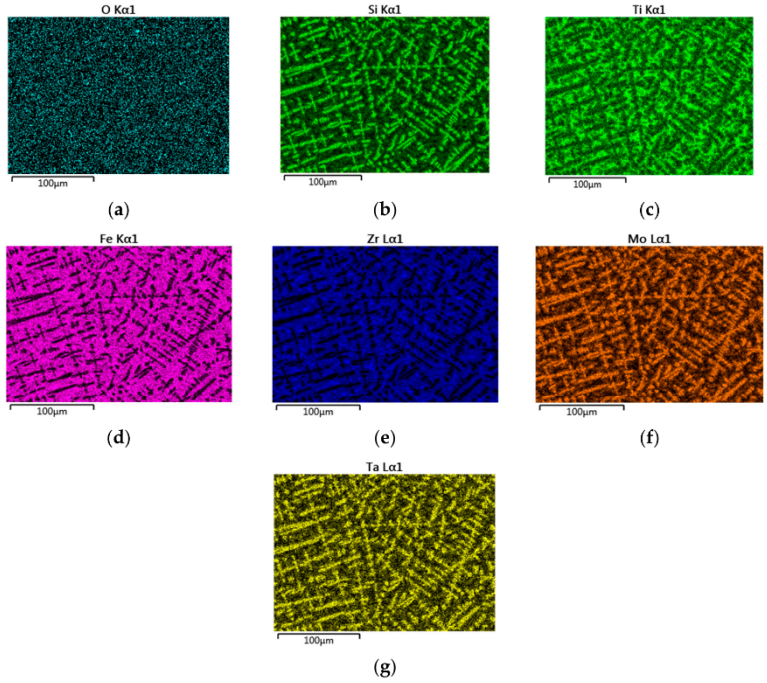

Figure 5. Map of the distribution of the elements in the microstructure of the FeMoTaTiZr alloy in the central region after casting: (**a**) O; (**b**) Si; (**c**) Ti; (**d**) Fe; (**e**) Zr; (**f**) Mo; (**g**) Ta.

The results yielded by the composition analysis were confirmed by X-ray diffraction tests. The diffraction patterns were captured with an angular increment of 0.040 at a scanning rate of 1 s per step. The qualitative analysis utilised the ICDD Release 2014 database. The X-ray diffraction diagram of the FeMoTaTiZr multicomponent alloy is shown in Figure 6.

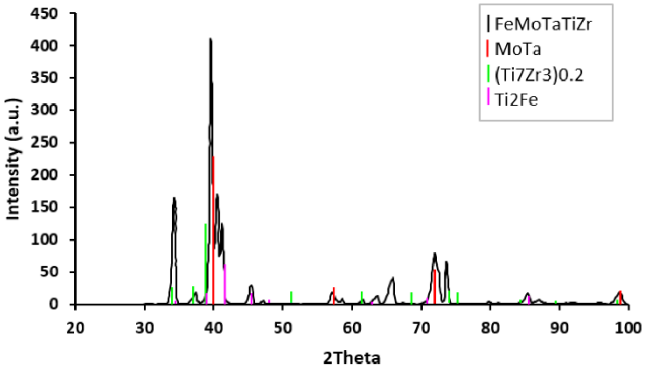

Figure 6. X-ray diffraction diagram of the as-cast FeMoTaTiZr multicomponent alloy.

The indications of the diagram in Figure 6 indicate the presence of the following constituents: bcc MoTa, hcp $(Ti_7Zr_3)_{0.2}$, fcc Ti_2Fe, and bcc Mo. The MoTa compound features the clearest indication (maximum peak), located at an angle of 2θ~40°. The presence validates the findings derived from mapping associated with the composition of dendrites in the FeMoTaTiZr high-entropy alloy. The other two constituents, $(Ti_7Zr_3)_{0.2}$ at an angle 2θ = 34° and Ti_2Fe at an angle 2θ = 41.5°, progressively separate from the metal melt at different temperatures, according to the mutual solubility and the electrochemical affinity of the constituent elements, contributing to the composition of the dendritic matrix.

To homogenise the solid solution, a first heat treatment (annealing followed by quenching) was performed. After the annealing, the homogeneity of the alloy was improved, the mass proportions of the constituents identified in the alloy being relatively close, but differences were found in terms of the constituents identified in the alloy in the cast state and those identified in the heat-treated state (Figure 7).

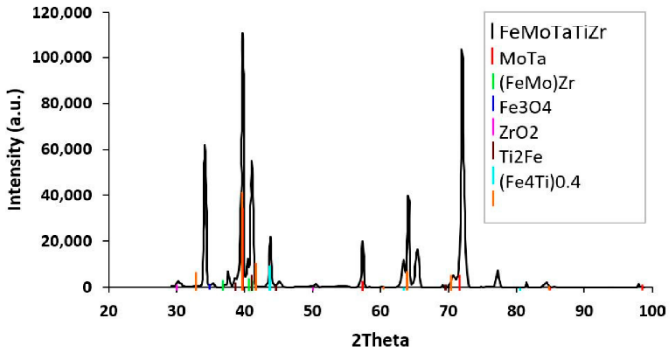

Figure 7. X-ray diffraction spectrum of FeMoTaTiZr alloy sample heat-treated in air at 900 °C/2 h, followed by fast cooling in water.

Some constituents, like oxides such as ZrO and Fe_3O_4, appeared in the solid solution due to the heat treatment conditions (heating in furnace atmosphere without protection, followed by cooling in water). Other compounds, such as $Fe_{0.2}Mo_{1.8}Zr$ and $(Fe_4Ti)_{0.4}$, are also present. The real changes brought to the alloy by heat treatment were obtained by annealing for 15 h in a controlled atmosphere (argon) at a temperature of 900 °C, followed by rapid cooling by argon flow purging.

In the analysis of the constituents identified (Figure 8), the long-period heat treatment led to the disappearance of the solid phase (FeMo)Zr and the appearance of new compounds, $Fe_{3.2}Mo_{2.1}$, $Mo_{0.93}Zr_{0.07}$, and $Zr(MoO_4)_2$. Also, the compounds based on Ti and Fe were modified, and instead of Ti_2Fe and Ti_7Zr_3, the compounds $Ti_{0.801}Fe_{0.197}$ and TiZr, respectively, appear. This is the consequence of maintaining for longer periods of time at high temperatures, when it is possible to separate some compounds from the initial solid solution matrix [31]. An additional microstructure study of the samples after a second annealing was conducted. A SEM image of the annealed area is shown in Figure 9, keeping a clear dendritic structure in which the tendency for dendrites to round is observed. Semi-quantitative composition spectra of different regions of the SEM image are shown in Figure 10.

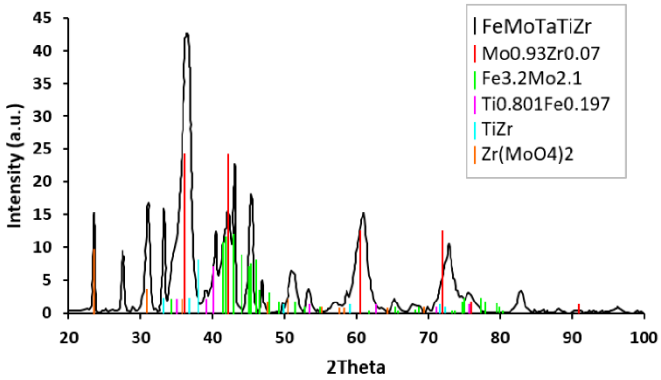

Figure 8. XRD results for FeMoTaTiZr alloy heat treated at 900 °C for 15 h in argon atmosphere followed by fast cooling in argon flow. The black and red lines represent the observed and calculated intensities in comparison.

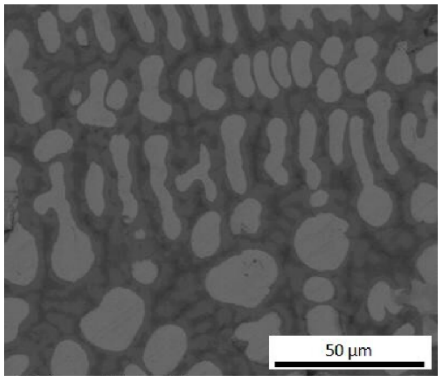

Figure 9. SEM micrograph of the FeMoTaTiZr alloy after annealing at 900 °C for 15 h.

In the semi-quantitative composition spectra (Figure 10), the dendrites in the annealed micro-areas are homogeneous from a compositional point of view. The chemical composition depends on the measurement area. Figure 10a shows the composition inside the dendrite, whereas Figure 10b–d shows the composition in the interdendritic regions. The chemical composition of the dendrites (Figure 10a) in the analysed micro area is within quite narrow limits, as follows (wt.%): Ta: 50.7–53, Mo: 36.8–38.2, Ti: 5.7–6.2, Zr: 2.4–2.6, and Fe: 1.3–1.7, and the oxygen content is constant, O: 0.9. These values clearly indicate that the dendrites are preferentially composed of chemical elements such as Ta and Mo, while in the interdendritic areas, the main elements are Zr, Fe, and Ti. The elements in the interdendritic region of the alloy had compositions within the following value ranges (wt.%): Zr: 33.8–37.8, Fe: 20.5–25.6, Ti: 15.1–19.7, Ta: 10.2–17.5, Mo: 5.6–11.9. Also, in this region, the oxygen content is constant at O: 1.2.

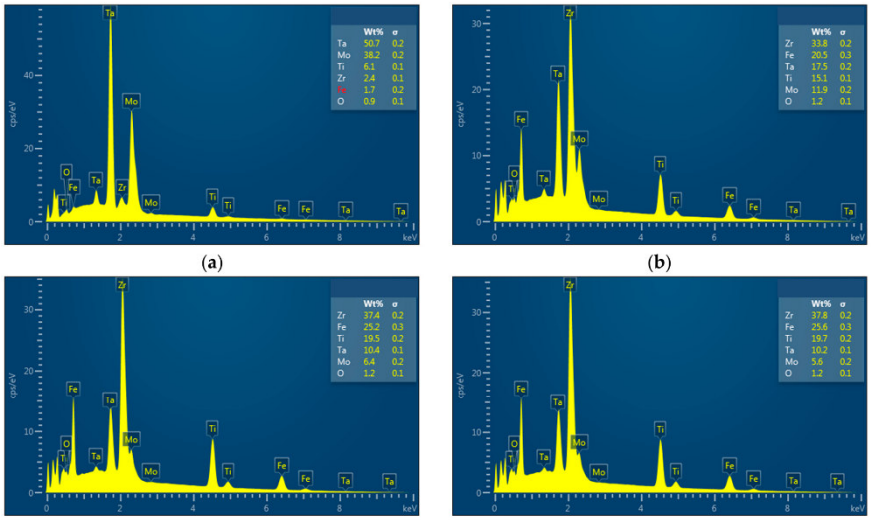

Figure 10. Image of secondary electrons and semi-quantitative composition of FeMoTaTiZr alloy after heat treatment at 900 °C for 15 h: (**a**) dendritic region and (**b**–**d**) interdendritic region.

3.2. Microhardness

The hardness was measured on both cast and heat-treated alloys, and the measurement values are shown in Table 2. The hardness measurements were performed in the homogenised zones of the ingots, on the cross-sections, using 10 different indentations, with a test force of 4.903 N and a load time of 10 s. The average hardness of the FeMoTaTiZr alloy in the cast state was 694 $HV_{0.5}$, and the heat treatment hardened it to 800 $HV_{0.5}$. The hardening level in the case of this alloy is more than 6% higher than the value obtained in the cast state.

Table 2. Microhardness values for FeMoTaTiZr samples in different thermal processing stages.

Alloy	Individual Values					Average Value	Variation Coefficient
As-cast (without heat treatment)							
FeMoTaTiZr	701	696	693	700	679	694	1.28
After annealing at 900 °C for 2 h							
FeMoTaTiZr	739	784	901	767	811	800	7.75
After annealing at 900 °C for 15 h							
FeMoTaTiZr	720	725	743	732	735	731	3.1

The considerable differences between the hardness values can be attributed to the presence of hard phases distributed in different zones of the metallic matrix. After performing the second annealing at 900 °C for 15 h, the microhardness decreased to 731 $HV_{0.5}$ due to stress relief effects; the dissolution of the solid phase (FeMo)Zr; and the appearance of new compounds like $Fe_{3.2}Mo_{2.1}$, $Mo_{0.93}Zr_{0.07}$, and $Zr(MoO_4)_2$.

3.3. Lactate Dehydrogenase (LDH) Cytotoxicity Assay

Lactate dehydrogenase (LDH) is an inert cytoplasmic enzyme present in all cells. LDH is swiftly released into the culture media when the plasma membrane of cultured cells is compromised during apoptosis, necrosis, and other types of cellular injury. The culture conditions provided enough cells (5–6 $\times$ 10^6 cells) for characterising cell viability and proliferation on the metallic substrate. Mesenchymal stem cells harvested from a 75 cm^2 tube were counted, checked for viability, and sub-cultured into two 75 cm^2 tubes (split ratio 1:2). The cells used to evaluate the biocompatibility of the alloys were human bone mesenchymal stem cells isolated in laboratory and a normal human fibroblast (NHF) cell line, kindly provided by Professor Mark Slevin from the Angiogenesis and Vascular Biology group at Manchester Metropolitan University.

Cells were stained with a Live/Dead Cell Double Staining Kit (Sigma cat. No. D4511-1KT-F) containing fluorochromes Propidium Iodide (PI) and Calcein AM. The optimal concentration established was 5 µL of PI and 10 µL of Calcein AM in 10 mL of phosphate-buffered saline (PBS) solution. Cytotoxicity was assessed by evaluating the activity of cytoplasmic enzymes produced from injured hBMSCs (human bone mesenchymal cells) and NHFs (normal human fibroblast cells). The degree of cell proliferation, viability, and adhesion of cells upon contact with the experimental alloy was monitored. The epifluorescence microscopy technique shows that cells have adhered to the alloy surface, making it necessary to investigate the adhesion and cellular morphology with specific markers in confocal microscopy. Using the same technique, cellular proliferation was observed both in the proximity of the alloy and on its surface. Cells in direct contact with the alloy samples were analysed in the Leica DMi8 inverted microscope using FITC and Rhodamine fluorescence cubes after incubation with Calcein AM and Propidium Iodide. The phase contrast image was also acquired on the same microscopic field of view (FOV), which allows for easy visualisation of the alloy sample in the well. For comparison, the evolution of the biological material prepared in the well without the presence of the metallic alloy was analysed after 5 and 10 days (Figure 11).

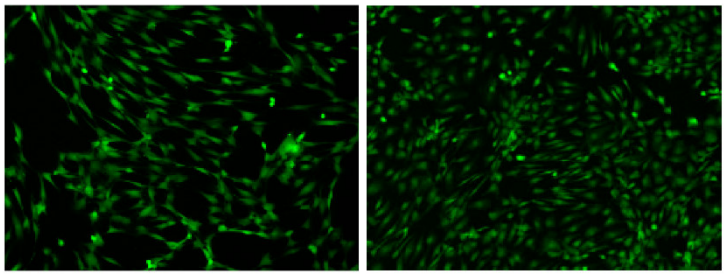

(**a**) (**b**)

Figure 11. Viability, adhesion, and proliferation of mesenchymal stem cells isolated from bone tissue in control wells, without alloy (fluorescence 100×): (**a**) after 5 days; (**b**) after 10 days.

At the same time, wells in which biological solutions were cultivated on discs taken from metal alloys were also examined after the same maintenance periods (Figure 12).

The phase contrast image was also acquired on the same microscopic field of view (FOV), which allowed for easy visualisation of the alloy sample in the well (Figure 13).

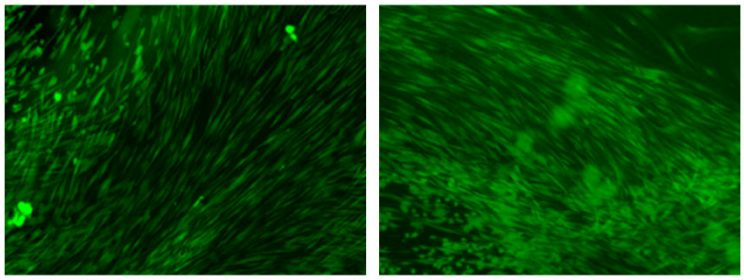

(**a**) (**b**)

Figure 12. Viability, adhesion, and proliferation of mesenchymal stem cells isolated from bone tissue in control wells with alloy (fluorescence 100×): (**a**) after 5 days; (**b**) after 10 days.

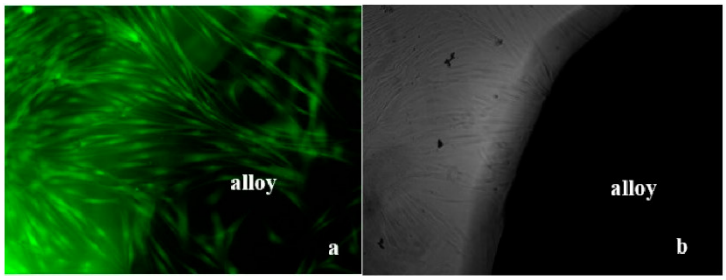

Figure 13. Viability, adhesion, and proliferation of human fibroblast cell line upon contact with FeMoTaTiZr alloys after 10 days. (**a**) Fluorescence, 100×; (**b**) phase contrast in same observation field, 100×.

In the images presented in Figures 11–13, it is observed that cellular proliferation from 80 to 90% confluence of the human fibroblast line was obtained both in the vicinity of the alloy and on its surface. In cytotoxicity tests performed on FeMoTaTiZr alloys, increases in LDH activity were recorded after 10 days in culture, with values double those in control wells with NHF and values 3.7 times higher than those in control wells with hBMSC.

The increase in LDH activity occurred both in the wells with cells cultured on alloys and in the wells with cells cultured without alloys, which means that it was not the presence of the metal alloy disc that led to certain cytolysis phenomena (cytotoxicity). At the same time, it was found that the greatest increases in LDH activity were recorded in the wells in which NHF were cultured. They have a higher proliferation capacity and cause overcrowding of the cell culture surface, causing the occurrence of apoptosis and necrosis in cell cultures.

4. Conclusions

The FeMoTaTiZr high-entropy alloy consisted of chemicals with low bio-toxicity for the human body, which occurs in classic alloys used in the manufacturing of non-implantable medical devices. The EDS analysis indicated a good agreement between the values of the chemical compositions proposed and obtained for the experimental alloys.

Values of mixing enthalpy and mixing entropy are in line with the formation of a solid solution, but the atomic size discrepancy among the constituent elements is slightly out

of range, which is not favourable for solid solution formation. Multi-phase solid solution formation is more likely to happen.

The morphological characterisation of the cast FeMoTaTiZr alloys highlighted a predominantly dendritic structure. The compositional analysis performed using the dispersive energy probe and the structural characterisation of the alloy, performed using X-ray diffraction, revealed the dendritic separation of the MoTa-type compounds in the fine dendritic matrix composed of $(Ti_7Zr_3)_{0.2}$ and Ti_2Fe-type constituents.

Annealing at 900 °C for 2 h performed in a furnace without a protective atmosphere, followed by quenching in water, promoted a high oxidation effect located preferentially on the interdendritic area. On the contrary, annealing at 900 °C for 15 h performed in an inert atmosphere (argon) followed by cooling in continuous argon flow created a better effect of homogenisation of the microstructure; dissolution of some compounds initially separated from the solid solution, like (FeMo)Zr; stress relief of the matrix; and reduction of hardness; as well as the appearance of new compounds, such as $Fe_{3.2}Mo_{2.1}$, $Mo_{0.93}Zr_{0.07}$, and $Zr(MoO_4)_2$.

Microhardness tests performed on the FeMoTaTiZr alloy, both in the as-cast state and after combined annealing and quenching heat treatments, revealed changes in the hardening effects of the metallic matrix.

Thus, annealing at 900 °C with a 2 h hold time in a furnace without a controlled atmosphere, followed by quenching in water, resulted in an increase in hardness from 694 $HV_{0.5}$ to 800 $HV_{0.5}$, the hardening level being over 6%. Annealing at the same temperature and a 15 h hold time in an inert atmosphere, followed by cooling in an argon flow, created a reduction in hardness from 800 to 730 $HV_{0.5}$.

Following cell proliferation tests and observations made using optical and phase contrast microscopy, it was established that the FeMoTaTiZr alloy allowed cell adhesion and multiplication to 80 and 90% confluence after 5 and 10 days of maintenance, respectively. Cytotoxicity tests showed that there is a slight cytotoxic reaction towards hBMSCs more sensitive than NHF cells. This phenomenon of cytolysis (cytotoxicity) occurred due to the more intense proliferation of this cell line because of the overcrowding of the culture surface with cells. Observations on the proliferation level with an increased intensity of NHF solutions led to the idea that a lower density per well, of approximately 10–20 $\times$ 10^4, is necessary.

Author Contributions: M.L.-R.: investigation, methodology and conceptualisation, and writing of the original draft; I.M.M.: investigation and methodology; V.G.: investigation, methodology, and writing—review and editing; I.V.: investigation, methodology, and writing—review and editing; J.M.-R.: data validation, project administration, visualisation, and review and editing. All authors have read and agreed to the published version of the manuscript.

Funding: This research received no external funding.

Data Availability Statement: The original contributions presented in this study are included in the article. Further inquiries can be directed to the corresponding authors.

Acknowledgments: We hereby acknowledge the project "The Smart Healthcare Engineering (SHEng)", with number 2023-1-RO01-KA220-HED-000159985, co-funded by the European Union. We also acknowledge Mark Slevin from the Angiogenesis and Vascular Biology group at Manchester Metropolitan University (UK), as well as the Hajnal Kelemen and Doina Manu from the University of Tg. Mures (Romania) for their assistance and advice in the cytotoxicity investigation.

Conflicts of Interest: The authors declare no conflicts of interest.

References

1. George, E.P.; Curtin, W.A.; Tasan, C.C. High Entropy Alloys: A Focused Review of Mechanical Properties and Deformation Mechanisms. *Acta Mater.* **2020**, *188*, 435–474. [CrossRef]
2. Han, L.; Zhu, S.; Rao, Z.; Scheu, C.; Ponge, D.; Ludwig, A.; Zhang, H.; Gutfleisch, O.; Hahn, H.; Li, Z.; et al. Multifunctional High-Entropy Materials. *Nat. Rev. Mater.* **2024**, *9*, 846–865. [CrossRef]
3. Mishra, R.S.; Haridas, R.S.; Agrawal, P. High Entropy Alloys—Tunability of Deformation Mechanisms through Integration of Compositional and Microstructural Domains. *Mater. Sci. Eng. A* **2021**, *812*, 141085. [CrossRef]
4. Yeh, J.-W.; Chen, S.-K.; Lin, S.-J.; Gan, J.-Y.; Chin, T.-S.; Shun, T.; Tsau, C.-H.; Chang, S.Y. Nanostructured High-Entropy Alloys with Multiple Principal Elements: Novel Alloy Design Concepts and Outcomes. *Adv. Eng. Mater.* **2004**, *6*, 299–303. [CrossRef]
5. Brito-Garcia, S.; Jimenez-Marcos, C.; Mirza-Rosca, J.; Voiculescu, I. Behavior of Ti-doped CoCrFeMoNi High Entropy Alloy. *Microsc. Microanal.* **2023**, *29*, 439–444. [CrossRef]
6. Zhang, E.; Zhao, X.; Hu, J.; Wang, R.; Fu, S.; Qin, G. Antibacterial Metals and Alloys for Potential Biomedical Implants. *Bioact. Mater.* **2021**, *6*, 2569–2612. [CrossRef] [PubMed]
7. Bandyopadhyay, A.; Mitra, I.; Goodman, S.B.; Kumar, M.; Bose, S. Improving Biocompatibility for next Generation of Metallic Implants. *Prog. Mater. Sci.* **2023**, *133*, 101053. [CrossRef]
8. Baltatu, M.S.; Spataru, M.C.; Verestiuc, L.; Balan, V.; Solcan, C.; Sandu, A.V.; Geanta, V.; Voiculescu, I.; Vizureanu, P. Design, Synthesis, and Preliminary Evaluation for Ti-Mo-Zr-Ta-Si Alloys for Potential Implant Applications. *Materials* **2021**, *14*, 6806. [CrossRef]
9. Yang, W.; Pang, S.; Liu, Y.; Wang, Q.; Liaw, P.K.; Zhang, T. Design and Properties of Novel Ti–Zr–Hf–Nb–Ta High-Entropy Alloys for Biomedical Applications. *Intermet* **2022**, *141*, 107421. [CrossRef]
10. Wang, S.-P.; Xu, J. TiZrNbTaMo High-Entropy Alloy Designed for Orthopedic Implants: As-Cast Microstructure and Mechanical Properties. *Mater. Sci. Eng. C* **2016**, *73*, 80–89. [CrossRef] [PubMed]
11. Todai, M.; Nagase, T.; Hori, T.; Matsugaki, A.; Sekita, A.; Nakano, T. Novel TiNbTaZrMo High-Entropy Alloys for Metallic Biomaterials. *Scr. Mater.* **2017**, *129*, 65–68. [CrossRef]
12. Wang, J.; Bai, S.; Tang, Y.; Li, S.; Liu, X.; Jia, J.; Ye, Y.; Zhu, L. Effect of the Valence Electron Concentration on the Yield Strength of Ti–Zr–Nb–V High-Entropy Alloys. *J. Alloys Compd.* **2021**, *868*, 159190. [CrossRef]
13. Oh, M.C.; Lee, H.; Sharma, A.; Ahn, B. Controlled Valence Electron Concentration Approach to Tailor the Microstructure and Phase Stability of an Entropy-Enhanced AlCoCrFeNi Alloy. *Metall. Mater. Trans. A* **2022**, *53*, 1831–1844. [CrossRef]
14. Yang, S.; Liu, G.; Zhong, Y. Revisit the VEC Criterion in High Entropy Alloys (HEAs) with High-Throughput Ab Initio Calculations: A Case Study with Al-Co-Cr-Fe-Ni System. *J. Alloys Compd.* **2022**, *916*, 165477. [CrossRef]
15. Mirza-Rosca, J.; Hulka, I.; Fratila, A.; Saceleanu, A. Surface Characterization of 5M NaOH Ti-Ta Treated Alloys Exposed to Simulated Body Fluid. *Microsc. Microanal.* **2023**, *29*, 1259–1261. [CrossRef]
16. Malatji, N.; Lengopeng, T.; Pityana, S.; Popoola, A.P.I. Effect of Heat Treatment on the Microstructure, Microhardness, and Wear Characteristics of AlCrFeCuNi High-Entropy Alloy. *Int. J. Adv. Manuf. Technol.* **2020**, *111*, 2021–2029. [CrossRef]
17. Wang, W.; Yang, K.; Wang, Q.; Dai, P.; Fang, H.; Wu, F.; Guo, Q.; Liaw, P.K.; Hua, N. Novel Ti-Zr-Hf-Nb-Fe Refractory High-Entropy Alloys for Potential Biomedical Applications. *J. Alloys Compd.* **2022**, *906*, 164383. [CrossRef]
18. Surmeneva, M.; Grubova, I.; Glukhova, N.; Khrapov, D.; Koptyug, A.; Volkova, A.; Ivanov, Y.; Cotrut, C.M.; Vladescu, A.; Teresov, A.; et al. New Ti–35Nb–7Zr–5Ta Alloy Manufacturing by Electron Beam Melting for Medical Application Followed by High Current Pulsed Electron Beam Treatment. *Metals* **2021**, *11*, 1066. [CrossRef]
19. Matsuno, H.; Yokoyama, A.; Watari, F.; Uo, M.; Kawasaki, T. Biocompatibility and Osteogenesis of Refractory Metal Implants, Titanium, Hafnium, Niobium, Tantalum and Rhenium. *Biomaterials* **2001**, *22*, 1253–1262. [CrossRef] [PubMed]
20. Gąsior, G.; Szczepański, J.; Radtke, A. Biodegradable Iron-Based Materials—What Was Done and What More Can Be Done? *Materials* **2021**, *14*, 3381. [CrossRef]
21. Chen, Q.; Thouas, G.A. Metallic Implant Biomaterials. *Mater. Sci. Eng. R Rep.* **2015**, *87*, 1–57. [CrossRef]
22. Xiang, T.; Zhao, M.; Du, P.; Xie, G. Heat Treatment Effects on Microstructure and Mechanical Properties of TiZrNbTa High-Entropy Alloy. *J. Alloys Compd.* **2023**, *930*, 167408. [CrossRef]
23. Guo, W.; Li, J.; Qi, M.; Xu, Y.; Ezatpour, H.R. Effects of Heat Treatment on the Microstructure, Wear Behavior and Corrosion Resistance of AlCoCrFeNiSi High-Entropy Alloy. *Intermet* **2021**, *138*, 107324. [CrossRef]
24. Brito-Garcia, S.; Jimenez-Marcos, C.; Mirza-Rosca, J.; Voiculescu, I. An investigation of elastic modulus in Zr doped CoCrFeMoNi HEA by three-point bending. *Microsc. Microanal.* **2023**, *29*, 439–444. [CrossRef]
25. Schuh, B.; Völker, B.; Todt, J.; Schell, N.; Perrière, L.; Li, J.; Couzinié, J.P.; Hohenwarter, A. Thermodynamic Instability of a Nanocrystalline, Single-Phase TiZrNbHfTa Alloy and Its Impact on the Mechanical Properties. *Acta Mater.* **2018**, *142*, 201–212. [CrossRef]
26. Senkov, O.; Scott, J.; Senkova, S.; Meisenkothen, F.; Miracle, D.; Woodward, C. Microstructure and Elevated Temperature Properties of a Refractory TaNbHfZrTi Alloy. *J. Mater. Sci.* **2012**, *47*, 4062–4074. [CrossRef]

27. Kuroda, D.; Kawasaki, H.; Yamamoto, A.; Hiromoto, S.; Hanawa, T. Mechanical Properties and Microstructures of New Ti–Fe–Ta and Ti–Fe–Ta–Zr System Alloys. *Mater. Sci. Eng. C* **2005**, *25*, 312–320. [CrossRef]
28. Chang, Y.-J.; Jui, C.-Y.; Lee, W.-J.; Yeh, A.-C. Prediction of the Composition and Hardness of High-Entropy Alloys by Machine Learning. *JOM* **2019**, *71*, 3433–3442. [CrossRef]
29. Yao, H.; Qiao, J.-W.; Hawk, J.; Ma, S.; Zhou, H. MoNbTaV Medium-Entropy Alloy. *Entropy* **2016**, *18*, 189. [CrossRef]
30. Liang, S.; Wang, Y.; Li, Y.; Gong, J.; Wu, W.; Hu, L.; Chen, Z. Structure and Mechanical Properties of Ambient Ductile TiZrNbHf Refractory High-Entropy Alloy: A First Principles and Experimental Study. *Vacuum* **2025**, *233*, 113910. [CrossRef]
31. Sheikh, S.; Bijaksana, M.K.; Motallebzadeh, A.; Shafeie, S.; Lozinko, A.; Gan, L.; Tsao, T.-K.; Klement, U.; Canadinc, D.; Murakami, H.; et al. Accelerated Oxidation in Ductile Refractory High-Entropy Alloys. *Intermet* **2018**, *97*, 58–66. [CrossRef]
32. Gartland, A.; Rumney, R.M.; Dillon, J.P.; Gallagher, J.A. Isolation and Culture of Human Osteoblasts. In *Human Cell Culture Protocols*; Picot, J., Ed.; Humana Press: Totowa, NJ, USA, 2005; pp. 29–54, ISBN 978-1-59259-861-8.
33. *ASTM E3-11*; Standard Guide for Preparation of Metallographic Specimens. ASTM International: West Conshohocken, PA, USA, 2017.
34. *ISO 10993-5*; Biological Evaluation of Medical Devices. Part 5: Tests for in Vitro Cytotoxicity. Springer: Berlin/Heidelberg, Germany, 2009.
35. Zhang, Y. Microstructures and Properties of High Entropy Alloys. *Prog. Mater. Sci.* **2014**, *61*, 1–93. [CrossRef]
36. Teatum, E.; Gschneidner, K.J.; Waber, J. *Compilation of Calculated Data Useful in Predicting Metallurgical Behavior of the Elements in Binary Alloy Systems*; Los Alamos National Laboratory (LANL): Los Alamos, NM, USA, 1959.
37. Calvo-Dahlborg, M.; Brown, S.G.R. Hume-Rothery for HEA Classification and Self-Organizing Map for Phases and Properties Prediction. *J. Alloys Compd.* **2017**, *724*, 353–364. [CrossRef]
38. Takeuchi, A.; Inoue, A. Calculations of Mixing Enthalpy and Mismatch Entropy for Ternary Amorphous Alloys. *Mater. Trans. JIM* **2000**, *41*, 1372–1378. [CrossRef]
39. Zhang, Y.; Zhou, Y.; Lin, J.; Chen, G.; Liaw, P. Solid-Solution Phase Formation Rules for Multi-component Alloys. *Adv. Eng. Mater.* **2008**, *10*, 534–538. [CrossRef]
40. Guo, S.; Hu, Q.; Ng, C.; Liu, C.T. More than Entropy in High-Entropy Alloys: Forming Solid Solutions or Amorphous Phase. *Intermet* **2013**, *41*, 96–103. [CrossRef]
41. Guo, S.; LIU, C.T. Phase Stability in High Entropy Alloys: Formation of Solid-Solution Phase or Amorphous Phase. *Progress. Nat. Sci.-Mater. Int.* **2011**, *21*, 433–446. [CrossRef]
42. Guo, S.; Ng, C.; Lu, J.; Liu, C. Effect of Valence Electron Concentration on Stability of Fcc or Bcc Phase in High Entropy Alloys. *J. Appl. Phys.* **2011**, *109*, 3587228. [CrossRef]

3. DOCUMENTO DE AUTORÍA

ULPGC

ULPGC Universidad de Las Palmas de Gran Canaria | Escuela de Doctorado

DOCUMENTO DE AUTORÍA PARA TESIS POR COMPENDIO

Los abajo firmantes, coautores del artículo titulado "*Effects of nickel content on the microstructure, microhardness and corrosion behavior of high-entropy AlCoCrFeNix alloys*", publicado en la revista "Scientific Reports" el 03 de diciembre de 2020:

The undersigned, co-authors of the article titled "*Effects of nickel content on the microstructure, microhardness and corrosion behavior of high entropy AlCoCrFeNix alloys*", published in the journal "Scientific Reports" on December 3, 2020:

- Reconocemos como autor principal del artículo a D. Miguel López Ríos, con DNI 44711206B.
  We recognize Mr. Miguel López Ríos, with DNI 44711206B, as the main author of the article.

- Renunciamos a utilizar esta publicación como núcleo principal de otras tesis doctorales, sin perjuicio de que dichas publicaciones puedan ser presentadas como méritos complementarios en las tesis doctorales que pudieran presentar los otros autores de dichas publicaciones.
  We renounce using this publication as the main nucleus of other doctoral theses, without prejudice to the fact that said publications may be presented as complementary merits in the doctoral theses that the other authors of said publications could present.

En Las Palmas de Gran canaria a 28 de febrero de 2025

Pedro Socorro Perdomo
Firmado digitalmente por Pedro Socorro Perdomo
Fecha: 2025.03.05 12:37:47 Z
P.P. Socorro Perdomo

I. Voiculescu

V. Geanta

V.Craciun

I. Boerasu

MIRZA ROSCA JULIANA CLAUDIA - 45360672A
Firmado digitalmente por MIRZA ROSCA JULIANA CLAUDIA - 45360672A
Fecha: 2025.03.07 10:00:18 Z
J.C.Mirza Rosca

ULPGC

ULPGC Universidad de Las Palmas de Gran Canaria | Escuela de Doctorado

DOCUMENTO DE AUTORÍA PARA TESIS POR COMPENDIO

Los abajo firmantes, coautores del artículo titulado "*Comparative Study of (Fe,Nb)MoTaTiZr High Entropy Alloys in Ringer Grifols Solution*", publicado en la revista "Metals" el 13 de diciembre de 2024:

The undersigned, co-authors of the article titled "*Comparative Study of (Fe,Nb)MoTaTiZr High Entropy Alloys in Ringer Grifols Solution*", published in the journal "Metals" on December 13, 2024:

- Reconocemos como autor principal del artículo a D. Miguel López Ríos, con DNI 44711206B.
  We recognize Mr. Miguel López Ríos, with DNI 44711206B, as the main author of the article.

- Renunciamos a utilizar esta publicación como núcleo principal de otras tesis doctorales, sin perjuicio de que dichas publicaciones puedan ser presentadas como méritos complementarios en las tesis doctorales que pudieran presentar los otros autores de dichas publicaciones.
  We renounce using this publication as the main nucleus of other doctoral theses, without prejudice to the fact that said publications may be presented as complementary merits in the doctoral theses that the other authors of said publications could present.

En Las Palmas de Gran canaria a 28 de febrero de 2025

Santiago Brito-Garcia

MIRZA ROSCA JULIANA CLAUDIA - 45360672A

Firmado digitalmente por MIRZA ROSCA JULIANA CLAUDIA - 45360672A
Fecha: 2025.03.07 10:00:48 Z

Julia Mirza-Rosca

Ionelia Voiculescu

ULPGC

ULPGC Universidad de Las Palmas de Gran Canaria | Escuela de Doctorado

DOCUMENTO DE AUTORÍA PARA TESIS POR COMPENDIO

Los abajo firmantes, coautores del artículo titulado "*New FeMoTaTiZr High-Entropy Alloys for Medical Applications*", publicado en la revista "Metals" el 24 de febrero de 2025:

The undersigned, co-authors of the article titled "*New FeMoTaTiZr High-Entropy Alloys for Medical Applications*", published in the journal "Metals" on February 27, 2025:

- Reconocemos como autor principal del artículo a D. Miguel López Ríos, con DNI 44711206B.
  We recognize Mr. Miguel López Ríos, with DNI 44711206B, as the main author of the article.

- Renunciamos a utilizar esta publicación como núcleo principal de otras tesis doctorales, sin perjuicio de que dichas publicaciones puedan ser presentadas como méritos complementarios en las tesis doctorales que pudieran presentar los otros autores de dichas publicaciones.
  We renounce using this publication as the main nucleus of other doctoral theses, without prejudice to the fact that said publications may be presented as complementary merits in the doctoral theses that the other authors of said publications could present.

En Las Palmas de Gran canaria a 28 de febrero de 2025

MIRZA ROSCA JULIANA CLAUDIA - 45360672A
Firmado digitalmente por MIRZA ROSCA JULIANA CLAUDIA - 45360672A
Fecha: 2025.03.07 10:01:23 Z
Julia Mirza-Rosca

Ileana Mariana Mates

Victor Geanta

Ionelia Voiculescu

5. OTRAS PUBLICACIONES

406
doi:10.1017/S1431927620014555

Microsc. Microanal. 26 (Suppl 2), 2020

AlCoCrFeNi High Entropy Alloys as Possible Nuclear Materials

Miguel Lopez Rios[1], Viviana Lucero Baldevenites[1], Ionelia Voiculescu[2] and Julia Mirza Rosca[1]

[1]University of Las Palmas de Gran Canaria, Las Palmas de GC, Canarias, Spain, [2]Politehnica University of Bucharest, Bucharest, Bucuresti, Romania

For maintaining a sustainable energy supply and ensuring the safe operation of nuclear reactors, the development of new and advanced nuclear materials is in high demand.

Recently, a new generation of structural materials, termed as multicomponent high-entropy alloys (HEAs), has been developing. The concept of high entropy provide a new path of developing advanced materials which may potentially break the properties limits of tradicional materials obtained by the conventional micro-alloying methods based on one dominant element. The HEAs consist of at least five principal metallic elements with an approximately equiatomic ratio for maximizing the compositional entropy and form a solid solution phase. Mixing of various elements results typically in high atomic-level stress, which leads to the possibility of achieving high irradiation resistances through unique damage healing mechanisms [1].

A typical HEA, the alloy AlCoCrFeNi, have been extensively studied and reported in the literature [2]. Aluminum is an interesting element because possesses the dualism of metal and nonmetal characteristics due to its special electronic structure and the properties of the alloy vary significantly with aluminum concentration. In this study, HEAs from AlxCoCrFeNi system with concentrations in aluminum varying from 0.6 to 1.0 were investigated using X-ray diffraction (XRD), optical microscopy (OM), scanning electron microscopy (SEM), transmission electron microscopy (TEM), Vickers hardness tester and Electrochemical Impedance Spectroscopy (EIS). The surface roughness was examined by Atomic Force Microscopy (AFM).

It can be observed that the particular elements of each alloy refer to the morphology of the phases and the general appearance of microstructures is dendritic. Thus, in the case of x = 1 and x = 0.6, the appearance of the dendrites is relatively rounded, while for x = 0.8 acicular formations oriented in different directions are observed. At higher magnification powers, the specific characteristics of each alloy are highlighted. Thus, in the case of x = 1, the microstructure is composed of phases arranged neatly in the metal matrix, surrounded by rectilinear grain boundaries. The microstructure of x = 0.8 sample shows the tendency of formation of the acicular phases, the grain boundaries being much wider. In the case of x = 0.6 sample, the microstructure is similar to that of x = 0.8, the presence of the two phases being better highlighted.

After EDAX analysis, two areas were considered on the HEA´s surface: one dendritic area (D) and another interdendritic area (ID) with clear differences in the element composition. A segregation parameter, segregation ratio (S_R), was introduced to demonstrate the degree of segregation of elements. The nanoscale analysis showed the D area with Fe and Co rich but Al and Ni depleted and the ID area with Al and Ni rich but Fe and Co depleted. Only Cr does not show evident differences in the two zones with a slightly higher concentration in interdrenditic area.

As Al concentration increases, the chromium effect is stronger and Co does not show evident difference in the two areas.

From Vickers tests and EIS measurements it can be observed that the increase of Aluminum concentration greatly enhanced hardness and, in consequence, the Young´s modulus and yield strength of these alloys.

Further studies regarding planned extensions in the operating life time for reactors are needed and must be supported by accompanying materials R&D for continued safe, reliable and cost-effective utilization of water-cooled nuclear reactors for electricity production.

References

[1] S. Xia, X. Yang, T. Yang, S. Liu, Y. Zhang, Irradiation resistance in AlxCoCrFeNi high entropy alloys, Jom, 67 (2015), pp. 2340-2344
[2] Zhang, Y. High-Entropy Materials A Brief Introduction, Springer Ed., 2019.

ULPGC

SMS 2019
SMART MATERIALS AND SURFACES

EGF2019
EUROPEAN GRAPHENE FORUM

NanoMedicine
2019

SMS 2019 / EGF 2019 / NanoMed 2019

Joint International Conferences and Exhibition

23 - 25 Oct. 2019

Lisbon - Portugal

Book of Abstracts

Organizer

Science Technology Engineering
SETCOR
Conferences & Exhibitions

www.setcor.org

EIS Characterization of Passive Films Formed on $Al_xCoCrFeNi$ Alloys

M.López Ríos,[1] N.Florido Suárez[1], I.Voiculescu[2], V.Geanta[2], J.C.Mirza Rosca[1]*

[1] Las Palmas de Gran Canaria University, Mech. Eng.Dept.,Spain
[2] Politehnica University of Bucharest, LAMET, Bucharest, Romania

Abstract:
Electrochemical Impedance Spectroscopy (EIS) measurements have been performed on High Entropy Alloys (HEAs) type $Al_xCoCrFeNi$ with different aluminium content (x = 0.6; 0.8 and 1.0) in order to characterize their passive film and corrosion resistance at 37ºC under simulated physiological conditions (Ringer´s solution) acidulated with HCl at pH=3. The impedance spectra were obtained at different potential values between E_{corr} and + 0.7 V vs. SCE.
Analysis of the impedance spectra was done by fitting the experimental data to different equivalent circuits. Two equivalent circuits, with one time constant and two time constants respectively, can be satisfactory used for fitting the spectra: one time constant represents the characteristics of the passive film and the second one is for the charge transfer reactions.
The polarization resistance and the double layer capacity were compared at different polarization potentials for the detection of the passive film structure and the roughness of the electrode surface.
It can be seen for both materials that the resistence of the passive film is very high and decreases slightly with the potential: the very high resistance of the passive film implies a high corrosion resistance which can be attributed to the formation of the protective oxide layer.
There is a decrease in the values of the parameter n of the CPE (constant phase element used in the mathematically modelling in order to consider also the electrochemical behavior of systems which do not correspond exactly to a pure capacitance) related to the rugosity of the electrode surface.

Keywords: high entropy alloys, aluminium, EIS, equivalent circuit, corrosion resistance, passivation, Ringer solution.

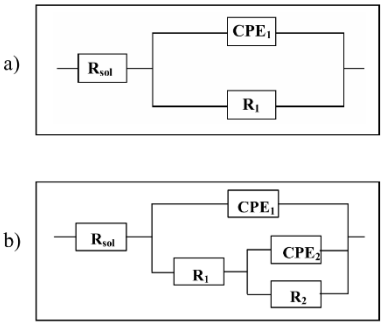

Figure 1: Figure illustrating the equivalent ciruits used for the fitting of the experimental data where R_{sol} is the ohmic resistance of the electrolyte. a) The first circuit has one time constant.
b) The second equivalent circuit fitted for HEAs in Ringer's solution of pH = 3 presents the second time constant which illustrates the slight porosity of the passive layer on the alloy surface (R_1 and CPE_1). So, the equivalent circuit contains in addition a parallel circuit for charge transfer reactions through the passive layer consisting of the double layer capacitance CPE_2 and charge transfer resistance R_2.

References:

1. B. Gwalani, S. Gorsse, D. Choudhuri, Y. Zheng, R.S.Mishra, R. Banerjee (2019) Tensile yield strength of a single bulk Al0.3CoCrFeNi high entropy alloy can be tuned from 160 MPa to 1800 MPa, *Scripta Materialia,* 162, 18-23
2. Z.Li, S.Zhao, R.O.Ritchie, M.A.Meyers (2019) Mechanical properties of high-entropy alloys with emphasis on face-centered cubic alloys, *Progress in Materials Science,* 102, 296-345.
3. D.B.Miracle, O.N.Senkov, A critical review of high entropy alloys and related concepts (2017), *Acta Materialia*, 122, 448-511.

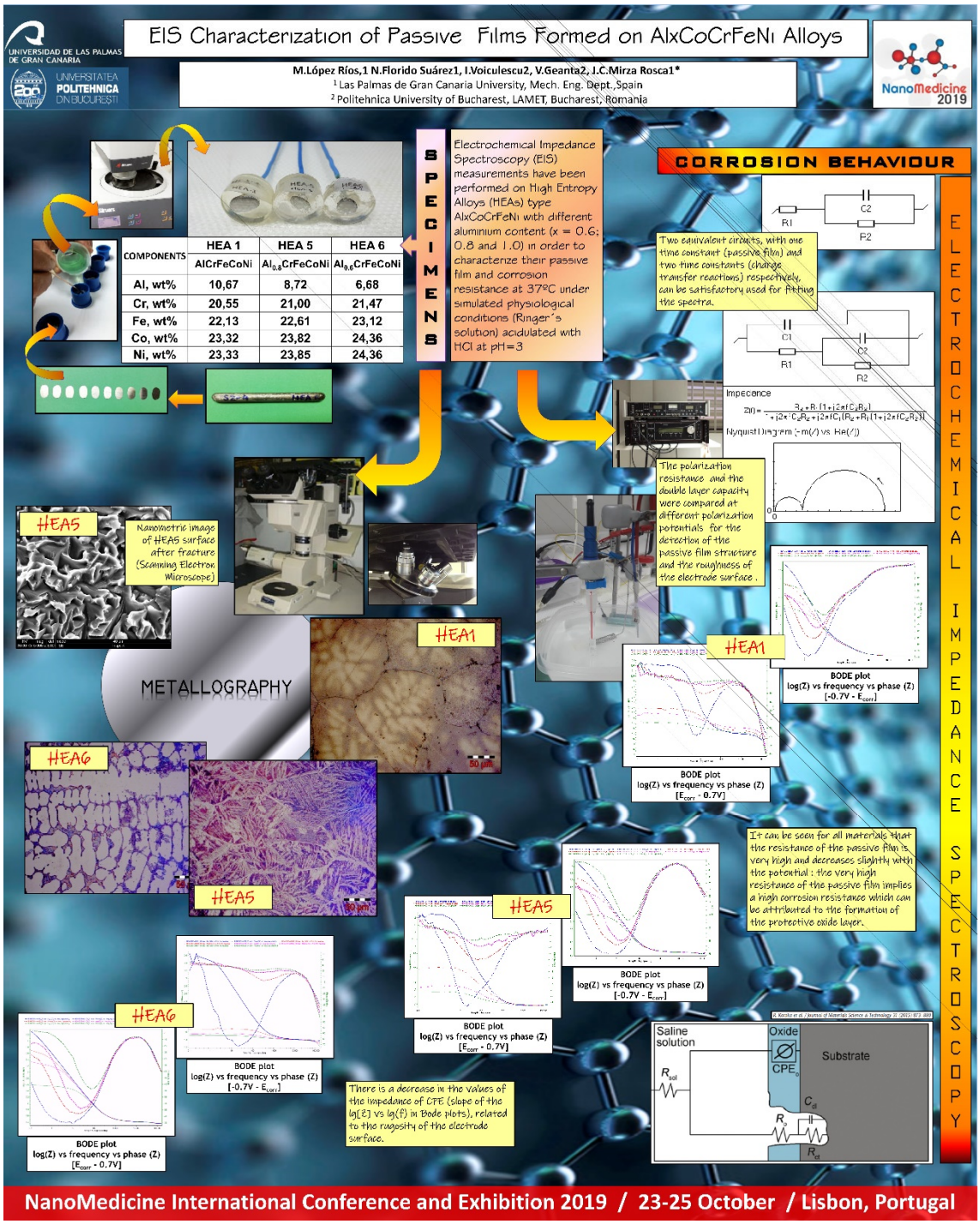
EIS Characterization of Passive Films Formed on AlxCoCrFeNi Alloys
M.López Ríos,1 N.Florido Suárez1, I.Voiculescu2, V.Geanta2, I.C.Mirza Rosca1*
[1] Las Palmas de Gran Canaria University, Mech. Eng. Dept.,Spain
[2] Politehnica University of Bucharest, LAMET, Bucharest, Romania
NanoMedicine 2019
SPECIMENS
Electrochemical Impedance Spectroscopy (EIS) measurements have been performed on High Entropy Alloys (HEAs) type AlxCoCrFeNi with different aluminium content (x = 0.6; 0.8 and 1.0) in order to characterize their passive film and corrosion resistance at 37ºC under simulated physiological conditions (Ringer´s solution) acidulated with HCl at pH=3
COMPONENTS | HEA 1 AlCrFeCoNi | HEA 5 Al0.8CrFeCoNi | HEA 6 Al0.6CrFeCoNi
Al, wt% | 10,67 | 8,72 | 6,68
Cr, wt% | 20,55 | 21,00 | 21,47
Fe, wt% | 22,13 | 22,61 | 23,12
Co, wt% | 23,32 | 23,82 | 24,36
Ni, wt% | 23,33 | 23,85 | 24,36
CORROSION BEHAVIOUR
Two equivalent circuits, with one time constant (passive film) and two time constants (charge transfer reactions) respectively, can be satisfactory used for fitting the spectra.
R1
C2
R2
C1
Impedance
Nyquist Diagram (-Im(Z) vs Re(Z))
The polarization resistance and the double layer capacity were compared at different polarization potentials for the detection of the passive film structure and the roughness of the electrode surface .
ELECTROCHEMICAL IMPEDANCE SPECTROSCOPY
HEA5
Nanometric image of HEA5 surface after fracture (Scanning Electron Microscope)
METALLOGRAPHY
HEA1
HEA6
HEA5
BODE plot
log(Z) vs frequency vs phase (Z)
[-0.7V - Ecorr]
It can be seen for all materials that the resistance of the passive film is very high and decreases slightly with the potential : the very high resistance of the passive film implies a high corrosion resistance which can be attributed to the formation of the protective oxide layer.
There is a decrease in the values of the impedance of CPE (slope of the lg[Z] vs lg(f) in Bode plots), related to the rugosity of the electrode surface.
Saline solution
Oxide
Substrate
CPE
Rsol
Rp
Cdl
Rct
NanoMedicine International Conference and Exhibition 2019 / 23-25 October / Lisbon, Portugal

Effects of Nickel Content on the Microstructure, Microhardness and Corrosion Behavior of High-entropy AlCoCrFeNi$_x$ Alloys

M.López Ríos,[1] P.P.Socorro Perdomo[1],
V.Lucero Baldevenites[1], I.Voiculescu[2], V.Geanta[2], J.C.Mirza Rosca[1*]

[1] Las Palmas de Gran Canaria University, Mech. Eng.Dept.,Spain
[2] Politehnica University of Bucharest, LAMET, Bucharest, Romania

Abstract:
The pioneering efforts in obtaining the high entropy alloys (HEAs) created the groundwork for a new concept in alloy design by finding new equiatomic combinations of elements for advanced materials with unique properties.
In this study we investigate the effect of different nickel concentration on the microstructure, hardness and corrosion properties of high entropy alloys from AlCrFeCoNi system.
The analyzed HEAs were AlCrFeCoNi$_x$ with x=1; 1.4 and 1.8. These alloys were obtained by vacuum arc remelting from raw materials with high purity.
The microscopy examination has revealed the dendritic morphology for the reference alloy (AlCrFeCoNi) and the increase of the width of the interdendritic zones by increasing the nickel concentration while Cr is segregated in the interdendritic regions more than in dendrites.
Hardness values decrease with increasing the percentage of nickel because of the dissolution of precipitates in a nickel rich matrix and in consequence forming continuous solid solutions.
The corrosion properties of the HEAs were evaluated using a potentiodynamic polarization method. The alloys were immersed in SBS (Simulated Body Fluid) during one week and the corrosion parameters were registered. The low corrosion rates, low corrosion currents and high polarization resistance attest the good stability of HEAs in simulated biological environment.

Keywords: high entropy alloys, nickel, corrosion resistance, corrosion currents, polarization resitance, passivation, Ringer solution.

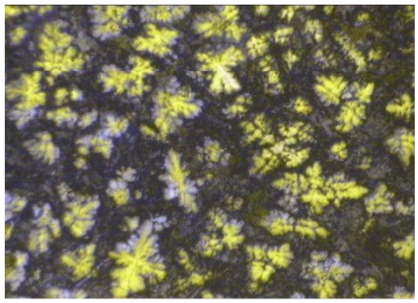

Figure 1: Figure illustrating the dendritic mor - phology of high-entropy AlCrFeCoNi$_{1.4}$ alloy after electrochemical etching in oxalic acid 10% for one minute.

References:

1. B. Gwalani, S. Gorsse, D. Choudhuri, Y. Zheng, R.S.Mishra, R. Banerjee (2019) Tensile yield strength of a single bulk Al0.3CoCrFeNi high entropy alloy can be tuned from 160 MPa to 1800 MPa, *Scripta Materialia,* 162, 18-23
2. Z.Li, S.Zhao, R.O.Ritchie, M.A.Meyers (2019) Mechanical properties of high-entropy alloys with emphasis on face-centered cubic alloys, *Progress in Materials Science,* 102, 296-345.
3. D.B.Miracle, O.N.Senkov (2017) A critical review of high entropy alloys and related concepts, *Acta Materialia*, 122, 448-511.
4. I.Voiculescu, V.Geanta, R.Stefanoiu, D.Patroi, H.Binchiciu (2013)Influence of the chemical composition on the microstructure and microhardness of AlCrFeCoNi high entropy alloy, *Revista de Chimie*, 12, 1441-1444.

Effects of Nickel Content on the Microstructure, Microhardness and Corrosion Behavior of High-entropy AlCoCrFeNi$_x$ Alloys

M .López Ríos,[1] P. P. Socorro Perdomo[1], V .Lucero Baldevenites[2], I.Voiculescu[2], V. Geanta[2], J. C. Mirza Rosca[1*]
[1] Las Palmas de Gran Canaria University, Mech. Eng. Dept.,Spain
[2] Politehnica University of Bucharest, LAMET, Bucharest, Romania

NanoMedicine 2019

UNIVERSIDAD DE LAS PALMAS DE GRAN CANARIA

UNIVERSITATEA POLITEHNICA DIN BUCUREŞTI

SPECIMENS PREPARATION

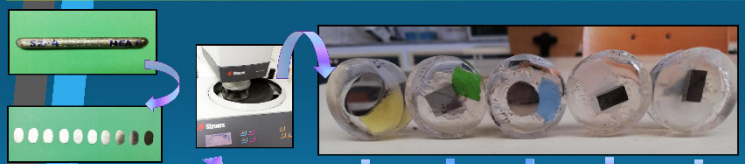

The pioneering efforts in obtaining the high entropy alloys (HEAs) created the groundwork for a new concept of solid solutions multi-principal element alloys with unique properties at the nanoscale. In this study we investigate the effect of different nickel concentration on the microstructure, hardness and corrosion properties of high entropy alloys from AlCrFeCoNi system.

COMPONENTS	HEA 1 AlCrFeCoNi	HEA 5 $Al_{0.8}$CrFeCoNi	HEA 6 $Al_{0.6}$CrFeCoNi	HEA 12 AlCrFeCoNi$_{1.4}$	HEA 14 AlCrFeCoNi$_{1.6}$
Al, wt%	10,67	8,72	6,68	9,76	8,99
Cr, wt%	20,55	21,00	21,47	18,8	17,32
Fe, wt%	22,13	22,61	23,12	20,24	18,65
Co, wt%	23,32	23,82	24,36	21,33	19,65
Ni, wt%	23,33	23,85	24,36	29,86	35,38

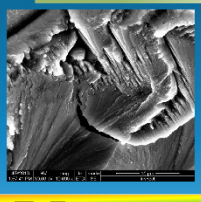

Nanometric image of HEA1 surface after fracture (Scanning Electron Microscope)

TESTS AND RESULTS

METALLOGRAPHY

HARDNESS

CORROSION

HEA1

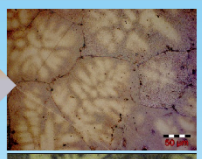

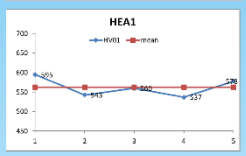

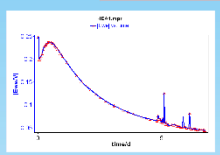

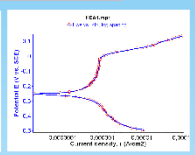

HEA12

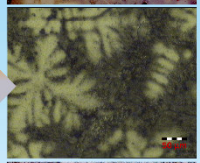

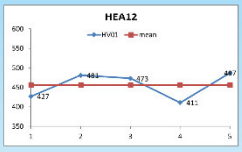

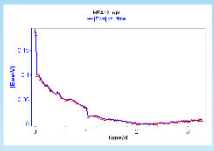

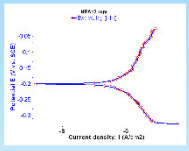

HEA14

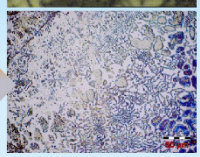

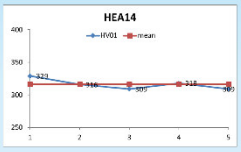

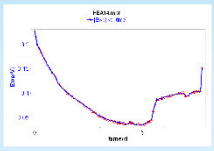

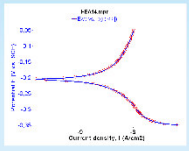

The microscopy examination reveals dendritic morphology for the reference alloy (AlCrFeCoNi) and the increase of the width of the interdendritic zones by increasing the nickel concentration.

Hardness values decrease with increasing the percentage of nickel because of the dissolution of precipitates in a nickel rich matrix and in consequence forming continuous solid solutions.

The alloys were immersed in SBS (Simulated Body Fluid) during one week . The low corrosion rates, low corrosion currents and high polarization resistance attest the good stability of HEAs in simulated biological environment.

NanoMedicine International Conference and Exhibition 2019 / 23-25 October / Lisbon, Portugal

6. CONCLUSIONES

Los tres estudios analizados contribuyen al campo de las aleaciones de alta entropía para aplicaciones biomédicas, proporcionando información valiosa sobre la relación entre la composición, la microestructura y las propiedades funcionales. Las conclusiones de este trabajo de investigación pueden consultarse en las publicaciones adjuntas en el presente documento de tesis doctoral. A modo de resumen, se exponen los siguientes puntos.

- El estudio de las aleaciones de alta entropía basadas en los elementos AlCoCrFeNi muestra la viabilidad de este sistema como base para biomateriales con buena resistencia a la corrosión.

  La observación de la microestructura mostró cómo la forma de los granos varió con el incremento de níquel, aumentando el tamaño de las regiones interdendríticas.

  Asimismo, el tratamiento térmico aplicado a las muestras mostró una distribución más uniforme de las fases para los tres niveles de níquel estudiados, así como un crecimiento de los granos.

  El ensayo de difracción de rayos X indicó la presencia de estructura cúbica en la aleación, y se observó que el aumento de níquel introdujo una nueva fase cúbica con estructura centrada en la cara (FCC). Adicionalmente, se observó en las muestras tratadas térmicamente, la aparición de una fase, también del tipo FCC, formada por aluminio y níquel. Todo lo anterior, junto con los resultados del estudio de espectroscopía de dispersión de electrones (EDS), mostró una buena homogeneidad en el material, con dos soluciones sólidas principales y algún compuesto minoritario segregado en la zona dendrítica.

  Por otro lado, las tres aleaciones mostraron buena estabilidad en el entorno biológico simulado, ya que se pudieron observar tasas bajas de corrosión.

  Finalmente, dentro del estudio de la dureza, se aprecia una tendencia a la disminución de la misma con el incremento de níquel. Este conocimiento ofrece una

vía para ajustar las propiedades mecánicas de las herramientas, según las necesidades específicas de su aplicación.

Como resumen de todo lo anterior, estos resultados muestran cómo la variación en el contenido en níquel y la aplicación de tratamientos térmicos influyen de forma significativa en la estructura y propiedades de estas aleaciones, lo que permite valorar la posibilidad de ajustar el diseño y la fabricación de aleaciones de este tipo para ajustarse a las necesidades de los instrumentos médicos en cuestión.

- El estudio de la sustitución del niobio por el hierro en el sistema de aleaciones formadas por los elementos MoTaTiZr, muestra cambios interesantes en la composición, en la dureza y en la resistencia a la corrosión de las aleaciones, las cuales fueron conformadas manteniendo porcentajes atómicos similares en ambos casos.

  En lo que a la microestructura y homogeneidad de la composición se refiere, la sustitución de niobio por hierro tiene una influencia significativa en la segregación de elementos, donde se puede ver que el hierro exhibe una mayor afinidad por las regiones interdendríticas, frente a la tendencia del niobio a repartirse entre las dos regiones (dendrítica e interdendrítica).

  Por otro lado, la variación de la resistencia a la corrosión en medio biológico simulado quedó patente por la mayor tasa de corrosión en el caso de FeHEA. Los mecanismos de corrosión de ambas aleaciones resultaron representados por el mismo circuito eléctrico equivalente en el análisis de espectroscopía de impendancia electroquímica (EIS), lo que permite concluir que ambas aleaciones muestran productos de corrosión y formación de capas similares. Pero la menor estabilidad de los productos de corrosión del hierro permite posiblemente una disolución selectiva que en este caso implica una mayor tasa de corrosión.

  Finalmente, los ensayos de microdureza no mostraron gran diferencia entre las dos aleaciones, aunque se pudo apreciar mayores valores de dureza en el caso de la aleación de hierro.

  El hallazgo de una mayor tasa de corrosión para la FeHEA, en comparación con la NbHEA, subraya la importancia de la composición en la estabilidad química de las

aleaciones de alta entropía en entornos biológicos, e implica la necesidad de una selección cuidadosa de los elementos constituyentes para estas aplicaciones. Futuras investigaciones podrían enfocarse en la pasivación y la liberación de iones a largo plazo de estas aleaciones.

- El estudio de las propiedades de una nueva aleación de alta entropía FeMoTaTiZr, diseñada con la finalidad de su aplicación en instrumentos médicos no implantables establece un punto de partida para el desarrollo de este sistema de aleaciones.

  Sobre las muestras fabricadas se realizó un análisis EDS que confirmó de forma experimental que los porcentajes composicionales de los distintos elementos en la aleación eran coherentes con los previstos en el diseño del material.

  En este estudio se expuso el valor de la entropía configuracional, el valor de la discrepancia del tamaño atómico entre los elementos constituyentes de la aleación (parámetro delta), el valor de la entalpía de mezcla, el valor del parámetro Ω y el valor de la concentración de electrones de valencia (VEC), calculados todos para la aleación diseñada en este artículo. Todos estos valores anteriores son algunos de los parámetros más utilizados para caracterizar a las aleaciones de alta entropía frente a las aleaciones tradicionales. Los resultados obtenidos indican la confirmación de la formación de una aleación de alta entropía y, en su mayoría, son consistentes con la formación de soluciones sólidas, con excepción de la discrepancia del tamaño atómico entre los constituyentes, que apuntan a la formación de una estructura multifase.

  La caracterización de la morfología de la microestructura después la fabricación por fusión muestra la presencia predominante de dendritas. Además, el análisis de composición y de fases mediante EDS y difracción de rayos X respectivamente, mostró la tendencia de un compuesto basado en molibdeno y tantalio a segregarse dendríticamente, sobre una matriz en la que se reconocen compuestos basados en titanio y zirconio y compuestos a base de titanio y hierro. El recocido posterior de las muestras a 900°C durante 15 horas en atmósfera inerte (argón), seguido de enfriamiento en flujo de argón, tuvo como resultado una mejor homogeneización de la microestructura, logrando la disolución de algunos de los compuestos inicialmente separados de la solución sólida, liberando de tensión la matriz y reduciendo la dureza. Asimismo, se observa la formación de nuevos compuestos basados en molibdeno.

Los ensayos de microdureza indicaron un aumento de los valores de dureza al aplicar un tratamiento térmico de recocido durante dos horas y temple en agua. Sin embargo, el efecto del recocido posterior durante 15 horas y posterior enfriamiento mediante normalizado produjo una reducción en estos valores de la dureza, aunque el resultado final se mantuvo por encima de los valores previos a los tratamientos. La modulación de la dureza mediante tratamientos térmicos es una característica importante para la conformación de herramientas.

Finalmente, el estudio se completó con ensayos de citotoxicidad basados en la actividad de la enzima lactata dehidrogenasa (LDH), para valorar la aparición de daño o muerte celular. El estudio se llevó a cabo con células madre mesenquimales de hueso humano (hBMSC) y con células del tipo fibroplasto humano normal (NHF) puestas en contacto con muestras de la aleación, en placas de cultivo. La comparación con las placas de referencia no mostró gran diferencia en la actividad de la enzima LDH, pero sí se observó diferencias entre las células NHF y las hBSMSC.

Investigaciones futuras podrían estudiar cómo optimizar los tratamientos térmicos para mejorar aún más la homogeneidad, así como evaluar la biocompatibilidad "in vivo".

En conjunto, esta tesis doctoral aporta conocimiento sobre el potencial de las aleaciones de alta entropía en el campo biomédico, proporcionando un punto de partida para el diseño y la optimización de nuevos materiales basados en estas familias de aleaciones, que admiten la obtención de propiedades a medida, para una variedad de aplicaciones médicas.

Con todo lo anterior, entendemos que los resultados obtenidos justifican la continuación de la investigación en este tipo de aleaciones de nueva generación.